THE G1 CYCLIN Cln3p REGULATES VACUOLE HOMEOSTASIS THROUGH PHOSPHORYLATION OF A SCAFFOLD PROTEIN, Bem1p, IN *Saccharomyces cerevisiae*

A Dissertation

by

BONG KWAN HAN

Submitted to the Office of Graduate Studies of
Texas A&M University
in partial fulfillment of the requirements for the degree of

DOCTOR OF PHILOSOPHY

December 2005

Major Subject: Biochemistry

THE G1 CYCLIN Cln3p REGULATES VACUOLE HOMEOSTASIS THROUGH PHOSPHORYLATION OF A SCAFFOLD PROTEIN, Bem1p, IN *Saccharomyces cerevisiae*

A Dissertation

by

BONG KWAN HAN

Submitted to the Office of Graduate Studies of
Texas A&M University
in partial fulfillment of the requirements for the degree of

DOCTOR OF PHILOSOPHY

Approved by:

Chair of Committee,	Michael Polymenis
Committee Members,	Donald W. Pettigrew
	Michael Kladde
	Z. Jeffrey Chen
Head of Department,	Gregory D. Reinhart

December 2005

Major Subject: Biochemistry

ABSTRACT

The G1 Cyclin Cln3p Regulates Vacuole Homeostasis through Phosphorylation of a Scaffold Protein, Bem1p, in *Saccharomyces cerevisiae*. (December 2005)

Bong Kwan Han, B.S., Seoul National University;

M.S., Korea Advanced Institute of Science and Technology

Chair of Advisory Committee: Dr. Michael Polymenis

How proliferating cells maintain the copy number and overall size of their organelles is not clear. In the budding yeast *Saccharomyces cerevisiae* the G1 cyclins Cln1,2,3p control initiation of cell division by regulating the activity of the cyclin-dependent kinase (Cdk) Cdc28p. We show that Cln3p controls vacuolar (lysosomal) biogenesis and segregation. First, loss of Cln3p, but not Cln1p or Cln2p, resulted in vacuolar fragmentation. Although the vacuoles of *cln3*Δ cells were fragmented, together they occupied a large space, which accounted for a significant fraction of the overall cell size increase in *cln3*Δ cells. Second, cytosol prepared from cells lacking Cln3p had reduced vacuolar homotypic fusion activity in cell-free assays. Third, vacuolar segregation was perturbed in *cln3*Δ cells. Our findings reveal a novel role for a eukaryotic G1 cyclin in cytoplasmic organelle biogenesis and segregation.

Furthermore we show that the scaffold protein Bem1p, a critical regulator of Cdc42p activity, is a downstream effector of Cln3p/Cdc28p complex. The Cdc42p GTPase is known to be required for vacuole fusion. Our results suggest that Ser72 on Bem1p is phosphorylated by Cdc28p in a Cln3p-dependent manner to promote vacuole

fusion. Replacing Ser72 with Asp, to mimic phosphorylation at an optimal Cdk-consensus site located in the first SH3 domain of Bem1p, suppressed vacuolar fragmentation in cells lacking Cln3p. Using *in vivo* and *in vitro* assays, we found that Cln3p was unable to promote vacuole fusion in the absence of Bem1p or in the presence of a non-phosphorylatable Bem1p-Ser72Ala mutant. Furthermore, activation of Cdc42p also suppressed vacuolar fragmentation in the absence of Cln3p. Our results provide a mechanism that links cyclin-dependent kinase activity with vacuole fusion through Bem1p and the Cdc42p GTPase cycle.

DEDICATION

To my wife and daughter, Hyewon Han-Park and Eu-Young Han. Without their incessant support, I might have gone astray in the journey.

ACKNOWLEDGEMENTS

I would like to give sincere thanks with all my heart to all the professors and colleagues in the Department of Biochemistry and Biophysics at Texas A&M University. Dr. Michael Polymenis was a fabulous advisor and mentor. His encouragement and advice made it possible for me to continuously and relentlessly explore the challenging field of science. He taught me how to do experimental science. I would like to acknowledge the help and comments of the members of my advisory committee: Dr. Donald W. Pettigrew, Dr. Sumana Datta, Dr. Michael Kladde and Dr. Z. Jeffrey Chen. I would like to give thanks to Dr. James C. Hu, who recruited me and gave me the opportunity to study, Dr. Donald W. Pettigrew, whose mentoring and support encouraged me, and Dr. Michael Kladde, whose Biochemical Genetics class opened my blind eyes. I would also like to give thanks to Dr. Ryland Young, Dr. Arthur E. Johnson, and Dr. Michael D. Manson for the learning-full and joy-full time of the journal club and Dr. Mary Bryk for help and encouragement. I would like to acknowledge the help and support of the members of the Polymenis laboratory including Dr. Lydia M. Bogomolnaya, Ritu Pathak, Jinbai Guo, James M. Totten, and Heidi M. Blank. I appreciate the help and support of my classmates, particularly Peter Cornish and Carrie Langlais, talks with whom were joyful, and Qingwu Yang, who became the best friend in my first year because, I think, we were the worst English speakers. We could communicate with each other somehow but not with others.

I am indebted to Dr. Lydia M. Bogomolnaya for some experiments (all the fluorescence microscopy experiments and Figures 4.3C, 4.5B&C, 4.7, 4.8D&E), Dr. Lawrence J. Dangott (Figure 4.6A), James M. Totten (Figures 4.4G, 4.5B,C&D), and Heidi M. Blank (Figures 4.5D, 4.8A&B). I am also indebted to Dr. Rodolfo Aramayo for fluorescence microscopy, Dr. Lawrence J. Dangott for the generous advice on protein gel electrophoresis, Dr. Deborah A. Siegele for the pulse-chase experiment, Dr. Ann Ellis for electron microscopy, Mrs. Jane Miller for flow cytometry, and Dr. R. Barhoumi for confocal fluorescence microscopy. Without their help, it would have been impossible to collect such numerous important data within the time period.

I believe that Aggieland was a destination for my training, not only as a scientist, but also as a human being. The last 5 years were full of learning and enlightment in many ways. Again, I would like to express my deep gratitude to all the Aggies and Texans.

TABLE OF CONTENTS

CHAPTER Page

LIST OF FIGURES

LIST OF TABLES

CHAPTER I

INTRODUCTION

The cell cycle

The mitotic cell cycle of eukaryotic cells is divided into four distinct phases; G1, S, G2 and M phase. S phase is a period when DNA is replicated. M phase is when the duplicated chromosomes are divided into two daughter cells. G1 and G2 are gap phases between the S and M phases.

Yeast cells have played crucial roles in unraveling molecular mechanisms of the cell cycle. The foundation for the molecular understanding of the cell cycle occurred in the early 1970's, when Lee Hartwell and his colleagues screened for mutants of genes regulating the cell cycle in *Saccharomyces cerevisiae*, which they baptized *cdc* (cell-division cycle) mutants (Pringle and Hartwell, 1981). Paul Nurse and his colleagues collected *cdc* mutants of *Schizosaccharomyces pombe* by a similar approach to Hartwell's (Nurse, 2002). These collections of *cdc* mutants have been invaluable resources for the cloning and characterization of each *CDC* gene and the molecular understanding of the cell cycle. Another breakthrough was the discovery by Tim Hunt and his colleagues of a protein, cyclin, which was observed to oscillate during cell cycle progression. This temporal oscillation of cyclins is crucial for driving the cell cycle (Nasmyth, 1996; Wittenberg et al., 1990).

This dissertation follows the style and format of Cell.

A key regulator in the yeast cell cycle is a cyclin-dependent kinase (CDK) encoded by *CDC28* in *Saccharomyces cerevisiae* and *cdc2* in *Schizosaccharomyces pombe*. Cyclins are primary regulators of the activity and probably the specificity of CDKs. Protein phosphorylation by the multiple cyclin-CDK complexes leads to events required at various cell cycle stages.

Cell size and G1 regulation

Cell size has been an important phenotype exploited in unraveling molecular mechanisms of the cell cycle. The reason was that the relative rate of progression through the cell cycle could be reflected through this easily measurable parameter. If the cell cycle progresses faster relative to cell growth, the cell will have a smaller size and vice versa. Therefore, measurement of size of cells with variant genotypes or environments would give important information on cell cycle progression in the corresponding condition. In fact, for a given condition, cell size remains unchanged after successive cell proliferations. Therefore, it was assumed that a mechanism existed whereby cell growth was coordinated with the cell cycle. Observations from earlier days showed that most eukaryotic cells spend a majority of time in G1 phase during the mitotic cell cycle and continue to grow until a commitment point for the initiation of DNA replication, which was named as “restriction point” for mammalian cells by Arthur Pardee (Pardee, 1974) and “Start” for *Saccharomyces cerevisiae* by Lee Hartwell (Hartwell and Unger, 1977).

A generally accepted model for cell size control states that the control of cell growth is performed at the point of the G1 to S transition. Understanding how cells decide to enter S phase has been one of the primary goals in the cell cycle field, especially because this research pertains to the better understanding of cancer cells, whose uncontrolled proliferation is thought to be due to their loss of tight regulation of the G1 to S transition. This essentially requires understanding of how complex signaling networks are processed from input signaling of extra-cellular growth factors and nutrients to give rise to the outcome of commitment to enter S phase. Because of this, biologists in the cell cycle field paid much attention to cell size control. In the 1970's, small cell size (*wee*) mutants were identified in *Schizosaccharomyces pombe* and similarly *whi* mutants from *Saccharomyces cerevisiae* (Sudbery et al., 1980; Thuriaux et al., 1978). One of the *wee* mutants mapped to the *cdc2* locus (Nurse and Thuriaux, 1980) and *wee2* is a kinase inhibiting *cdc2* function by phosphorylating *cdc2* on tyrosine15 (Parker et al., 1992). Several *WHI* genes turned out to be involved in the regulation of the G1 to S transition, which is consistent with the notion that the major cell size control point of *Saccharomyces cerevisiae* occurs at the G1 to S transition. For example, the *WHI1-1* mutant is a gain-of-function mutant of a G1 cyclin, which was later re-named as *CLN3* (Nash et al., 1988; Richardson et al., 1989). *WHI3* is a negative regulator of Cln3p.

The other G1 cyclins of *Saccharomyces cerevisiae*, *CLN1* and *CLN2*, were isolated as high copy suppressors of G1 arrest in a *cdc28* mutant by Steven Reed and his

colleagues (Hadwiger et al., 1989). Cells removed all three G1 cyclins are non-viable but cells with any single G1 cyclin can proliferate (Richardson et al., 1989).

Cyclins and cyclin-dependent kinases

Saccharomyces cerevisiae has five CDKs, *CDC28*, *PHO85*, *KIN28*, *SSN3*, and *CTK1*, but only *CDC28* is essential (Mendenhall and Hodge, 1998). The analogous gene in *Schizosaccharomyces pombe* is *cdc2* (Doree and Hunt, 2002). CDKs are serine/threonine protein kinases. The CDK full consensus phosphorylation site is S/T-P-x-K/R and its minimum consensus site is S/T-P. Crystallographic study of Cdk2p by Sung-Ho Kim and his colleagues provides an important insight into a structural basis of CDK action (De Bondt et al., 1993). It has an active site cleft surrounded by two lobes formed by the N-terminus and the C-terminus. The N-terminal lobe contains the conserved PSTAIRE helix. The position of the T-loop, located in the C-terminus lobe, plays a crucial role in CDK activity. Without cyclin binding, the T-loop prevents access of a substrate to the active site cleft of CDK. Upon binding with cyclin it dislocates and the cleft is accessible to CDK's substrates. CDK activity is regulated by four main mechanisms: cyclin binding, CDK inhibitors (CKIs) binding, activation by phosphorylation by CDK activating kinase (CAK), and inhibition by phosphorylation (Mendenhall and Hodge, 1998).

Cyclins are defined as proteins containing the cyclin box, which is a 100-amino acid residue region required for Cdk binding and activation. They are a family consisting of very diverse proteins, whose size ranges from 35 to 90 kD. The conserved cyclin box

forms the cyclin fold composed of a 5-helix bundle (De Bondt et al., 1993). Helices 3 and 5 of the cyclin fold interact with the PSTAIRE helix of the active site cleft of CDKs. Such cyclin binding appears to influence significantly the conformation of the active site of CDKs.

Cdc28p associates with 9 cyclins, of which three are G1 cyclins (Cln) and six are B-type cyclins (Clb). All the cyclins except for Cln3p temporally oscillate during the cell cycle (Nasmyth 1996). Two mechanisms are crucial for cyclin oscillation, transcriptional regulation and proteasome-mediated proteolysis. The abundance of Cln1p, 2p and Clb5p, 6p peaks in late G1, while that of Clb3p, 4p peaks at G2/M, and that of Clb1p, 2p peaks at M. G1 cyclins are very unstable because they contain a PEST region at their C-termini, which is required for their proteasome-mediated proteolysis (Mendenhall and Hodge, 1998; Tyers et al., 1992). *CLN3-1* and *CLN3-2* alleles produce stable forms of Cln3p because they lack the PEST region. Clbs have a destruction box at the N-termini, which is required for their proteasome-mediated proteolysis (Mendenhall and Hodge, 1998).

Although it was long presumed that Cdc28p might directly phosphorylate many key components of cell cycle machinery, attempts to find the targets of Cdc28p were not very successful. Only a dozen proteins were identified as Cdc28p targets including H1 histone (Langan et al., 1989), Far1p (Peter et al., 1993), Ste20p (Leeuw et al., 1998), and Sic1p (Verma et al., 1997). However, the recent development of many toolkits for yeast genetics and molecular biology facilitated the identification of Cdc28p substrates. The Cdc28as mutant protein, which can utilize a bulky ATP analogue, N^6-(benzyl) ATP,

made it possible to follow the labeled proteins from ^{32}P-N^{6}-(benzyl) ATP because the other cellular kinases cannot use the analogue. This allowed proteins phosphorylated by Cdc28as protein to be discernible from proteins phosphorylated by other kinases. David Morgan and his colleagues performed genome-wide studies for putative Cdc28p substrates (Loog and Morgan, 2005; Ubersax et al., 2003). It was estimated that as many as 8% of yeast genes might encode putative substrates of the Clb2p/Cdc28p kinase complex. These results will provide a valuable resource for further detailed molecular studies.

Cdc28p plays a crucial role in almost every point during the cell cycle. Different substrates seem to be phosphorylated by a different cyclin-Cdc28p kinase complex at various time points during the cell cycle. For example, Gin4p is phosphorylated in a Clb2p/Cdc28p-dependent manner, while Ste20p is phosphorylated by Cln2p/Cdc28p (Altman and Kellogg, 1997; Leeuw et al., 1998). However there seems to be substantial redundancy between cyclins because deletion of one cyclin gene often does not give rise to any discernible phenotypes. How Cdc28p's substrate specificity is achieved has long been an issue of debate. Different spatial distributions and different temporal oscillations of individual cyclins may contribute to the Cdc28p's substrate specificity (Edgington and Futcher, 2001; Miller and Cross, 2000). In fact, the abundance of Cdc28p does not oscillate and is relatively much higher than that of cyclins at a given time and space. As a consequence, presumably the identity and activity of cyclin will be a dominant determining factor for the activity and specificity of Cdc28p. Another possible

mechanism to accomplish substrate specificity of Cdc28p is by different spatial distribution and different temporal oscillation of its substrates.

A mechanistic understanding of cell cycle regulation by cyclin/Cdc28p kinases provides an important insight into how CDKs execute cell cycle transitions in higher organisms because most key regulators of the cell cycle are evolutionary conserved. This premise was for example the basis of how Paul Nurse and his colleagues succeeded in cloning human Cdk1p by complementation using a *Schizosacchomyces pombe cdc2* mutant (Lee and Nurse, 1987). Steven Reed and his colleagues cloned human cyclins (cyclins C, D, and E) using *Saccharomyces cerevisiae* cyclin mutants (Lew et al., 1991). Similarly, Stephen Elledge and Matthew Spottswood cloned human Cdk2p using a *Saccharomyces cerevisiae cdc28* mutant (Elledge and Spottswood, 1991).

G1 to S transition (START)

In early G1 phase the activity of Cdc28p remains low, as low Cdc28p kinase activity is necessary for anaphase to take place. However, the commitment to initiate DNA replication requires high activity of Cdc28p. Before this commitment point, cells grow and the process of ribosome biogenesis actively takes place. Accordingly, a cell's protein synthesis capability increases and this leads to an increase of Cln3p/Cdc28p activity, which is an upstream regulator of G1 to S transition (Polymenis and Schmidt, 1997; Jorgensen and Tyers, 2004).

A protein kinase, TOR (target of rapamycin), plays a key role in integrating nutrient-dependent signaling pathways to regulate translation and as a result cell size control (Raught et al., 2001). S6 kinase (S6K) and 4E-BP are two important effectors of TOR signaling. S6K phosphorylates ribosomal S6 protein and consequently positively regulates translation. 4E-BP is a negative regulator of the translation initiation factor, eIF4E, and is inhibited by TOR-mediated phosphorylation. The ultimate effect of this TOR action is thought to increase the abundance of Cln3p in late G1. Michael Polymenis and Emmett Schmidt found that abundance of Cln3p is regulated by translation in G1 (Polymenis and Schmidt, 1997).

Extensive molecular studies of the yeast cell cycle have revealed key features of the G1 to S transition regulation. A key event for the G1 to S transition is the activation of the G1 transcription program, which leads to a burst expression of more than 200 genes including Cln1p, Cln2p, Clb5p and Clb6p (Spellman et al., 1998). These gene products play crucial roles in S phase processes such as DNA replication and bud formation. At the center of G1 transcription are two transcription factors, SBF (SCB (Swi4-Swi6-dependent cell cycle box) binding factor) and MBF (MCB (*MluI* cell cycle box) binding factor). SBF is a complex comprised of Swi4p and Swi6p, and MBF is a complex of Mbp1p and Swi6p. Swi4p and Mbp1p each bind specific DNA sequences. SBF and MBF remain bound to their promoters but in association with their inhibitor, Whi5p, until late G1 phase. The transcription of the target genes stays in a repressed state in this period.

Cln3p/Cdc28p and Bck2p positively regulate SBF and MBF by independent pathways (Wijnen and Futcher, 1999). Curt Wittenberg and his colleagues finally identified the long-pursued target of Cln3p/Cdc28p kinase in G1 transcription regulation (de Bruin et al., 2004). At late G1 when the activity of Cln3p/Cdc28p in the nucleus is thought to reach a critical threshold, Cln3p/Cdc28p phosphorylates Whi5p and dissociates it from SBF and MBF, leading to de-repression of the target genes (Costanzo et al., 2004; de Bruin et al., 2004). Whi5p then re-localizes from the nucleus into the cytoplasm. In mammals, the tumor suppressor protein Rb binds to and inhibits E2Fs, which are transcription activators for the genes required for the G1 to S transition. In many cancer cells, the function of Rb as a gate keeper of cell cycle entrance is lost (Chau and Wang, 2003). Whi5p appears to play an analogous role in *Sacchromyces cerevisiae* (Schaefer and Breeden, 2004). Whi5p and Rb have homology not in structure but in logic of function. How Bck2p activates SBF and MBF is currently unknown.

Abundance and activity of Cln3p do not oscillate as the other cyclins do during cell cycle progression (Nasmyth, 1996). Cell growth appears to be required for Cln3p's activation and the sub-cellular localization of Cln3p appears to be important in its positive regulation role for SBF and MBF (Edgington and Futcher, 2001; Wang et al., 2004). Whi3p regulates Cln3p's sub-cellular localization (Wang et al., 2004).

At START, three prominent cell cycle events take place: DNA replication, bud formation and spindle pole body duplication. Cln1, 2p/Cdc28p trigger initiation of bud emergence (Gulli et al., 2000). Cln1, 2p/Cdc28p also phosphorylate Sic1p and Cdh1p and inactivate them through proteasome-mediated proteolysis (Nasmyth, 1996).

Degradation of Sic1p and Cdh1p, which are inhibitors of Clb-Cdc28p, leads to activation of Clb5, 6p/Cdc28p. This in turn initiates DNA replication and S phase starts.

In addition to the transcriptional regulation mediated by SBF and MBF, there are multiple layers of regulation in G1 so that a cell does not enter S phase prematurely. CDK inhibitor proteins (CKIs) play a crucial role in S phase entrance. They prevent Cdc28p from being activated in G1 phase. The action of three CKIs, Sic1p, Far1p and Cdh1p, is well understood about how they antagonize Cdc28p activity. Far1p is expressed only in haploid cells and is a specific inhibitor of Cln/Cdc28p whereas Sic1p is a specific inhibitor of Clb/Cdc28p (Mendenhall and Hodge, 1998). Both Far1p and Sic1p are capable to exclude substrates from the Cdc28p active site. During late anaphase and G1, Cdh1p binds to the APC/C (anaphase-promoting complex/cyclosome), an E3 ubiquitin ligase. APC/C-Cdh1p complex recognizes Clbs for ubiquitination and then their proteolysis. The ultimate effect of these inhibitory pathways is to ensure that overall activity of Cdc28p remains low until late G1. G1 to S transition requires accumulated Cln/Cdc28p activity, which can override the multiple inhibitory actions and which can only be obtained in late G1. Cln/Cdc28p phosphorylates and inactivates Far1p through proteasome-mediated degradation (Henchoz et al., 1997). Similarly, Sic1p is phosphorylated by Cln/Cdc28p and marked for proteasome-mediated proteolysis (Nash et al., 2001). Intriguingly multiple phosphorylation of Sic1p provides molecular information of its switch-like degradation (Nash et al., 2001). Cdh1p is phosphorylated by Clb/Cdk1p and then dissociated from the APC/C complex, which then cannot recognize Clbs anymore for proteolysis (Zachariae et al., 1998).

Bud emergence and polarized growth

For bud emergence to take place in the G1 to S transition, cells must re-organize the structure of the actin cytoskeleton. *Saccharomyces cerevisiae* has at least four distinct structures of actin cytoskeleton: actin cables, cortical patches, a cytokinetic ring, and the cap (Adams and Pringle, 1984). In late G1, cortical patches assemble to an area where the bud tip is to form, and actin cables orient from the patches. The assembled actin structures guide the delivery of secretory vesicles, which are required for bud emergence and growth (Pruyne et al., 2004).

In late G1, Bud1p/Rsr1p GTPases seem to play a key role in the determination of incipient bud site (Casamayor and Snyder, 2002). Around Bud1p/Rsr1p, a large protein complex, composed of Bem1p, Cdc24p, Cdc42p, Cla4p, and Ste20p, is formed (Bose et al., 2001). Cln1, 2p/Cdc28p are thought to play an important role in this process by regulating Cdc24p phosphorylation (Gulli et al., 2000). *BEM1* was identified as a gene required for bud emergence. It is a scaffold protein containing two SH3 domains, a PX domain and a PB domain from N- to C-termini (Irazoqui et al., 2003). The second SH3 domain interacts with Cla4p, Ste20p, Boi1p and Boi2p. The PX domain interacts with phosphoinositides and the PB domain interacts with Cdc24p. Bem1p also interacts with Cdc42p through its N-terminal region. Formation of a complex including Bem1p, Cdc42p, Cla4p, and Ste20p appears to be important to the establishment of a polarized actin cytoskeleton. Actin cables formed toward the bud tip provide a road for the secretory vesicles to migrate to the bud, supplying materials required for the growth of bud.

Organelle inheritance

In a eukaryotic cell, organelles are not *de novo* synthesized but instead are inherited from the mother cell (Warren and Wickner, 1996; Weisman, 2003). Inheritance processes of some organelles such as the Golgi apparatus are quite contrasting between *Saccharomyces cerevisiae* and mammalian cells (Warren and Wickner, 1996). Inheritance of human Golgi apparatus takes place in M phase through Golgi fragmentation into many smaller vesicles, which partition into two daughter cells. The vesicles from mitotic Golgi fragmentation then fuse in G1 phase to form a new copy of Golgi. In *Saccharomyces cerevisiae*, organelle inheritance usually starts in S phase when the bud grows. A part of the mother cell's organelles moves along actin cables into the bud, where they form new organelles by homotypic fusion.

Homotypic fusion is defined as membrane fusion between the same compartments. During the whole process of organelle inheritance, the organelle is first fragmented in the mother cell to smaller vesicles, which are then translocated to the daughter cell and finally fused to form a new copy of the organelle. All of these processes will be closely related with homotypic fusion. To coordinate organelle inheritance with the cell cycle, homotypic fusion may somehow be linked to the cell cycle machinery. In fact, a human Golgi's tethering factor, GM130, was shown to be phosphorylated *in vitro* by cyclinB/Cdk1p and its phosphorylation disrupts trans-interaction with another tethering factor, p115, on other membrane (Lowe et al., 1998). This phosphorylation was proposed to be crucial for mitotic Golgi fragmentation.

At present we do not have an established molecular picture of organelle inheritance. Studies on yeast vacuole inheritance have provided some important insights into molecular mechanisms of organelle inheritance.

Vacuole/lysosome

The yeast vacuole is an organelle equivalent to the mammalian lysosome and the most extensively studied organelle in *Saccharomyces cerevisiae*. The main function of the vacuole is to maintain cellular homeostasis. Vacuole serves as a reservoir of small molecules such as amino acids, small ions, and polyphosphates, and so it has a lower density than other organelles (Wiemken and Durr, 1974). It also contains a large amounts of various hydrolases, including carboxypeptidase Y (CPY), alkaline phosphatase (ALP), proteinase A (PrA), proteinase B (PrB), and aminopeptidase I (API) (Bryant and Stevens, 1998). The vacuole is the main site for degradation of proteins, lipids and even of whole organelles, and is also involved in the regulation of receptor-mediated signaling pathways.

The vacuole is a large organelle, occupying about 25% of total cell volume (Wiemken and Durr, 1974), and has a low copy number, 1-5 vacuoles per cell (Wickner, 2002). There are several vacuole-specific dyes which are commercially available. In particular, CDCFDA and FM4-64 are very useful (Vida and Emr, 1995). They facilitate molecular and cellular studies on the vacuole. CDCFDA diffuses into the cytoplasm and is hydrolyzed by vacuolar hydrolases in the vacuolar lumen (Breeuwer et al., 1995). The cleaved product becomes fluorescent in the acidic vacuole lumen. It becomes charged

after cleavage and is thus retained in the vacuole. FM4-64 is a lipophilic fluorescent compound which can stain the vacuolar membranes. It is internalized from the plasma membrane by endocytosis and then targeted into the vacuolar membrane.

Wild-type vacuoles have a round-shaped morphology. Genes required for the normal morphology were identified and termed as *VAM* (vacuole morphology). Vacuole morphology is categorized into five classes (Class A, B, C, D, and E) (Catlett and Weisman, 2000). Class A is wild-type vacuole morphology. Class B is vacuole morphology of multiple small vacuoles. Class C is highly fragmented vacuoles. Class D is a single, enlarged vacuole morphology. Class E vacuoles have a large vacuole compartment surrounded by many membrane vesicles. Vacuolar pH is about 6.2 in wild-type cells. VPH (vacuole pH) genes were identified, which are required for acidic vacuolar pH (Preston et al., 1989).

There are five targeting pathways to the vacuole (Bryant and Stevens, 1998; Burd et al., 1998). Two pathways, the ALP pathway and the CPY pathway, share the ER to late Golgi pathway along the secretory pathway. The ALP pathway takes a route from the late Golgi to the vacuoles. The CPY pathway takes a route from the late Golgi through the prevacuolar endosome to the vacuoles. The other vacuole targeting pathways are the cytoplasm-to-vacuole pathway, the autophagy pathway, and the endocytosis pathway. API takes the cytoplasm-to-vacuole pathway, in which a soluble protein in the cytoplasm is surrounded by a membrane to form a vesicle, which is finally fused with vacuolar membrane. The autophagy pathway recently received much attention because dysfunction of human homologs of some genes involved in the pathway is known to be

linked to some diseases (Shintani and Klionsky, 2004). Autophagy involves the formation of an autophagosome, a double-layered membrane-bound structure engulfing cytoplasmic composites. The autophagosome fuses with vacuolar membrane and a single membrane-bound structure enters into the vacuole lumen, where it is degraded by vacuolar hydrolases. In the endocytosis pathway, small vesicles formed by invagination of plasma membrane, which are first delivered to early endosomes, then to multivesicular late endosomes, and finally to vacuoles. The vesicles in the lysosome/vacuole are degraded by vacuolar hydrolases. This, also called multi-vesicular body (MVB) pathway, is one pathway that extra-cellular stimuli use to reach the cytoplasm to execute cellular effects. This pathway is thought to down-regulate the growth factor/pheromone signaling. This pathway is especially important for signal transduction pathways involved in the control of cell growth and development (Katzmann et al., 2002). The genes involved in each pathway are well characterized. 46 complementation groups of *VPS* (vacuolar protein sorting) genes have been identified (Jones et al., 1997). Some of these genes are involved in the Golgi-to-endosome, the endosome-to-vacuole, or the retrograde endosome-to-Golgi pathway (Jones et al., 1997).

Membrane fusion

Membrane fusion is a reaction of fundamental importance in eukaryotic cells, essential for membrane trafficking, protein targeting and organelle inheritance. James Rothman and his colleagues identified key players of the membrane fusion machinery in the 1980's. Using *in vitro* membrane fusion assays, they identified NSF (N-ethyl maleimide-

sensitive factor), SNAP (soluble NSF attachment protein) and SNARE (SNAP receptor), all of which play crucial roles in membrane fusion (Rothman, 1994). Randy Schekman and his colleagues identified 23 genes required for protein targeting along the yeast secretory pathways (*sec* genes), some of which are involved in membrane fusion (Bonifacino and Glick, 2004; Novick et al., 1981; Novick et al., 1980).

NSF is an ATPase, a founding member of the AAA protein family (ATPases associated with diverse cellular activities) and forms a hexameric ring (Bonifacino and Glick, 2004). SNAP is required for NSF to bind to the membrane. SNAREs are membrane-associated receptors of SNAP. Rothman and his colleagues proposed the SNARE hypothesis that the specificity of membrane fusion between two compartments is determined by trans-SNARE interaction (Sollner et al., 1993). It asserts that the interaction between a SNARE on the vesicle membrane (v-SNARE) and a SNARE on the target membrane (t-SNARE) is a determining factor for the specificity of two membranes. The trans-SNARE complex has a four-helix bundle structure comprised of three t-SNAREs and one v-SNARE (Sutton et al., 1998). The SNARE hypothesis triggered extensive studies on molecular mechanisms of membrane fusion and its specificity (Chen and Scheller, 2001; Guo et al., 2000; Pfeffer, 1996; Rothman, 2002). The trans-SNARE complex was shown to be the minimal machinery (SNAREpin) required for membrane fusion (Weber et al., 1998) and a determining factor for compartmental specificity of membrane fusion at least in artificial liposomes (McNew et al., 2000). Furthermore, each membrane compartment appears to have unique SNAREs (Hay and Scheller, 1997; Pelham, 1999). All these support the SNARE hypothesis.

However, the SNARE complex is probably not the only factor that determines compartmental specificity *in vivo* because specific inhibition of the SNAREs does not block vesicle docking (Guo et al., 2000; Pfeffer, 1999). In addition, t-SNAREs are distributed uniformly over the plasma membrane rather than on a limited area of vesicle fusion in *Drosophila* and the squid giant synapse.

Membrane fusion is a multi-step process which can be defined as a sequence of distinct steps, such as priming, tethering, docking and fusion (Pfeffer, 1999). In priming, NSF disassembles cis-SNARE complex on the same membrane. Tethering was proposed as a loose interaction state in which the associations extend over distances of more than about half the diameter of a vesicle from a given membrane surface (>25 nm). Remarkably, a tethering factor Uso1p has a coiled-coil structure of 150 nm long, which is suited for a tethering function. Docking was proposed as a tighter and more stable state, in which two membranes are within a bilayer's distance (<5-10 nm), and the trans-SNARE complex is established between two membrane compartments. Fusion is a stage where two membrane bilayers become one continuing membrane bilayer. All these processes are driven by protein-protein interactions. Membranes of each compartment have different tethering and docking factors (Guo et al., 2000; Pfeffer, 1999). Tethering and docking factors probably play an important role in determining compartment specificity.

Vacuolar inheritance and vacuolar homotypic fusion

Vacuoles, like other organelles, are not *de novo* synthesized in a daughter cell but inherited from the mother cell (Warren and Wickner, 1996; Weisman, 2003). Vacuolar inheritance is thought to be coordinated with cell cycle progression. In S phase, a tubular vesicle structure is formed from the mother cell's vacuoles and moves along an actin cable toward the bud, where they fuse to form a new copy of vacuoles by vacuolar homotypic fusion. Genes involved in vacuolar inheritance (*VAC*) have been identified. Key players in vacuolar inheritance are Myo2p, Vac8p and Vac17p (Tang et al., 2003). Vac17p is a component of the vacuole-specific Myo2p receptor. Vac8p is a vacuolar membrane protein, which interacts with Vac17p. Myo2p is a motor protein, capable of moving along actin cables. Myo2p/Vac17p/Vac8p complex connects a vacuole vesicle to the actin cable. The motoring action of Myo2p produces the driving force for the vesicle movement. Transported vesicles are deposited in the bud by dissociating the Myo2p/Vac17p/Vac8p complex through degradation of the PEST domain of Vac17p (Tang et al., 2003).

A current molecular picture of vacuolar homotypic fusion is shaped by the extensive studies performed by Bill Wickner and his colleagues (Wickner and Haas, 2000). They established an *in vitro* fusion assay, which is an important tool for the biochemical study of the fusion reaction. Like other analogous *in vitro* membrane fusion assays, this assay exploits biochemical complementation. Vacuole liposomes are prepared from two strains of *pho8*Δ cells and *pep4*Δ*/prb1*Δ cells. They are mixed with cytosol, ATP, and salts and incubated to allow for vacuole fusion to take place. *PHO8*

encodes alkaline phosphatase (ALP). *PEP4* and *PRB1* encode vacuolar hydrolases, which are required for the processing of pro-ALP to mature active ALP. Only when two vacuole membranes fuse and their components are mixed, can fully matured active ALP form. ALP activity can be measured by spectrophotometry. Alternatively, vacuole fusion can be directly evaluated by microscopy after vacuole staining.

Using this biochemical assay, combined with genetics, Bill Wickner and his colleagues identified many players involved in the fusion reaction. Vam3p and Vam7p are vacuolar t-SNAREs (Wickner, 2002). Nyv1p, Vti1p and Ykt6p are vacuolar v-SNAREs. HOPS (homotypic fusion protein sorting) complex is composed of tethering factors of vacuolar homotypic fusion. It is composed of Vps 11, 16, 18, 33, 39, 41p. Sec17p is yeast SNAP and Sec18p is yeast NSF, both of which are involved in vacuolar homotypic fusion (Haas and Wickner, 1996). Several small GTPases such as Ypt7p, Cdc42p, and Rho1p are known to play a key role in the vacuole membrane fusion.

Phosphoinositides also play a crucial role in vacuolar membrane trafficking and fusion (Burd et al., 1998). S*accharomyces cerevisiae* has phosphoinositol (PI), phosphoinositol 3-phosphate (PI(3)P), phosphoinositol 4- phosphate (PI(4)P), and phosphoinositol 3, 5-diphosphate ($PI(3,5)P_2$). Membranes of different organelles have characteristic distribution of PI or PIPs of their own. The Golgi membrane has PI(3)P and PI(4)P while the endosome has PI(3)P and $PI(3,5)P_2$. Vps34p is a PI 3-kinase converting PI to PI(3)P on the Golgi and endosome membranes. Pik1p is a PI 4-kinase catalyzing PI to PI(4)P on Golgi membrane. Fab1p is a PI(3)P 5-kinase catalyzing the conversion of PI(3)P to $PI(3,5)P_2$ on the endosome and vacuole membranes. PI or PIPs

interact with specific protein domains. PI(3)P interacts with the FYVE (Fab1p, Ygl023p, Vac1p, Eea1p) domain. PH (Pleckstrin homology) domain interacts with various PI or PIPs (Maffucci and Falasca, 2001). The different distributions of PI or PIPs endow identity to individual organelles by recruiting different proteins. The importance of phosphoinositides in vacuolar physiology is well exemplified by *fab1*Δ mutant cells, which have a very enlarged single vacuole filling almost the entire cell volume (Efe et al., 2005). The cells are very sick, probably because of vacuolar dysfunction. In fact, phosphoinositides play an important role in the regulation of human cell proliferation (Mayo and Donner, 2002).

Bill Wickner and his colleagues proposed that vacuolar homotypic fusion is composed of four sequential steps named priming, tethering, docking and fusion (Mayer et al., 1996). They characterized a temporal sequence of the vacuolar homotypic fusion reaction using several inhibitors and antibodies, which were known to block a specific step. In the priming step, the cis-SNARE complex is first disassembled, which is dependent on Sec18p (yeast NSF) and Sec17p (yeast SNAP). Then, the tethering factor HOPS complexes on the opposing membranes interact, this interaction being dependent on Ypt7p. The trans-SNARE complex then forms and finally Ca^{++} triggers the membrane fusion.

Overall, vacuolar homotypic fusion appears to be a very complex reaction, which is a multi-step reaction involving many proteins. Several lines of evidence favor this notion. First, a genome-wide study showed that more than 100 genes are involved in the vacuolar homotypic fusion reaction (Seeley et al., 2002). Second, cis-SNAREs exist in a

large 65S complex before the priming step. It seems that large complex assembly/disassembly takes place during the entire fusion reaction from the priming step to final membrane fusion. Third, at least three GTPases are known to be involved in the vacuolar homotypic fusion. This adds an additional layer to an already complex regulatory network because the activity of each GTPase is regulated by a specific GTPase activing protein (GAP), GTP exchange factor (GEF) and GTPase dissociation inhibitor (GDI) in each case. A GTPase, Ypt7p, is required for the tethering step. Rho1p and Cdc42p act after Ypt7p to regulate vacuole docking (Eitzen et al., 2001; Muller et al., 2001).

Cdc42p appears to be involved in vacuolar homotypic fusion through the regulation of actin polymerization. The reports on how actin regulates membrane fusion are quite contradictory (Eitzen, 2003). Actin was generally thought to be a negative regulator of membrane fusion because it seemed to act as a barrier to formation of trans-SNARE complex. However, after the docking stage, in which trans-SNARE complex forms, it might facilitate membrane fusion. Therefore, the role of actin in membrane fusion seems quite complicated, and it can facilitate or inhibit membrane fusion depending on at which step it acts.

Membrane traffic, cell size control and *CLN3*

A feature of eukaryotic cells is that they have many intracellular membrane-bound organelles. These intracellular membrane-bound structures were observed as early as the late nineteenth century by Camillo Golgi and Elie Metchnikoff (Mellman and Warren, 2000). In the middle of the twentieth century, George Palade and his colleagues showed the existence of biochemically and physically distinct organelles using cell fractionation and enzymatic assays combined with electron microscopy (Palade, 1975). They elucidated the basic principles of the secretory pathway using EM autoradiography. Proteins were pulse-labeled and after various chase periods, the cell was observed by EM to follow the labeled proteins' pathway. They found that secretory proteins are synthesized in the endoplasmic reticulum (ER), translocated into the Golgi complex and secreted across the plasma membrane by exocytosis. Proteins are translocated between distinct organelle compartments via transport vesicles, which bud from one organelle and fuse into another.

Another important pathway in membrane traffic is endocytosis. This is the pathway for extracellular materials to enter the cell. After binding to a cognate receptor on the plasma membrane, the extracellular material is internalized into the cell as a vesicle and targeted to late endosomes.

There are numerous, dynamic fluxes of vesicles between the plasma membrane and organelles as well as between organelles. For *Sacchromyces cerevisiae* to grow, continuous expansion of the cell wall and plasma membrane is required. Materials

should be continuously carried by secretory vesicles and supplied to the area of the cell wall and plasma membrane from intracellular compartments by exocytosis. Membrane trafficking may be closely involved in the regulation of cell size and morphogenesis. Cell size and morphogenesis will be altered as a result of a net change of the vesicle fluxes between compartments. However, most, if not all, mechanistic explanations of cell size control were provided in terms of molecule-to-molecule interactions, and without taking into account the compartmentalization of eukaryotic cells.

CLN3 is a well-known cell size regulator. Mutations in *CLN3* give rise to significant cell size changes. Hypermorphic alleles, *CLN3-1* and *CLN3-2*, make a cell small, whereas *CLN3* deletion leads to an enlarged cell. A generally accepted molecular explanation is that Cln3p/Cdc28p regulates the G1 transcription program and as a consequence temporally controls the G1 to S transition. According to this model, gain-of-function mutations in *CLN3* will activate the transcriptional program at an earlier point. Cells can enter S phase at a smaller cell size, and as a consequence, the overall cell size of this mutant will be diminished. As for loss-of-function *CLN3* mutants, the opposite effect will occur for the opposite reason. This model seems to be well suited for explaining the cell size phenotypes of *CLN3* mutants because the role of *CLN3* to activate the G1 transcription program is well established. Furthermore, this model is consistent with the recent observation of the genome-wide study by Mike Tyers and his colleagues that cell size deregulation was observed among gene deletion mutants of the ribosome biosynthesis pathways, which impact on the regulation of G1 to S transition (Jorgensen et al., 2002).

However it should be mentioned that they also observed that most of the cell size mutant genes do not control G1 to S transition. Therefore, although the G1 to S transition is an important point for the coordination of the cell cycle with cell growth, the possibility should not be overlooked that overall cell size may be determined by diverse ways at various points during cell cycle progression. In fact, cells continue to grow after the G1 to S transition. Though ribosome biogenesis and translation efficiency were proposed as the main theme for cell size control, the broad diversity of the genes involved in cell size control may reflect that cell size is determined at multiple levels during cell division and cell growth.

Another scenario is that the size of individual organelles is autonomously controlled by the genetic program and the environment, and that the size of individual organelles disproportionately contributes to overall cell size in different genetic and environmental conditions. However, this possibility was almost out of consideration until recently, when we showed that there is a disproportional change in vacuole size compared to overall cell size change in *cln3*Δ cells of *Saccharomyces cerevisiae* (Han et al., 2003). To our surprise Cln3p/Cdc28p directly regulates vacuolar homotypic fusion and vacuolar copy number by a post-translational mechanism. This reveals a novel role of Cln3p independent of its well-established function in the activation of G1 transcription. It is the first demonstration in yeast that a cell cycle regulator directly regulates an organelle's membrane fusion. I will describe these exciting findings in CHAPTER III.

Remarkably we succeeded in identifying the target of Cln3p/Cdc28p in vacuole fusion. A scaffold protein, Bem1p, is required for the vacuolar function of Cln3p. Furthermore we succeeded in pinpointing the target site (Ser72) of Cln3p/Cdc28p on Bem1p, whose phosphorylation gives rise to a crucial biological consequence in vacuole fusion. In CHAPTER IV, I will describe these surprising and exciting findings.

CHAPTER II

MATERIALS AND METHODS

Strains and DNAs

Cell cultivation, media and yeast molecular biology techniques were performed as described by Kaiser et al (Kaiser et al., 1994), unless otherwise indicated. Most of the strains and plasmids used in this study are listed in Tables 2.1 and 2.2, respectively. The *YEp-VAC8* and *YEp-CLN2* plasmids were gifts from L. Weismanm (Wang et al., 2001) and B. Andrews (Ogas et al., 1991), respectively. The plasmid used to disrupt *CLN3* in *vac8*Δ cells (BY4741 background) has been described previously (Polymenis and Schmidt, 1997).

The *CLN3-2* strains were generated by transformation of the corresponding wild-type strains with a $URA3^{+}$ low-copy-number centromeric plasmid carrying the *CLN3-2* allele (Cross, 1990). In the *cln2*Δ strain (BY4741 background), we disrupted *CLN1* (*cln1*Δ*::URA3*) by PCR-based single-step gene replacement (Kaiser et al., 1994). The PCR-product was generated by amplification of *URA3* sequences with the following oligonucleotide primers: 5'-CCACCACTCCACTGCTCGTTAGCTATTTCTGTAAAATAAATAAAAAGATCATGTCGAAAGCTACATATAAGGAACG –3', and 5'-TAGTATTCCGTTATTAATTAAGTATATATGTAGGCTTGATGAGAAAATGGTCAGTTTTGCTGGCCGCATCTTCTC-3'.

Table 2.1 *Saccharomyces cerevisiae* strains and their relevant genotypes

Strain	Relevant genotype	Source
BY4741	*MAT*a *his3*Δ *leu2*Δ *met15*Δ *ura3*Δ	Res. Genetics
BY4742	*MAT*α *his3*Δ *leu2*Δ *met15*Δ *ura3*Δ	Res. Genetics
BY4743	BY4741/BY4742	Res. Genetics
W303a	*MAT*a *ade2 trp1 leu2 his3 ura3 can1*	B. Futcher
A364A	*MATa ade1 ade2 ura1 his7 lys2 tyr1 gal1 SUC mal*	ATCC
185-3-4g	*cdc28::cdc28-1* (A364A otherwise)	ATCC
GT106	*cln3*Δ*::URA3* (W303a otherwise)	B. Futcher
GT108	*CLN3-3HA::URA3* (W303a otherwise)	B. Futcher
MT240	*CLN2-3HA::URA3* (W303a otherwise)	B. Futcher
7503198	*CLN2-TAP::his3MX* (BY4741 otherwise)	Open Biosystems
7499374	*BEM1-TAP::his3MX* (BY4741 otherwise)	Open Biosystems
33340	*bem1*Δ*::kanMX/bem1*Δ*::kanMX* (BY4743 otherwise)	Res. Genetics
DKY6281	*MAT*a *lys2 trp1 ura3 his3 leu2 suc2 pho8*Δ*::TRP1*	W. Wickner
BJ3505	MATa *lys2 trp1 ura3 his3 gal2 can prb1 pep4*Δ*::HIS3*	W. Wickner
13340	*bem1*Δ*::kanMX* (BY4742 otherwise)	Res. Genetics
SCMSP47	*cln1*Δ*::KanMX cln2*Δ*::URA3* (BY4741 otherwise)	(Han et al., 2003)
SMY01	*bem1*Δ*::KanMX cln3*Δ*::URA3* (BY4741 otherwise)	This study
30366	*cln3*Δ*::kanMX/cln3*Δ*::kanMX* (BY4743 otherwise)	Res. Genetics
366	*cln3*Δ*::kanMX* (BY4741 otherwise)	Res. Genetics
1036	*cln2*Δ*::kanMX* (BY4741 otherwise)	Res. Genetics
4105	*pep3*Δ*::kanMX* (BY4741 otherwise)	Res. Genetics
253	*vac8*Δ*::kanMX* (BY4741 otherwise)	Res. Genetics
4738	*clb1*Δ*::kanMX* (BY4741 otherwise)	Res. Genetics
5534	*clb2*Δ*::kanMX* (BY4741 otherwise)	Res. Genetics

Table 2.1 continued.

Strain	Relevant genotype	Source
3853	*clb3*Δ*::kanMX* (BY4741 otherwise)	Res. Genetics
4159	*clb4*Δ*::kanMX* (BY4741 otherwise)	Res. Genetics
5535	*clb5*Δ*::kanMX* (BY4741 otherwise)	Res. Genetics
4739	*clb6*Δ*::kanMX* (BY4741 otherwise)	Res. Genetics
DOM90	*bar1::HisG* (W303a otherwise)	D. Morgan
DOM30	*cdc28::cdc28-as1* (DOM90 otherwise)	D. Morgan

Table 2.2 Plasmids and their relevant characteristics

Plasmid	Relevant characteristic	Source
p205	CEN [*CLN3-2^{D}*] *URA3*	F. Cross
PDLB2226	CEN [*BEM1-12MYC*] *LEU2*	D. Lew
PDLB2226-S72A	CEN [*BEM1-S72A-12MYC*] *LEU2*	This study
PDLB2226-S72D	CEN [*BEM1-S72D-12MYC*] *LEU2*	This study
PTH113	2μ [*CDC24*] *LEU2*	T. Höfken
PTH114	2μ [*CDC42*] *LEU2*	T. Höfken
PDLB2374	2μ [*BEM1-12MYC*] *LEU2*	D. Lew
PDLB2375	2μ [*BEM1-P208L-12MYC*] *LEU2*	D. Lew
PDLB2377	2μ [*BEM1-P355A-12MYC*] *LEU2*	D. Lew
PDLB2378	2μ [*BEM1-R369A-12MYC*] *LEU2*	D. Lew
PDLB2379	2μ [*BEM1-K482A-12MYC*] *LEU2*	D. Lew
pBAD-DCR2	[P_{BAD}-*DCR2-TAG*]	This study
pBAD-CLN3	[P_{BAD}-*CLN3-TAG*]	This study
pBAD-BEM1	[P_{BAD}-*BEM1-TAG*]	This study
pBAD-BEM1-S72A	[P_{BAD}-*BEM1-S72A-TAG*]	This study
pBAD-BEM1-S72D	[P_{BAD}-*BEM1-S72D-TAG*]	This study
pBAD-CDC42	[P_{BAD}-*CDC42-TAG*]	This study
BG1805-DCR2	2μ [P_{GAL1}-*DCR2-TAG*] *URA3*	Open Biosystems
BG1805-CLN3	2μ [P_{GAL1}-*CLN3-TAG*] *URA3*	Open Biosystems
BG1805-BEM1	2μ [P_{GAL1}-*BEM1-TAG*] *URA3*	Open Biosystems
BG1805-BEM1-S72A	2μ [P_{GAL1}-*BEM1-S72A-TAG*] *URA3*	Open Biosystems
BG1805-BEM1-S72D	2μ [P_{GAL1}-*BEM1-S72D-TAG*] *URA3*	Open Biosystems
BG1805-CDC42	2μ [P_{GAL1}-*CDC42-TAG*] *URA3*	Open Biosystems

To generate the *bem1*Δ *cln3*Δ strain (SMY01) we disrupted one *CLN3* copy in diploid *bem1*Δ cells as described previously (Polymenis and Schmidt, 1997). The resulting heterozygote was sporulated, and the segregants were obtained by random spore analysis (Kaiser et al., 1994). All the single cyclin deletions and the *bem1*Δ strain in the BY4741 background were obtained by sporulation of the corresponding homozygous diploid deletion strains distributed from Research Genetics. The phenotypes reported for each strain were obtained after examining several independent transformants or segregants for the strain in question.

The putative phosphorylation site amino acid substitutions were introduced in the *BEM1-12MYC* low copy centromeric plasmid pDLB2226 (Irazoqui et al., 2003). We first PCR-amplified *BEM1* sequences from pDLB2226 using forward primers that encoded the desired mutation (BEM1-S72A-FWD: 5'-CCAAAAAACAGACATAATTCTAAAGATATTACTGCTCCAGAGAAAGTTATAAAAGCCAAATAC-3'; BEM1-S72D-FWD: 5'-CCAAAAAACAGACATAATTCTAAAGATATTACTGATCCAGAGAAAGTTATAAAAGCCAAATAC-3'), and a reverse primer corresponding to sequences up to position +574 of the *BEM1* ORF (BEM1-(+574)-REV: 5'-CGACCAATTGGCTTAGCAATGAACC-3'). The PCR products were purified by agarose gel electrophoresis and used as primers in a second PCR reaction with pDLB2226 as template and a forward primer corresponding to *BEM1* sequences up to position –186 (BEM1-(-186)-FWD: 5'-ATTACCCTAAACGGACAAATG-3'). The PCR product of this reaction was also purified by agarose gel electrophoresis and co-

transformed into yeast cells together with plasmid pDLB2226, which was previously linearized with SmaI and HindIII digestion (cutting at positions -166 to +330 of the *BEM1* ORF, respectively). The gap-repaired plasmid derivatives were then recovered from yeast transformants by standard methods (Kaiser et al., 1994).

To construct plasmids for bacterial expression, we digested the BG1805-based plasmids (purchased from Open Biosystems, CA; see Table 2.2) with AgeI, which cuts once in the *GAL1* promoter all the BG1805 plasmids used here. The digested plasmids were then transformed into a Ura^- yeast strain for gap-repair together with an oligonucleotide that encodes the arabinose P_{BAD} promoter and ribosome binding site (Guzman et al., 1995) (GAL1-PBAD-FWD: 5'-CGGGAACGGATTAGAAGCCGCCGAGCGGGTGACGCTTTTTATCGCAACTCTCTACTGTTTCTCCATACCCGTTTTTTTGGATGGAGTGAATATACCTCTATACTTTAACGTCAAGGAGAA-3'). GAL1-PBAD-FWD at its 5’ end carries sequences complementary to *GAL1* sequences upstream of the AgeI site, and at its 3’ end sequences complementary immediately upstream of the ATG start codon of the ORF in the BG1805 plasmids, which correspond to the bacteriophage λ attR1 site.

The mutant plasmid derivatives were sequenced to verify the introduced mutation and the absence of any other mutations at the Genome Technologies Laboratory of Texas A&M University.

Microscopy and flow cytometry

For microscopic examination of vacuolar membranes the cells were stained with FM4-64, N-(3-triethylammoniumpropyl)-4-(6-(4-diethylamino)phenyl)hexatrienyl)pyridinium dibromide, as described by Wang et al (Wang et al., 1996). Briefly, $3x10^6$ cells were collected from exponentially growing cells at a cell density of $5x10^6$/ml in YPD and re-suspended in 0.25ml of YPD. 1 μl of 20mM FM4-64 (Molecular Probes, Eugene, OR) was added. It was incubated at 30°C in a shaking incubator for about 1-2 cell population doublings. Cells were collected, sonicated and washed with YPD. After re-suspending in about 10 μl of YPD, cells were mounted on a glass slide to observe under the microscope. For the experiments shown in the figure on p.50 with the temperature-sensitive *cdc28-1* strain, the cells were shifted to their non-permissive temperature (37 °C) for 3h, stained with FM4-64 for 1 h at 37 °C, cultured in dye-free medium at 37 °C for 2 h, and then examined microscopically.

Cells and purified vacuoles were stained with the vital vacuolar stain CDCFDA, as described previously (Roberts et al., 1991). CDCFDA was added at 10 μM in the culture media (with 50 mM sodium citrate, pH 5.0) for 20 minutes. The cells were then examined either by fluorescence microscopy or flow cytometry.

For samples analyzed by confocal microscopy, total cellular volume was evaluated by staining the exterior of the cells with Rhodamine Red, according to the manufacturer's instructions (Molecular Probes, OR), while vacuoles were visualized using CDCFDA as we described above. Data for each strain were obtained from at least

3 different microscope fields, and we examined a minimum of 20 planes for each microscope field. The fluorescent area per cell was measured using Adobe Photoshop® software. The sum of the areas corresponding to each cell was then used as an estimate of volume.

Electron microscopic analysis of ultrathin sections and acid phosphatase localization using cerium chloride as a capture agent to visualize the vacuole was carried out at the Texas A&M Microscopy and Imaging Center. Cells were fixed in a 2% acrolein, 0.1M sodium cacodylate solution (pH 7.4) on ice for 30 min. The cells were then washed four times, 15 min each time, in 5% sucrose, 1% DMSO, 0.1M sodium cacodylate solution (pH 7.4). The reaction mixture for acid phosphatase localization was 0.1M sodium acetate (pH 5.0), 5% sucrose, 1mM β-glycerophosphate, 2mM cerium chloride, and 0.01% Triton X-100. The cells were first incubated for 30 min at 30ºC in reaction mixture lacking the substrate (β-glycerophosphate), followed by a 1h incubation in complete reaction medium at 30ºC. The reaction was stopped by two washes in ice-cold solution of 0.1M sodium acetate (pH 5.0), 5% sucrose, followed by two washes in ice-cold 0.1M sodium cacodylate solution (pH 7.4). The cells were then incubated overnight at 4ºC in a solution containing 1% OsO_4, 5% sucrose and 0.1M sodium cacodylate (pH 7.4). The samples were then dehydrated in graded ethanol series, embedded in epoxy resin, sectioned and examined without post-staining.

For flow cytometry for cellular DNA content (the figure on p.61), cells ($1x10^7$ cells/ml) were fixed overnight in an Ethanol-PBS solution (mixed at a 7:3 ratio). They were then re-suspended in 50 mM sodium citrate buffer (pH 7.0). The sample was

treated with RnaseA (0.25 mg/ml) overnight at 37 °C. Finally, the sample was re-suspended in a 50 mM sodium citrate buffer (pH 7.0) containing 1 mM Sytox Green (Molecular Probes, OR), before it was evaluated by flow cytometry. To generate the DNA content histograms (the figure on p.61), the same number of cells (30,000) was collected for any given strain.

Vacuole staining with CDCFDA

Vacuole staining with CDCFDA (5-(and-6)-carboxy-2', 7'-dichlorofluorescein diacetate), Molecular Probes) was performed based on the manufacturer's instruction. Cells were grown in SC medium (Kaiser et al., 1994). In the exponential growth phase at a cell density of $5x10^6$/ml, 10^6 cells were taken and re-suspended in 50mM sodium citrate buffered-SC medium, pH 5.1 μl of 10mM CDCFDA (in DMSO) was added and incubated for about 20 minutes at room temperature. The stained vacuoles were then evaluated with microscopy or flow cytometry.

Vacuole purification

Vacuole purification was performed based on the protocols by Roberts et al. and Conradt et al (Conradt et al., 1992; Roberts et al., 1991) . DKY6281 (*pho8Δ*) and BJ3505 (*pep4Δ, prb1Δ*) cells were grown in YPD medium. $4x10^{10}$ cells were collected from the exponential growth phase and washed with distilled water at room temperature. The cells

were pelleted and re-suspended in 100ml of 1M sorbitol, to which 1ml of Zymolyase solution (50mM Tri-HCl, pH 7.7, 1mM EDTA, 50% glycerol, 20mg (400 units)/ml Zymolyase 20T: ICN Immunobiologicals) was added and incubated with gentle shaking at 30^{o}C for 90 minutes. Spheroplasts were collected by centrifugation at 2,200g for 5 minutes and washed once with 1M sorbitol. The spheroplasts were broken by homogenizing (by pipetting) in 25ml buffer A (10mM 2-(MES)/Tris, pH 6.9, 0.1mM $MgCl_2$, 12% Ficoll 400). The lysate was centrifuged at 2,200g for 10 minutes at 4^{o}C. The supernatant was saved and transferred to Beckman SW 28 rotor and about 13ml of buffer A was overlayed. Then it was subjected to centrifugation at 60,000g for 30 minutes at 4^{o}C. The white wafer floating on top was collected with a spatula and homogenized in 6mL of buffer A. It was transferred to Beckman SW 41 Ti rotor and overlayed with 6ml buffer B (10mM MES/Tris, pH 6.9, 0.5mM $MgCl_2$, 8% Ficoll 400) and centrifuged at 60,000g for 30 minutes at 4^{o}C. Again, the white wafer floating on top was collected and re-suspended in 0.3ml of 2X buffer C (20mM MES/Tris, pH 6.9, 10mM $MgCl_2$, 50mM KCl). After homogenizing by pipetting, an equal volume of 1X buffer C was added. Vacuoles were aliquoted and stored at –80^{o}C until use. Protein quantification was done to measure the concentration of purified vacuoles after solubilizing vacuoles with 2% SDS.

Cytosol preparation for *in vitro* vacuole fusion assay

2 x 10^9 cells grown in SC medium till exponential growth phase were collected and washed with cold 0.25M sorbitol buffer (0.25M sorbitol, 20mM Pipes/KOH, pH 6.8, 150mM potassium acetate, 5mM magnesium acetate). The cells were collected and re-suspended in 200 μl of 0.25M sorbitol buffer with 1mM DTT and 0.5mM PMSF. Cell lysis was performed by bead beating of 10 cycles of 30 seconds vortex and 30 seconds chilling at 4°C. The lysate was clarified by sequential centrifugations at 3,000g for 5 minutes at 4°C and 14,000g for 10 minutes at 4°C. Finally, the supernatant was centrifuged at 150,000g for 30 minutes at 4°C. The cytosol was aliquoted and quick frozen in liquid nitrogen and kept at –80°C until use. Protein quantity was measured as above.

***In vitro* vacuole fusion assay**

The *in vitro* vacuole fusion assay was performed based on the procedure by Mayer et al (Mayer et al., 1996). The vacuole fusion reaction mixture was composed of 0.01mg/ml of purified vacuoles from *pho8*Δ and *pep4*Δ *prb1*Δ cells, 3.2 μl of 10X salt buffer (100mM Pipes/KOH. pH 6.8, 1M sorbitol, 50mM $MgCl_2$, 1M KCl, 0.5M K-acetate), 1.75 μl of 10X ATP-regenerating system (400mM creatine phosphate, 20mg/ml creatine phosphokinase, 10mM MgATP), 1~2mg/ml cytosol and 1X reaction buffer (20mM Pipes/KOH, pH 6.8, 0.3M sorbitol, 100mM KCl, 50mM K-acetate, 5mM $MgCl_2$), filled

to a final overall volume of 33 μl. The reaction mixture was incubated at 27°C for 90 minutes. To measure alkaline phosphatase (ALP) activity, 465 μl of assay reaction solution (250mM Tris/HCl, pH 8.0, 0.4% Triton X-100, 10mM $MgCl_2$, 1mM *p*NPP (ρ-nitro-phospho-phenol)) was added and incubated at 30°C for 5 minutes. ALP enzyme reaction was stopped by addition of 500 μl of termination solution (1M glycine/KOH, pH 11). Absorbance at 400nm was measured. This assay generated reliable results when comparing *in vitro* vacuole fusion activities among fusion reactions prepared from the same batch of reaction mixture. However, large deviations occurred when comparing *in vitro* vacuole fusion activities from different batches of reaction mixtures. Therefore, most relative fusion activities measured in this study were performed by comparing between fusion reactions with adding an inhibitor or buffer to an aliquot from the same batch of reaction mixture. In the experiment for the figure on p.71 to measure fusion activity the reaction mixture was equally split, and to each aliquot the same volume of buffer with inhibitor (or antibody) was added. Buffer-added aliquots were incubated at 27 °C or on ice, the fusion activities of which were measured after 90 min and set as 100% or 0% fusion activity, respectively. Inhibitor-added aliquot was incubated at 27 °C for the same time and its fusion activity was measured to evaluate the relative fusion activity.

For the immuno-depletion experiments, cytosolic extracts were incubated for 1 h at 4 °C with 60 μg of 12CA5 monoclonal anti-HA antibody prepared from ascites fluid, followed by an 1 h incubation at 4 °C with 50 μl of a protein G-Agarose bead solution (Pierce, IL). The beads were then removed and the cytosolic extracts were used in

vacuole fusion reactions as described above. Mock-depleted cytosols were prepared from the same batches of extracts but with the same volume of PBS instead of the anti-HA antibody. The effects of each immunodepleted Cln (Cln2p or Cln3p) on the fusion activity were evaluated by comparing it to its mock-depleted counterpart.

Vacuolar morphology and size

For microscopic examination of vacuolar membranes the cells were stained with N-(3-triethylammoniumpropyl)-4-(6-(4-diethylamino)phenyl)hexatrienyl)pyridinium dibromide, FM4-64 (Molecular Probes, Eugene, OR), and then examined microscopically with a Nikon Eclipse TS100 inverted fluorescence microscope.

Vacuolar size was evaluated by flow cytometry after staining with the vital vacuolar stain 5' (and 6')- carboxy-2',7'-dichlorofluorescein diacetate, CDCFDA (Molecular Probes, Eugene, OR).

Budding index, DNA content, cell size and doubling time measurements

The percentage of budded cells (budding index) was evaluated as described elsewhere (Zettel et al., 2003). DNA content was evaluated by flow cytometry as described previously (Bryan et al., 2004). The mean cell volume of live unfixed samples was measured using a Beckman Coulter® Z2 Channelyzer. The data were analyzed using the manufacturer's AccuComp software. The geometric mean is indicated in each case. For

population doubling (generation) time measurements we used absorbance measurements at 600nm (A) at multiple time points (t) during the exponential growth of the culture. From the slope of the line obtained after plotting ln(A) vs. t, we got the specific growth rate constant of the culture (k). The culture's doubling time (g) was then calculated from the formula $g = \ln 2/k$.

Protein analysis

Unless otherwise indicated, the gels for SDS-PAGE (Laemmli, 1970) contained 8% of a 29:1 acrylamide/bis-acrylamide solution. For the immunoblots shown in the figure on p.55, cytosolic extracts were prepared as described above, while total cellular extracts were prepared as described previously (Kaiser et al., 1994), separated by SDS-PAGE on a 10% acrylamide gel, and transferred onto nitrocellulose. The blots were blocked in PBS containing 5% w/v dry non-fat milk and 0.1% v/v Tween-20. Between incubations the blots were washed three times 10 min each, in PBS. All the antibodies were added in blocking solution. The 12CA5 monoclonal antibody against HA was used at a 1:1,000 dilution. The primary antibodies against yeast Prc1p (CPY), Pho8p (ALP) and Pgk1p were from Molecular Probes (OR), and they were used according to their instructions. Secondary antibody horseradish peroxidase conjugates were from Pierce (NJ) and used at 1:5,000 dilution. The blots were developed with chemiluminescent peroxidase reagent from Sigma, according to their instructions.

Immunoprecipitations and TEV cleavage of TAP-tagged Bem1p were performed according to the protocols and reagents recommended by Rigaut et al (Rigaut et al., 1999). Briefly, $5x10^9$ cells of untagged or TAP-tagged *BEM1* cells from the exponential phase of growth were used. Cell extracts were prepared in the presence of protease and phosphatase inhibitor cocktails (Sigma, St. Louis, MO). After the first immunoprecipitation with IgG-agarose beads, the beads were washed twice with RIPA buffer and once with TEV reaction buffer. 80U of TEV for 30 min at 30 °C was used to cleave the protein A domain. The phosphatase experiment shown in the figure on p.77 was done as described previously (Liakopoulos et al., 2003). For the phosphatase experiments in the figure on p.77, Bem1p-CBP on Calmodulin beads was washed three times with RIPA buffer and once with λ-phosphatase reaction buffer. Then 500U of λ-phosphatase and 10x of protease inhibitor cocktail were added and incubated at 30 °C for 30 min in the presence or absence of 10x phosphatase inhibitor cocktail.

For protein surveillance, cell extracts were prepared using a urea extraction buffer as described by Ubersax et al (Ubersax et al., 2003). The differences in Bem1p's electrophoretic mobility in 1D SDS-PAGE are better resolved if the samples are desalted prior to electrophoresis (using a kit from Pierce (Rockford, IL), according to their instructions), and electrophoresis is performed at a constant voltage of 70V (instead of the typical 200V applied to mini-gels).

2D gel electrophoresis was performed using carrier ampholytes (pH 4-6; GE Healthcare, UK) in acrylamide tubes according to the method of O'Farrell (O'Farrell, 1975). 7 cm long tube gels containing 0.5% ampholytes were focused for approximately

1,000 volt hours without pre-focusing. The tubes were extruded and soaked, sequentially, in SDS sample buffer containing dithiothreitol or iodoacetamide. The tube gels containing the reduced and alkylated proteins were subsequently placed on top of 8% polyacrylamide slab minigels and subjected to SDS PAGE (Laemmli, 1970). Prior to immunostaining, the proteins were electroblotted onto PVDF membranes (Immobilon P^{sq}; Millipore, MA) at 100 – 200 mAmps overnight using 10 mM CAPS, 10% methanol, pH 11.

For immunostaining, protein A fusion proteins were detected with the Peroxidase-Anti-Peroxidase (PAP) soluble complex reagent from Sigma (St. Louis, MO). The anti-Pgk1p antibody was from Molecular Probes (Eugene, OR). The anti-phospho [ST]P, anti-CBP, anti-HA and anti-Myc antibodies were from Abcam (Cambridge, MA). The horseradish peroxidase-conjugated secondary antibodies used for immunoblotting were also from Abcam (Cambridge, MA). All antibodies were used at the dilutions recommended by the manufacturers. The blots were processed with reagents from Pierce (Rockford, IL).

Bacterial expression

The pBAD-based plasmids were transformed into *E. coli* (strain XL1-Blue). For protein expression we followed previously published procedures (Guzman et al., 1995). From 50-100 ml cultures we obtained soluble protein from all the constructs we describe here. The exception was Cln3p, which required larger cultures (0.5l-1l) because the majority

of the recombinant protein appeared to be insoluble. We purified the recombinant proteins through their 6xHis epitope, using TALON Co^{2+} affinity beads (BD Biosciences, CA), according to their instructions.

Kinase assays

Human Cdc2/cyclin B and Cdk2/cyclin A were from New England Biolabs (Beverly, MA), and used at 5U per reaction. Cln3p-associated activity was obtained from yeast cells (strain W303a) carrying plasmid BG1805-CLN3 (see Table 2.2), using TALON Co^{2+} affinity beads (BD Biosciences, CA), according to their instructions. The Cln3p-associated activity was from ~10^{10} cells initially grown in raffinose, but 4h prior to harvesting the culture was induced with 2% galactose. Histone H1 was from Sigma (St. Louis, MO), and used as a substrate at 5 μg per reaction. Bem1p was obtained from bacteria as described above. The reactions also contained 5 μCi [γ-^{32}P] ATP, 100 μM ATP, 50 mM Tris-HCl pH 7.5, 10 mM $MgCl_2$, 1mM EGTA, 2mM DTT and 0.01% Brij 35. All the reactions (30 μl total volume) were performed at room temperature for 20 min.

Immunofluorescence microscopy

Unless otherwise indicated, we followed the protocols of the Botstein lab as described at http://genome-www.stanford.edu/group/botlab/. 4'6-diamidino-2-phenylindole, DAPI,

was from Sigma (St. Louis, MO). The anti-tubulin primary antibody and the secondary FITC-conjugated antibody were from Abcam (Cambridge, MA). For the experiment shown in the figure on p.89, the cells were grown at 37 °C to exacerbate the bud emergence defect of *bem1Δ* cells. The samples were examined with a Nikon Eclipse TS100 inverted fluorescence microscope.

CHAPTER III

THE G1 CYCLIN Cln3p CONTROLS VACUOLAR BIOGENESIS IN *Saccharomyces cerevisiae*[*]

Introduction

Overall organelle morphology and copy number in proliferating cells remain constant, despite successive cell divisions. In yeast, as in animal cells, the enzymes that catalyze cell cycle transitions are complexes of a cyclin-dependent kinase (Cdk) and activating regulatory subunits called cyclins. In *Saccharomyces cerevisiae*, START is thought to represent a nodal point in late G1, where various aspects of the cell's physiology are measured or monitored prior to initiation of DNA replication (Pringle and Hartwell, 1981). START is brought about by the activity of Cdc28p (a Cdk) in association with one of the G1 cyclins, Cln1,2,3p (Wittenberg and Reed, 1996). Cells lacking all three *CLN* genes are inviable and cannot complete START (Richardson et al., 1989). During vegetative growth the only essential "collective" function of Clns is to promote the phosphorylation and subsequent proteolysis of the B-type cyclin kinase inhibitor Sic1p (Schneider et al., 1996; Tyers, 1996).

None of the *CLN* genes alone, however, is necessary for the cell's survival. This

---

[*]Reprinted with permission from "The G1 cyclin Cln3p controls vacuolar biogenesis in *Saccharomyces cerevisiae*" by Han, B.-K., Aramayo, R., and Polymenis, M., 2003, Genetics *165*, 467-476. Copyright 2003 by the Genetics Society of America.

apparent redundancy has been challenged in the last few years, with Cln1,2p and Cln3p being functionally distinct. It is now thought that Cln3p functions upstream of Cln1,2p activating the G1/S transcription program (Dirick et al., 1995; Levine et al., 1996; Stuart and Wittenberg, 1995; Tyers et al., 1993), where >100 genes (*CLN1,2* among them) are transcribed in a temporal manner at the G1/S transition (Spellman et al., 1998). Cln1,2p/Cdc28p complexes may regulate polarized growth during budding (Benton et al., 1993; Cvrckova and Nasmyth, 1993). They may also serve as upstream activators of the protein kinase C (Pkc1p), which is involved in cell wall biosynthesis (Heinisch et al., 1999). Thus, it seems that Cln3p controls the correct timing of G1/S transcription, while Cln1,2p tethers G1/S progression with the morphogenetic and biosynthetic aspects of making a bud.

The vacuole in *Saccharomyces cerevisiae* is a large compartment, occupying a significant fraction (~25%) of the total cellular volume (Wiemken and Durr, 1974). Vacuoles serve as repositories of metabolites and low molecular weight compounds and they are analogous to the lysosomes of animal cells, containing numerous hydrolases (Jones et al., 1997; Roberts et al., 1991). In all eukaryotic cells, the lysosomes or vacuoles play major cellular turnover roles, including autophagy where entire organelles are delivered to them for turnover (Klionsky and Emr, 2000). These lysosomal or vacuolar functions are evident during responses to stress or nutrient limitation, and also impact on developmental processes and human disease states (Klionsky and Emr, 2000). Vacuoles, as many other organelles (*e.g.* the Golgi), are not usually synthesized *de novo* in daughter cells, but instead they are inherited from mother cells. It is possible,

however, for a daughter cell to slowly synthesize a new vacuole (the same is true for the Golgi) if it did not inherit one (Catlett and Weisman, 2000). Since this is a slow and inefficient process, a vacuolar inheritance mechanism is believed to have evolved. Vacuolar morphology and inheritance is dynamic and is somehow coordinated with cell cycle progression (Catlett and Weisman, 2000). Yeast cells typically contain only one to three vacuoles, and their segregation to daughter cells follows an ordered pattern (Warren and Wickner, 1996). Beginning at the G1/S transition of the cell cycle, vesicles from the vacuole of the mother cell form a tubular structure and are transported into the newly formed bud, where they will eventually establish the vacuolar compartment of the daughter cell (Bryant and Stevens, 1998; Catlett and Weisman, 2000). However, it is not known whether the molecular machinery that regulates cell cycle progression also affects vacuolar inheritance and *vice versa*.

Here we show that the G1 cyclin Cln3p regulates vacuolar biogenesis and segregation. Our findings suggest an unexpected role for a G1 cyclin that is specific to Cln3p and it is not shared by other G1 cyclins.

Results

Vacuolar morphology in cln3Δ cells

To examine vacuolar morphology we first visualized the vacuoles with the vital amphiphilic styryl dye FM4-64 (see Materials and Methods), which stains the vacuolar membrane (Hill et al., 1996). The vacuolar compartment in about 60-70% of *cln3*Δ cells

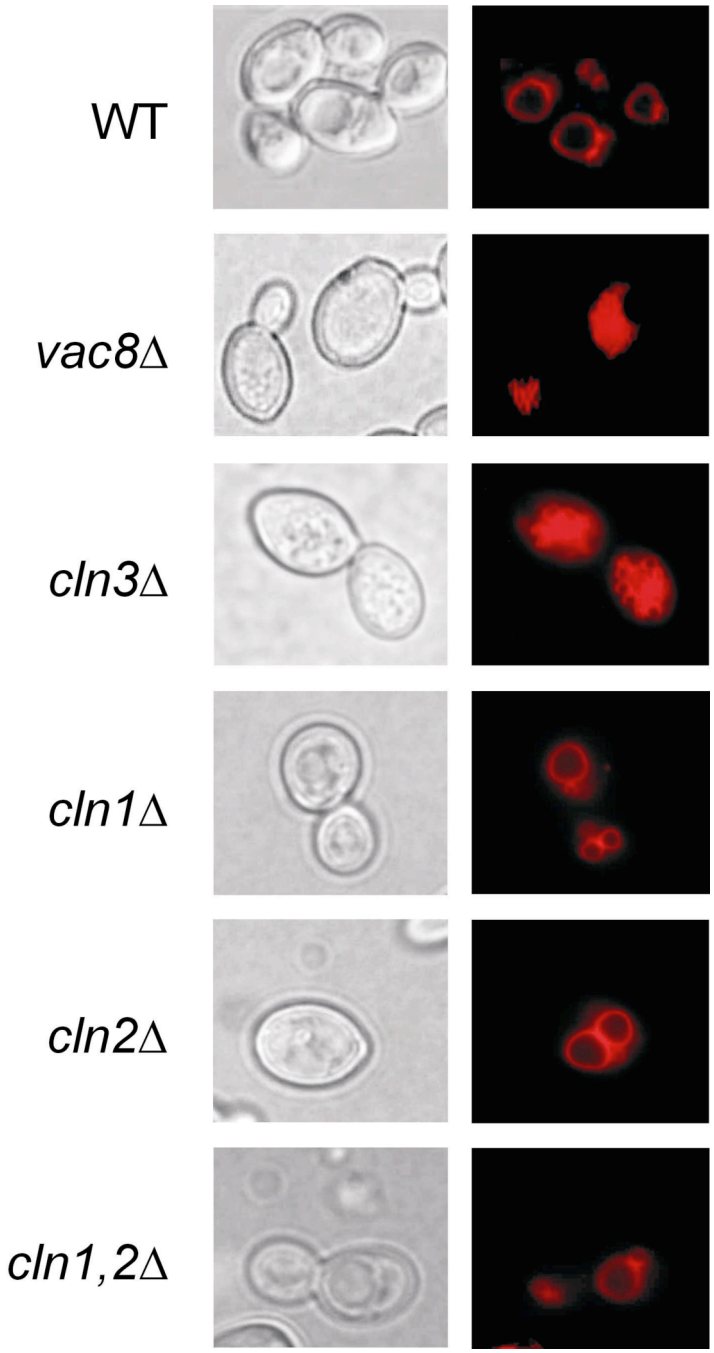

FIGURE 3.1. Vacuolar fragmentation in cells lacking *CLN3*. Diploid cells of the indicated genotype (all in the BY4743 background) were exposed to FM4-64, a vital dye that stains the vacuolar membrane (see Materials and Methods), and photographed through phase optics (left panels) and by fluorescence microscopy with a rhodamine filter (right panels).

had a fragmented and multilobular appearance (Fig. 3.1). This was not the case, however, for cells lacking Cln1p and Cln2p (Fig. 3.1). The extent of vacuolar fragmentation was comparable to that of *vac8*Δ cells(Fig. 3.1), which are defective in vacuolar inheritance (Catlett and Weisman, 2000), and they display extensive vacuolar fragmentation (Wang et al., 2001). We also examined cells carrying the *CLN3-2* allele, which effectively over-express Cln3p because they produce a truncated but stable form of the protein (Cross, 1988), but the vacuolar morphology of these cells was indistinguishable from wild-type cells (data not shown). Next, we evaluated wild-type and *cln3*Δ cells by electron microscopy (Fig. 3.2). Consistent with the fluorescence data, cells lacking Cln3p had more but smaller vacuoles (Fig. 3.2). We also observed extensive vacuolar fragmentation of *cdc28-1* cells shifted to their non-permissive temperature (Fig. 3.3). This is consistent with the known role of Cln3p, as a regulatory subunit in a complex with Cdc28p important for the G1/S transition. These observations suggest that Cln3p, but not Cln1,2p, may be necessary for the maintenance of vacuolar morphology.

The vacuolar compartment in *cln3*Δ cells occupied a significant portion of the cell (Figs. 3.1 and 3.2), and we decided to address this issue in more detail. We examined living cells carrying a wild-type (*CLN3*$^{+}$), null (*cln3*Δ), or a dominant (*CLN3-2*) *CLN3* allele. The cells were stained with a vacuolar fluorescent probe, 5-carboxy-2',7'-dichlorofluorescein diacetate (CDCFDA). CDCFDA is localized in the vacuole by diffusion, where it is hydrolyzed into an impermeant fluorescent anionic derivative (Preston et al., 1989). The cells were then examined either by fluorescence microscopy

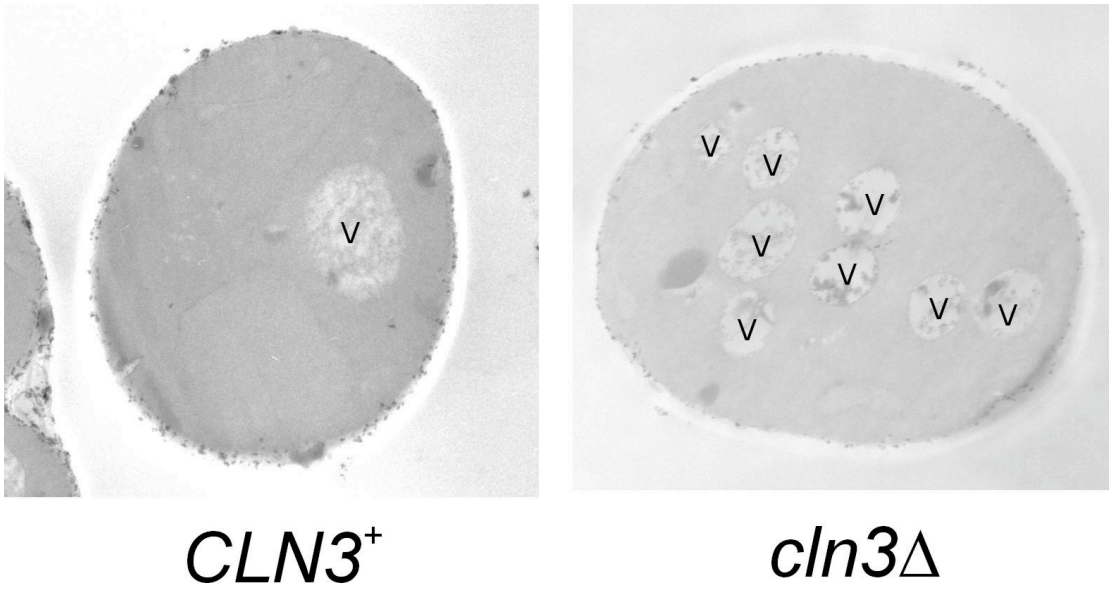

FIGURE 3.2. Electron micrographs of wild-type and *cln3*Δ cells. V indicates the vacuole**.**

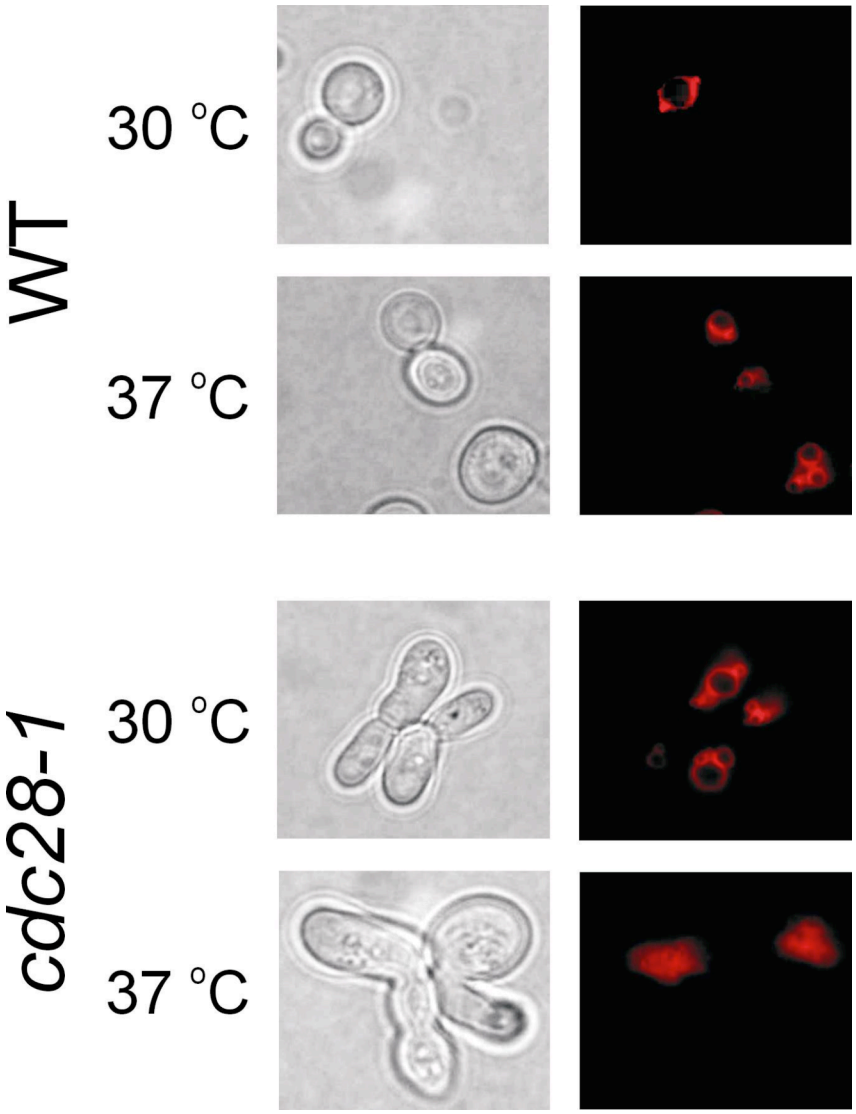

FIGURE 3.3. Vacuolar fragmentation in *cdc28-1* cells. Wild-type and *cdc28-1* cells (in the A364A background, see Materials and Methods) were exposed to FM4-64 and photographed through phase optics (left panels) and by fluorescence microscopy with a rhodamine filter (right panels). The cells were photographed both during growth at room temperature and after they were shifted for 6 h to 37 ºC, the non-permissive temperature of the *cdc28-1* strain (see Materials and Methods).

(Fig. 3.4A) or flow cytometry (Fig. 3.4B). CDCFDA-fluorescence intensity, representing vacuolar size, of live cells was quantified by flow cytometry (Fig. 3.4B) from the same samples that were used to obtain the forward angle scattering cell size estimates, to simultaneously obtain both parameters. Note that this analysis confirmed the expected small vacuolar compartment of *pep3*Δ cells (Table 3.1), which are known to have small vacuolar vesicles (Preston et al., 1991). In Table 3.1, we summarize the values of cell size and vacuolar size in *CLN3*$^{+}$, *cln3*Δ and *CLN3-2* cells in the BY4741 background. Importantly, we noticed disparities in vacuolar size that did not correlate with cell size differences. For example, *cln3*Δ cells are 30% larger overall than *CLN3*$^{+}$ cells, but their vacuole is 80% larger. This disproportional enlargement of the vacuolar compartment in *cln3*Δ cells was evident ($P<0.05$, based on a Student's *t* test) in all strains tested, irrespective of ploidy, haploid BY4741 vs. diploid BY4743, and genetic background, strains BY4741 vs. W303, (data not shown). Note that the above differences in vacuolar volume were not due to intra-vacuolar pH differences which may alter the fluorescence of the vacuolar probe we used, for two reasons: First, both *cln3*Δ and *CLN3-2* cells had a vacuolar pH in the same range as wild-type cells (≥ 5.98 and ≤ 6.14; data not shown). Second, the vacuolar size differences were evident even after the intra-vacuolar pH was equilibrated to that of external buffers (data not shown).

We also estimated cell size and vacuolar size using confocal microscopy. For *CLN3*$^{+}$, *cln3*Δ, and *CLN3-2* haploid cells in the BY4741 strain background, cultured in defined SC media, the relative cell volume values were 1±0.24 (n=20), 1.35±0.35

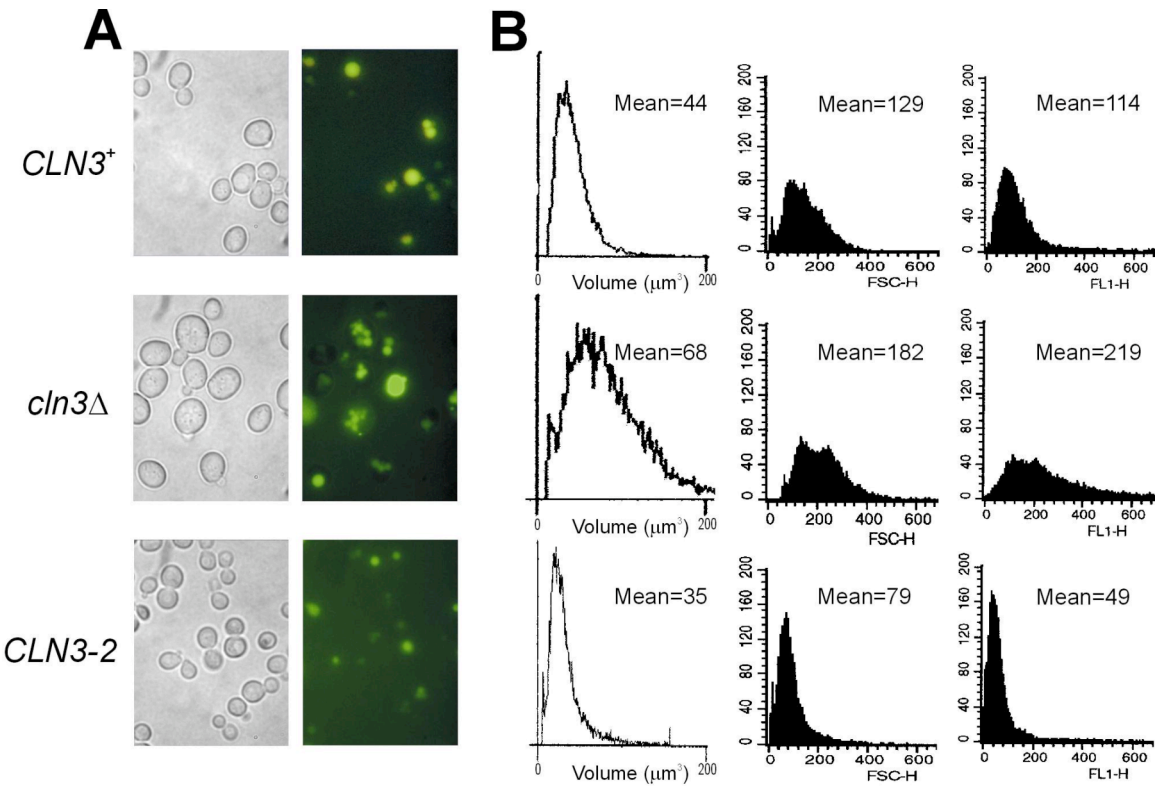

FIGURE 3.4. Cell and vacuole size in cells carrying different *CLN3* alleles. All the strains shown were in the haploid BY4741 background. *A*, Cells were photographed through phase optics (left panels) and by fluorescein fluorescence (right panels) to visualize the vacuole of exponentially growing cells in rich defined SC media (see Materials and methods). *B*, Cell volume of the indicated strains was measured using a Channelyzer (left panels), or flow cytometry by forward angle scattering (FSC, middle panels). Vacuolar fluorescence was measured by flow cytometry (right panels). In every panel, the measured parameter is shown on the x-axis, and the number of cells on the y-axis. The geometric mean is shown in each case.

TABLE 3.I. Loss of Cln3p disproportionately enlarges the vacuole

Strain	Relative cell size[a]		Relative
	Channelyzer	FSC	vacuolar size
CLN3^{+}	1±0.06 (4)	1±0.05 (5)	1±0.09 (5)
*Cln3*Δ	1.35±0.17 (4)	1.53±0.06 (5)	1.92±0.19 (5)
CLN3-2	0.68±0.05 (4)	0.63±0.02 (7)	0.51±0.06 (7)
*Cln2*Δ	1.07±0.02 (6)	2.13±0.04 (4)	0.96±0.17 (4)
*Cln1,2*Δ	1.59±0.16 (6)	1.42±0.06 (3)	0.80±0.06 (3)
*Pep3*Δ	0.84±0.06(20)	0.92±0.03 (3)	0.45±0.04 (3)

[a]Means and standard deviations of standardized values are shown. The number in parentheses indicates independent cultures analyzed in each case. For cell and vacuolar size the geometric mean is used. For the *CLN3-2* plasmid-transformed strain the cultures examined were from independent transformants and compared to the parental strain transformed with an empty low-copy centromeric plasmid. The cellular parameters of the parental strain transformed with the empty low-copy vector were similar to those of the un-transformed strains (not shown). All the strains were grown in synthetic SC media.

(n=23), and 0.71±0.19 (n=20), respectively. In contrast, the vacuolar size of *CLN3*$^{+}$, *cln3*Δ, and *CLN3-2* cells, relative to the overall cell size of wild-type cells was 0.25±0.13 (n=40), 0.55±0.17 (n=50), and 0.14±0.07 (n=22), respectively. Our results are in very good agreement with earlier estimates of vacuolar size (25% of total cellular volume)(Wiemken and Durr, 1974), and our own data regarding the relative vacuolarand cell size parameters in *cln3*Δ cells we reported above (Table 3.1).

However, the vacuolar size in cells that lack another G1 cyclin, Cln2p, was not significantly affected (Table 3.1). Even in cells that lacked both *CLN1* and *CLN2* and were quite large overall, the vacuole was not disproportionately enlarged. Instead, we noticed a decrease in vacuolar size in *cln1,2*Δ cells (Table 3.1). Thus, based on our results with the *cln1,2*Δ strain, we conclude that a decrease in vacuolar size is not necessarily accompanied by overall cell size decrease. Specifically in the case of *cln3*Δ cells, however, loss of Cln3p clearly increases the size of the vacuolar compartment to a greater extent than what was predicted from cell size differences.

Cells that lack Cln3p are defective in vacuole homotypic fusion

Given the fragmented vacuolar morphology of *cln3*Δ cells, we then decided to test Cln3p's effects in an *in vitro* vacuole homotypic fusion assay developed by Wickner and colleagues (Wickner and Haas, 2000). The process of vacuole vesicle fusion is crucial in determining the overall vacuole copy number and vacuolar biogenesis in general (Wickner and Haas, 2000). Vacuoles were purified and then mixed in the presence of cytosol and ATP. To evaluate vacuole fusion microscopically (Fig. 3.5A), the fused

FIGURE 3.5. Cln3p regulates vacuole homotypic fusion *in vitro*. *A* and *B*, Purified vacuoles were allowed to fuse in the presence of ATP and cytosol and stained with CDCFDA, before they were photographed. *A*, vacuole fusion in the presence of cytosol prepared from the indicated strains, all in the BY4743 background. To visualize the vacuoles in the absence of ATP and cytosol (lower right panel), we exposed for 30 sec, because shorter exposures were insufficient. In contrast, fused vacuoles, in the presence of ATP and cytosol, fluoresce much more intensely, so for wild-type cytosol (upper left panel) we exposed for 6 sec, while for *CLN3-2* cytosol (lower-left panel) the fluorescence was so intense that the exposure was only 4 sec. For *cln3*Δ cytosol (upper right panel), or for the no cytosol control (middle right panel), we exposed for 10 sec. Aliquots of the vacuole fusion reactions shown were evaluated colorimetrically, based on the reconstitution of alkaline phosphatase activity. The average and standard deviations from at least seven independent experiments of relative alkaline phosphatase activity, normalized for background (no cytosol), obtained from the indicated reactions is shown. *B*, vacuole fusion in the presence of cytosol from untagged, *CLN2-HA*, or *CLN3-HA* tagged strains. All the cytosols were immuno-depleted using an anti-HA monoclonal antibody (see Materials and Methods) before they were used in the vacuole fusion reactions. The precipitated (P) and the supernatant (S) fractions were evaluated by immunobloting using the anti-HA antibody, to measure the extent of cyclin depletion. (*) indicates non-specific bands. Fusion was evaluated microscopically, and the exposure time was the same (10 sec) for all the photographs shown. Aliquots of the vacuole fusion reactions shown were also evaluated colorimetrically, based on the reconstitution of alkaline phosphatase activity. The average and standard deviation from three independent experiments of relative alkaline phosphatase activity, normalized for background (no cytosol), obtained from the indicated reactions is shown. *C*, The intracellular steady-state levels of Pgk1p and the pro- and mature (m) forms of CPY and ALP in cells of the indicated genotype were evaluated by immunobloting. The *pep4*Δ*, prb1*Δ strain was BJ3505 (see Methods), while all the others were in the BY4743 background. *D*, Homotypic fusion reactions using cytosol from $CLN3^{+}$ and *cln3*Δ cells (in the BY4743 background) transformed with an empty (vector) or *CLN2*-containing (*CLN2*) high copy plasmid, were evaluated colorimetrically as described above. The average and standard deviations from four independent experiments of relative alkaline phosphatase activity, normalized for background (no cytosol), obtained from the indicated reactions is shown.

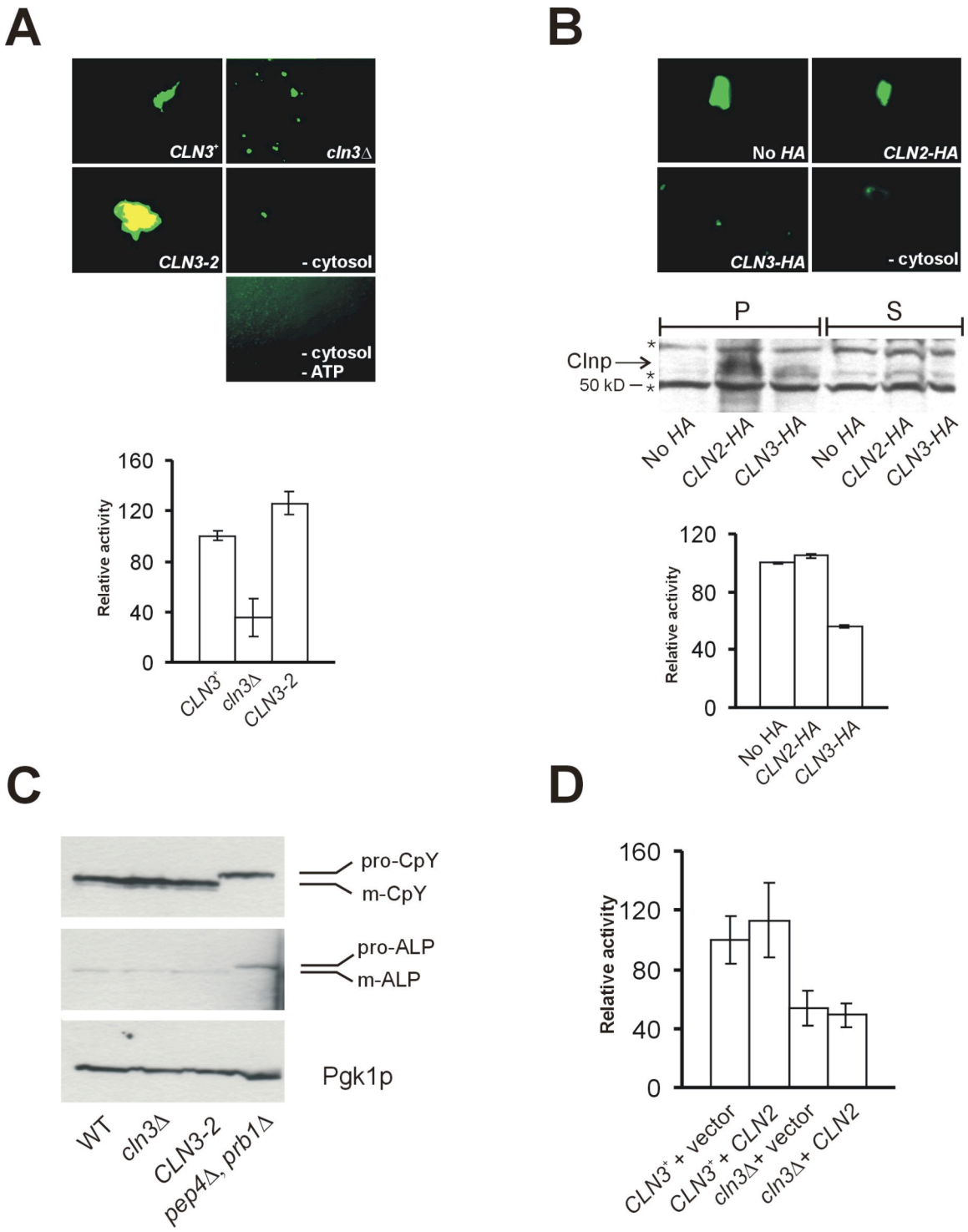
A
CLN3+
cln3Δ
CLN3-2
- cytosol
- cytosol
- ATP
Relative activity
160
120
80
40
0
CLN3+
cln3Δ
CLN3-2
B
No HA
CLN2-HA
CLN3-HA
- cytosol
P
S
Clnp
50 kD
No HA
CLN2-HA
CLN3-HA
No HA
CLN2-HA
CLN3-HA
Relative activity
120
80
40
0
No HA
CLN2-HA
CLN3-HA
C
pro-CpY
m-CpY
pro-ALP
m-ALP
Pgk1p
WT
cln3Δ
CLN3-2
pep4Δ, prb1Δ
D
Relative activity
160
120
80
40
0
CLN3+ + vector
CLN3+ + CLN2
cln3Δ+ vector
cln3Δ+ CLN2

vacuoles were stained with CDCFDA. Cytosol from cells lacking Cln3p had significantly reduced fusion activity (Fig. 3.5A). The extent of vacuole fusion can also vacuoles were stained with CDCFDA. Cytosol from cells lacking Cln3p had significantly reduced fusion activity (Fig. 3.5A). The extent of vacuole fusion can also be evaluated colorimetrically, because the purified vacuoles in this assay were prepared from two different strains, each lacking the ability to produce active alkaline phosphatase (encoded by *PHO8*). One of the strains lacks *PHO8*, while the other lacks vacuolar proteases necessary for Pho8p maturation. In this assay, processed vacuolar alkaline phosphatase can be produced only if the vacuolar constituents from the two strains mix after fusion (Wickner and Haas, 2000). Although the enzymatic assay was not as sensitive as the direct microscopic observation, it was still clear that alkaline phosphatase activity, which reflects vacuole fusion, was lower ($P<0.05$, based on a Student's *t*-test) in the presence of cytosol from *cln3*Δ cells (Fig. 3.5A).

To more directly test the role of Cln3p in vacuolar homotypic fusion, we prepared cytosol from wild-type cells, and from cells carrying epitope-tagged versions of Cln2p (*CLN2-HA*) and Cln3p (*CLN3-HA*). These epitope-tagged Cln2p and Cln3p are fully functional (Tyers et al., 1993; Tyers et al., 1992). Cytosol from the untagged and tagged strain was incubated with either an antibody against the epitope for immunodepletion, or mock-depleted with PBS, and we then carried out immunoprecipitations, to deplete the HA epitope-carrying polypeptides from the cytosolic extracts. The extent of immunodepletion was significant (>90%), as shown on the immunoblot below the micrographs on Fig. 3.5B. The immuno-depleted or mock-

depleted cytosolic extracts were then evaluated for vacuole homotypic fusion activity (Fig. 3.5B). It is clear that depletion of Cln3p, but not Cln2p, reduced homotypic fusion activity (Fig. 3.5B). These results further strengthen the notion that Cln3p is required for homotypic fusion activity.

To test whether *CLN3* deletion or over-expression might somehow affect secretory pathways of vacuolar protein sorting (Jones et al., 1997), we evaluated the maturation of two vacuolar enzymes, carboxypeptidase Y (CPY) and vacuolar membrane alkaline phosphatase (ALP), in *CLN3*$^{+}$, *cln3*Δ and *CLN3-2* cells (all in the BY4743 background). The CPY precursor, Prc1p, traffics through the ER, Golgi, and pre-vacuolar compartments before it is sorted to the vacuole (Jones et al., 1997). ALP bypasses the pre-vacuolar compartment. We found that steady-state levels of mature CPY and ALP was similar among wild-type, *cln3*Δ and *CLN3-2* cells (Fig. 3.5C). Thus, it does not appear that the secretory processes that are involved in CPY and ALP maturation are grossly affected in *CLN3-2* or *cln3*Δ cells.

Finally, increasing the dosage of another G1 cyclin, *CLN2*, could not suppress the defect in homotypic fusion observed in *cln3*Δ cells (Fig. 3.5D). We also examined vacuolar morphology of these cells after staining with the vacuolar membrane stain FM4-64, and we found that the vacuolar fragmentation of *cln3*Δ cells we described above (Fig. 3.1), was not rescued by introducing *CLN2* on a high-copy plasmid (data not shown).

Cln3p and vacuolar segregation

After examining photographs of budded *cln3*Δ cells we noticed that in several cases the signal associated with the vacuolar compartment was not equally distributed between the bud and the mother cell (Fig. 3.6A). This is different from wild-type cells, which distribute their vacuoles between the mother and the bud. In the known vacuolar inheritance mutants the bud fails to receive vacuoles, as was evident in *vac8*Δ cells (Fig. 3.6A). Note that the vacuoles stained by FM4-64 do not represent all the vacuoles in the cell, because between the time of staining and the time of observation, new vacuoles are synthesized in the cell, which are not stained (see Materials and Methods). We were particularly surprised to find that there was also a fraction of *cln3*Δ cells that distributed their vacuoles almost exclusively in the bud and not in the mother (Fig. 3.6A and B). This has not been observed in known *vac* mutants.

VAC8 and CLN3

We next examined vacuolar morphology and cell cycle progression of cells mutant for *VAC8* and *CLN3* (Fig. 3.7). Combined loss of *CLN3* and *VAC8* does not lead to an apparent additive effect and the cells still have visible but fragmented vacuoles. In addition, over-expression of *CLN3* in *vac8*Δ cells, and vice versa, does not suppress the vacuolar fragmentation defects of the singly mutant strains either (Fig. 3.7). Thus, it does not appear that *CLN3* and *VAC8* function in a simple linear pathway.

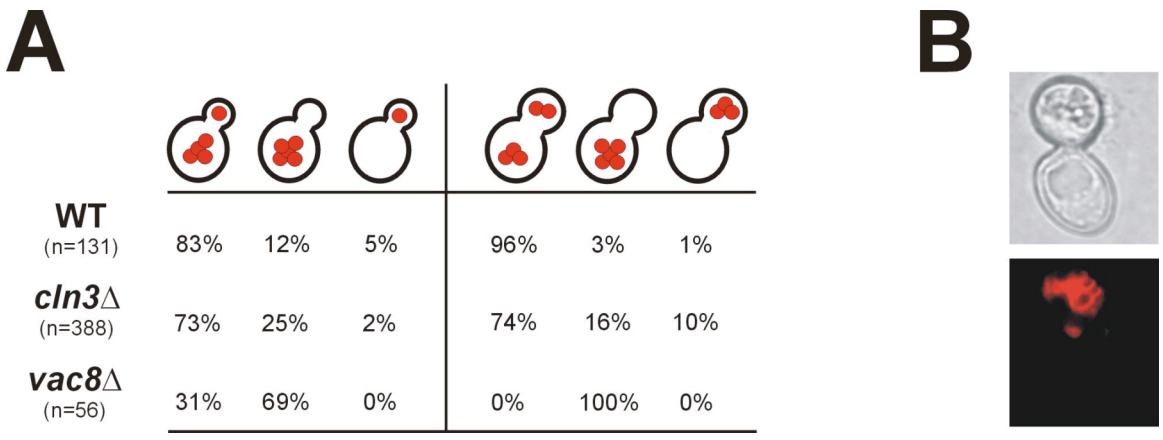

FIGURE 3.6. Cells lacking *CLN3* are defective in vacuolar segregation. Cells of the indicated genotype (all in the BY4743 background) were stained with FM4-64 to visualize vacuole membranes. *A*, Random fields of cells were examined for vacuolar segregation, 2 h after vacuolar staining with FM4-64 (see Materials and Methods). The number of cells examined is shown in parentheses. The scored cells were grouped into two groups based on bud size, and within each group the percentage of cells with the indicated vacuolar morphology is shown. *B*, Unequal vacuolar segregation in homozygous diploid *cln3*Δ cells, stained and photographed as described in the legend of Fig. 3.1.

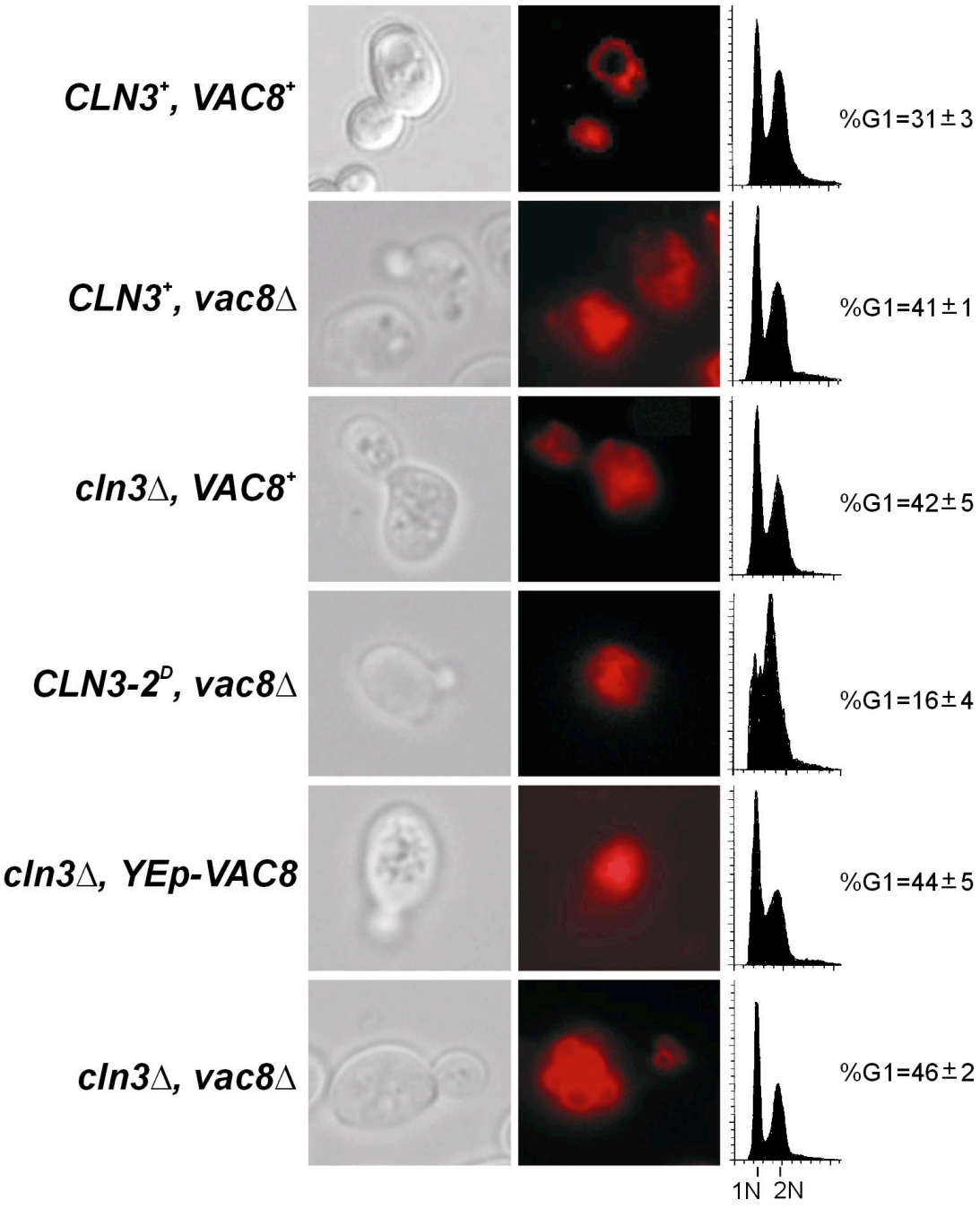

FIGURE 3.7. *CLN3* and *VAC8* in vacuolar biogenesis and cell cycle progression. Cells of the indicated genotype (all in the BY4741 background) were exposed to FM4-64 and photographed through phase optics (left panels) and by fluorescence microscopy with a rhodamine filter (middle panels). Their cellular DNA content (right panels) was determined by FACS. For each strain, the percentage of cells in G1, calculated by the ModFit software, is indicated. Cell numbers are plotted on the y-axis and the x-axis represents fluorescence.

We also examined cell cycle progression of these strains by flow cytometry (Fig. 3.7, right panels). Note that *vac8*Δ cells proliferated at the same rate as wild-type or *cln3Δ* cells (data not shown). Interestingly, in *vac8*Δ cells there was an increase in the percent of cells in the G1 phase of the cell cycle. Thus, as is the case for *cln3*Δ cells (Cross, 1988; Nash et al., 1988), it appears that *vac8*Δ cells stay longer in G1 but there is a compensatory shortening of subsequent cell cycle phases, resulting in no net change in doubling time. Over-expression of Vac8p had no effect on cell cycle progression (data not shown). Importantly, however, Cln3p over-expression in *vac8*Δ cells accelerated completion of START, without suppressing the vacuolar fragmentation of these cells (Fig. 3.7), suggesting that, at least in this case, vacuolar fragmentation is not necessarily linked to the timing of START. Taken together, our results indicate that Cln3p's role in vacuolar biogenesis is distinct from that of Vac8p and also separate from Cln3p's established function in G1/S progression.

Discussion

Besides the chromosomes in the nucleus, the size and copy number of all organelles must also be maintained during cell proliferation. This work documents a novel role for a eukaryotic G1 cyclin in vacuolar (lysosomal) homeostasis, suggesting that the same cell cycle machinery that initiates cell division may also perform a separate function in the control of vacuolar biogenesis and segregation.

There are usually 1-3 vacuoles per cell (Warren and Wickner, 1996). In *cln3*Δ (but not *cln1*Δ and/or *cln2*Δ) cells, the vacuolar compartment was fragmented (Fig. 3.1 and 3.2). Interestingly, the overall vacuolar compartment of *cln3*Δ cells was disproportionately enlarged (Fig. 3.4). Even though vacuole size does not always dictate overall cell size (for example, *cln3*Δ and *cln1,2*Δ cells are both large but the size of their vacuolar compartment differs by 3-4 fold, see Table 3.1), this result underscores the complexity of cell size regulation. Organelle contribution to overall cell size is not usually taken into consideration in studies of cell size control. How could Cln3p regulate vacuolar biogenesis? We provide evidence that Cln3p controls vacuolar homotypic fusion activity *in vitro* (Fig. 3.5). These findings raise the issue of Cln3p's sub-cellular localization. Cln3p is certainly found in the nucleus (Miller and Cross, 2000), but a more recent report clearly showed that Cln3p is also found in the cytoplasm (Gari et al., 2001). Note also that cytosolic extracts immuno-depleted for Cln3p could not support homotypic fusion (Fig. 3.5), arguing for a post-translational mechanism of regulation of homotypic fusion by Cln3p. Whether Cln3p needs to exit the nucleus or simply acts on a nuclear factor which then exits the nucleus is unclear at present, since our cytosolic preparations are not devoid of soluble nuclear proteins. Since forcing Cln3p in the cytoplasm leads to cell size enlargement (Edgington and Futcher, 2001), and since we show here (Fig. 3.4) that the large size of *cln3*Δ cells is largely due to vacuolar enlargement, it is perhaps likely that Cln3p still functions in the nucleus where it perhaps modifies a factor that in turn exits into the cytoplasm and affects vacuolar biogenesis. In

any case, it is clear that Cln3p's function in vacuolar biogenesis is separate from its established role in activating the G1/S transcriptional program.

Self (homotypic) fusion of organelle vesicles is essential for organelle homeostasis (Wickner and Haas, 2000). In animal cells, inhibition of Golgi homotypic fusion in mitosis results in extensive fragmentation of the Golgi. This is important for Golgi inheritance because the resulting Golgi vesicles stochastically disperse in equal numbers in both daughter cells where, after completion of mitosis, they will fuse to re-generate the Golgi (Warren and Wickner, 1996). Warren and colleagues have shown that mitotic inhibition of Golgi homotypic fusion is mediated by the cyclin-dependent kinase Cdc2 (Lowe et al., 1998; Nelson, 2000). Is it possible that aspects of this established paradigm also operate in Cln3p's role during vacuolar biogenesis? Perhaps. Note that while the Cln3p/Cdc28p complex may be necessary for high vacuolar homotypic fusion activity, the mammalian Cdc2/cyclinB complex does the opposite, because it inhibits Golgi vesicle fusion. Overall, however, we think it is intriguing that, although in each case different organelles are affected at different cell cycle points, in both cases organelle homotypic fusion may be sensitive to changes in the activity of cyclin/Cdk complexes.

Loss of Cln3p not only affects vacuolar morphology, but it also impacts on vacuolar segregation (Fig. 3.6). To our knowledge, this is the first evidence linking a cell cycle regulator with vacuolar segregation. Overall, how do the vacuolar phenotypes of *cln3*Δ cells compare to those of other vacuolar mutants? We think that although *cln3*Δ cells share some characteristics with other vacuolar mutants, the combination of these

characteristics makes them unique. For example, vacuolar enlargement and a concomitant overall cell enlargement are evident in *fab1* mutants (Gary et al., 1998; Jorgensen et al., 2002). But, in contrast to *cln3*Δ cells, the vacuole of *fab1* cells is not fragmented, *fab1* cells lose vacuolar acidity, and vacuolar protein sorting is impaired as well (Gary et al., 1998). During the course of this work, the fragmented vacuole of *cln3*Δ cells was also mentioned in a genome-wide study of vacuolar morphology (Seeley et al., 2002). The fragmented vacuolar morphology of *cln3*Δ cells corresponds to class B vacuolar protein sorting (*vps*) mutants, and is apparently similar to *vac8*Δ cells (Seeley et al., 2002). Furthermore, both Vac8p (Wang et al., 2001) and Cln3p (Fig. 3.5) appear to be required in vacuole fusion. However, based on our results, we think there are important differences between *vac8*Δ and *cln3*Δ cells. For example, note that in *vac8*Δ cells vacuolar fragmentation is not accompanied by overall vacuolar and cellular enlargement (see Figs. 3.1 and 3.6). Furthermore, our analysis of double *CLN3* and *VAC8* mutants argues against a simple linear relationship of the two gene products in vacuolar biogenesis (Fig. 3.7). In known *vac* mutants (including *vac8*Δ cells), it is the daughter cells that do not receive enough vacuoles (Catlett and Weisman, 2000). However, in *cln3*Δ cells it appears that at least in some cases the opposite is true (Fig. 3.6). Although known *vac* mutants are not defective in vacuolar retention, retention in the mother cell can play an important role during organelle partition, and it is an established aspect of mitochondria segregation in yeast (Yang et al., 1999). Finally, loss of Vac8p apparently delays the G1/S transition (Fig. 3.7), but it is not clear at this point whether vacuolar biogenesis can causally alter cell cycle progression. Note that vacuolar

fragmentation *per se* in *vac8*Δ cells is not blocking acceleration of START in the context of the dominant *CLN3-2* allele (Fig. 3.7).

Based on the results we report here, it appears that the seemingly separate events of the nuclear cell division cycle and the cytoplasmic processes that control organelle segregation might be controlled by separate functions of the same machinery. Our finding that Cln3p is involved in vacuolar biogenesis at least provides a handle towards a more detailed understanding of these phenomena in yeast. Since regulatory mechanisms of cell division and organelle biogenesis are highly conserved between yeast and humans, findings from yeast studies should be relevant to these processes in other organisms.

CHAPTER IV

Bem1p, A SCAFFOLD SIGNALING PROTEIN, MEDIATES CYCLIN-DEPENDENT CONTROL OF VACUOLAR HOMEOSTASIS IN *Saccharomyces cerevisiae*

Introduction

Overall cell size and macromolecular composition remain unaffected after successive rounds of cell division. This phenomenon also extends to intracellular membrane-bound organelles, because the copy number and size of any given organelle compartment remain constant in dividing cells (Shorter and Warren, 2002; Warren and Wickner, 1996). Implicit in this central aspect of cellular physiology is a tight coordination between cell division and organelle biogenesis, but in most cases the mechanisms remain mysterious (Shorter and Warren, 2002; Warren and Wickner, 1996).

Vacuoles in *Saccharomyces cerevisiae* serve as repositories of metabolites and low molecular weight compounds and are analogous to the lysosomes of animal cells, containing numerous hydrolases (Jones et al., 1997; Roberts et al., 1991). The vacuole is a low-copy organelle, and yeast cells typically contain 1-3 vacuoles. The large size of the vacuolar compartment {~25% of the total cellular volume (Wiemken and Durr, 1974)} and the availability of vacuole-specific vital fluorescent dyes facilitate observations of overall vacuolar morphology. Defects in self (homotypic) fusion of vacuolar vesicles lead to vacuolar fragmentation (Seeley et al., 2002). Thus, homotypic fusion is very important for vacuolar homeostasis and it can also be evaluated *in vitro*

(Wickner and Haas, 2000). Although daughter cells of certain vacuolar inheritance mutants can be born without a vacuole, they must form a new one before they can pass through a point in late G1 called START and initiate DNA replication and a new round of cell division (Weisman, 2003). A recent report also suggested that in *Candida albicans* the vacuolar compartment may impact on cell cycle progression and hyphal development (Barelle et al., 2003). Nonetheless, it is not known how the molecular machinery that regulates cell cycle progression also affects vacuolar biogenesis or vice versa.

In late G1, START completion is mediated by Cdc28p (a cyclin-dependent kinase, CDK) in association with one of the G1 cyclins, Cln1,2,3p. Cells lacking all three *CLN* genes are inviable and cannot complete START (Richardson et al., 1989). Cln3p functions upstream of Cln1,2p activating the G1/S transcription program (Dirick et al., 1995), where ~200 genes (*CLN1,2* among them) are transcribed (Spellman et al., 1998). Cln3p/Cdc28p phosphorylates Whi5p, a repressor of the G1/S transcription factor SBF, thereby releasing Whi5p from SBF and activating START transcription (Costanzo et al., 2004; de Bruin et al., 2004; Schaefer and Breeden, 2004). In addition, our earlier findings provided evidence for a novel function of Cln3p in vacuolar homotypic fusion, separate from its role in G1/S transcription and not shared by other G1 cyclins (see CHAPTER II).

A central polarity-establishment factor in a variety of organisms (from yeast to humans) is Cdc42p, a Rho-type small GTPase that orchestrates numerous processes necessary for polarization, such as septin and actin organization and membrane

trafficking, in response to cell cycle transitions and environmental cues (Etienne-Manneville, 2004; Irazoqui and Lew, 2004). Cdc42p membrane localization is not restricted to the plasma membrane but includes internal membranes, notably vacuolar membranes (Richman et al., 2004). Furthermore, Cdc42p is one of several GTPases required for vacuolar homotypic fusion (Eitzen et al., 2001; Muller et al., 2001). Reorganization of vacuole-bound actin is needed for vacuolar homotypic fusion, and proteins of the Cdc42p-dependent processes necessary for actin remodeling are enriched on vacuolar membranes (Eitzen et al., 2002). Among numerous Cdc42p effectors and interacting proteins, the scaffold protein Bem1p is critical for proper Cdc42p activation (Irazoqui et al., 2003). After the Cln3p/Cdc28p-mediated initiation of the G1/S transcription program, the burst of late G1 phase Cdk activity involving Cln1,2p/Cdc28p and Pcl1,2p/Pho85p (another cyclin/Cdk complex) triggers a pathway that leads to phosphorylation of Cdc24p. Cdc24p is a Cdc42p guanine nucleotide exchange factor (GEF). Once at the bud site, Cdc24p binds Bem1p and Cdc42p-dependent actin reorganization necessary for bud emergence takes place (Bose et al., 2001; Gulli et al., 2000; Moffat and Andrews, 2004).

In this report, we show that Bem1p is required for vacuolar homotypic fusion and that the overall vacuolar compartment in *bem1*Δ cells is enlarged but fragmented, similar to *cln3*Δ cells. Furthermore, Bem1p is phosphorylated in a Cln3p-dependent manner at Ser72. A single S72D substitution in Bem1p (which mimics phosphorylation), or over-expression of *CDC42* or *CDC24* suppresses the vacuolar fragmentation of *cln3*Δ cells. Conversely, substituting Ser72 in Bem1p with Ala blocks the ability of Cln3p to

promote vacuole fusion, *in vivo* and *in vitro*. The results we report here suggest that Cln3p impacts on vacuolar homeostasis through Bem1p and Cdc42p.

Results

Cln3p is required for an early step of vacuolar homotypic fusion

We had previously shown that Cln3p is required for vacuolar homotypic fusion (CHAPTER II). Vacuolar homotypic fusion is composed of several distinct sequential steps: Priming, docking, and fusion (Wickner and Haas, 2000). To study the kinetics of the reaction, order of addition experiments can be done, whereby the fusion reaction progressively becomes resistant to the addition of various inhibitors, once the inhibitor-sensitive step has been completed. For example, placement on ice blocks all steps and thus results in a "late-stage" inhibition profile, which is also similar to the GTP-γ-S inhibition profile. There are several GTPases involved in more than one step, including the last fusion step, which leads to a "late-stage" inhibition profile by GTP-γ-S (Eitzen et al., 2001; Eitzen et al., 2000). On the other hand, the ionophore FCCP blocks the docking step and it does not significantly inhibit the overall reaction if added late. Using this approach, we decided to determine the stage of the overall reaction that requires Cln3p for its completion, with cytosol from cells expressing HA-tagged Cln3p. We then added an anti-HA antibody as an inhibitor at various time points during the reaction, and measured the overall fusion activity at the end of the 90 min incubation period (Fig. 4.1). This experiment was done in parallel with several other reactions, to

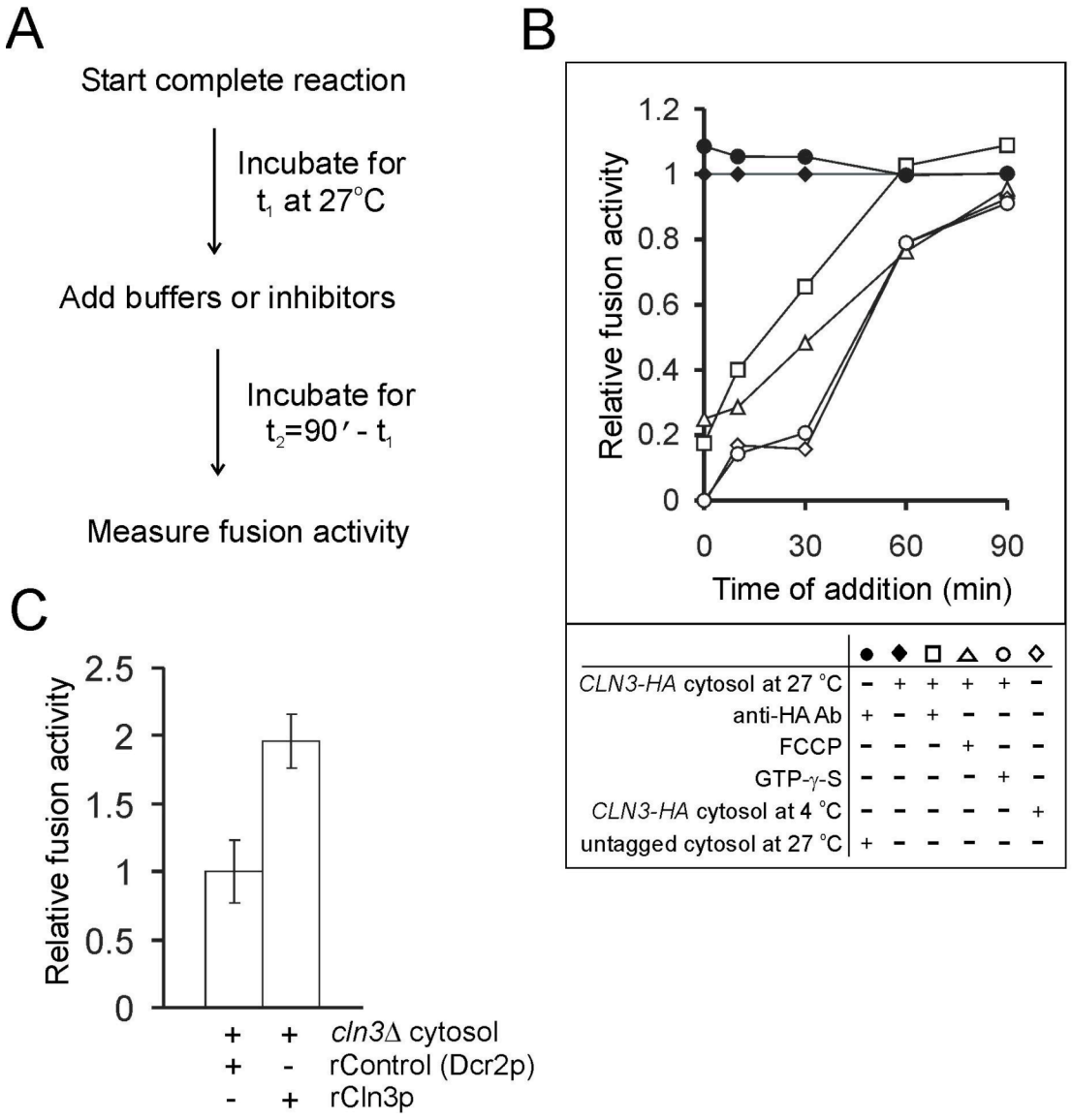

Figure 4.1. Cln3p is required for an early step during vacuole fusion. *A*, A schematic of the experimental strategy is shown. *B*, Fusion reactions were incubated at 27°C with cytosol from a *CLN3-HA* strain. At the indicated times of addition (t_1) shown on the x-axis, aliquots were removed and added to tubes containing anti-HA Ab, FCCP, GTP-γ-S, or buffer and incubated at 27°C. The activity from the buffer-containing tube at 27°C was set as 100% fusion activity. Another buffer-containing tube was incubated on ice and its activity was set at 0% fusion activity. As a control, aliquots of reactions with cytosol from the untagged isogenic strain were also added at various time points to tubes containing the anti-HA Ab (●) or buffer, and treated in the same manner as above. Reactions were incubated for a total of 90 min and then assayed for alkaline phosphatase, the relative values of which are shown on the y-axis. *C*, Fusion reactions were performed as described in Materials and Methods, using cytosol from *cln3*Δ cells and recombinant proteins from bacteria as indicated. Fusion was evaluated colorimetrically and the average and standard deviation of the relative fusion activities from at least three independent experiments is shown.

compare the profile of Cln3p withdrawal to the profiles of known fusion inhibitors (Fig. 4.1). From this analysis, it appears that the reaction becomes resistant to removal of Cln3p with kinetics slightly earlier than the kinetics for FCCP addition (Fig. 4.1). Thus, once docking is complete, Cln3p is not required for vacuolar homotypic fusion.

To further test whether the requirement for Cln3p in vacuole fusion is direct, and not somehow due to indirect effects resulting from Cln3p's role in G1/S transcription, we performed the *in vitro* fusion reaction using cytosol from *cln3*Δ cells, supplemented with Cln3p expressed in bacteria (Fig. 4.1C). Addition of recombinant Cln3p, but not of the unrelated control protein Dcr2p (Pathak et al., 2004), increased fusion activity (Fig. 4.1C). These results argue that there is a direct requirement for Cln3p in vacuole fusion.

Bem1p impacts on vacuolar biogenesis, downstream of Cln3p

To understand Cln3p's vacuolar function, we reasoned that one of the numerous known regulators of homotypic fusion might be targeted by Cln3p. Possible downstream effectors of Cln3p/Cdc28p in vacuolar homotypic fusion may display the following properties: loss of function mutations should lead to vacuolar and overall cell size enlargement; loss of function mutations should lead to vacuolar fragmentation; and the putative effectors should be Cdk targets. Recent genome-wide studies focused on these properties, namely altered cell size (Jorgensen et al., 2002; Zhang et al., 2002); fragmented vacuolar morphology (Seeley et al., 2002); and proteins that are phosphorylated by Cdc28p in whole-cell extracts (Ubersax et al., 2003). There are more than a hundred gene products in each data set (Fig. 4.2A). For example, there were 181

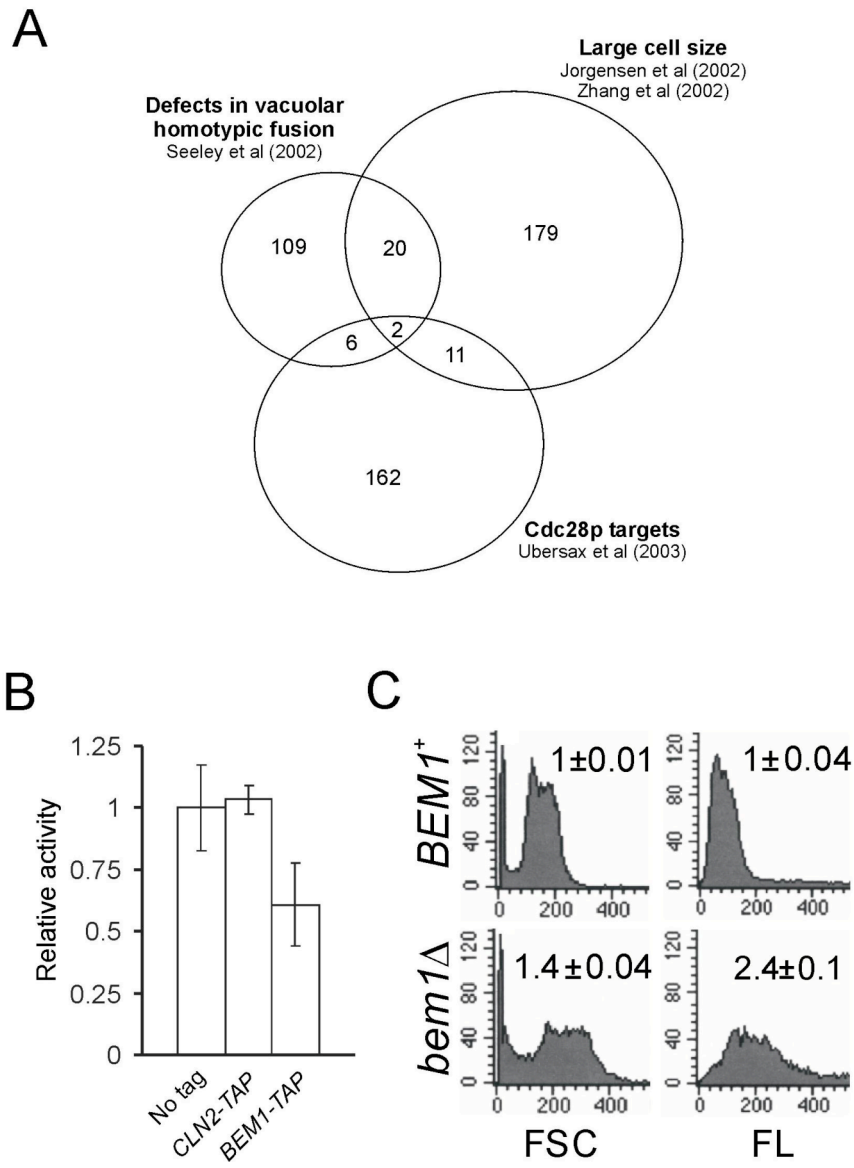

Figure 4.2. Bem1p is required for vacuole fusion and vacuolar size homeostasis. *A*, Venn diagrams from the indicated genome-wide studies, with the number of genes corresponding to different phenotypes in each case is shown. *B,* Vacuole fusion using cytosol from untagged, *CLN2-TAP*, or *BEM1-TAP* tagged strains (see Table 2.1), carried out in the presence of rabbit IgG antibody. Each measurement was evaluated upon addition of rabbit IgG or buffer. The buffer-containing reactions were then incubated at 27°C or ice (setting the 100% and 0% values of fusion activity). The IgG-containing reactions were incubated at 27°C. Fusion was evaluated colorimetrically and the average and standard deviation from at least three independent experiments is shown. *C*, Cell and vacuole size of live CDCFDA-stained *BEM1*$^{+}$ and *bem1*Δ cells (in the diploid BY4743 background) was evaluated by flow cytometry. The number of cells is shown on the y-axis, and the x-axis indicates forward angle scattering, which is indicative of cell size (FSC), or vacuolar fluorescence (FL). The average and standard deviation from five independent measurements in each case is shown.

proteins that were significantly phosphorylated by Clb2p/Cdc28p (with a P-score ≥2, which is the logarithm of the amount of phosphate incorporated per ng of protein). Yet, only Cln3p itself and Bem1p were present in all three data sets (Fig. 4.2A).

Using the *in vitro* fusion assay, we found that reactions with cytosol from *BEM1-TAP* cells in the presence of inhibitory rabbit IgG (which targets the TAP domain) had significantly reduced fusion activity (Fig. 4.2B). Loss of Bem1p or Cln3p also leads to vacuolar fragmentation in about 40-60% of the cells {see Figs. 4.2-4.3A,B and (Han et al., 2003; Seeley et al., 2002)}. Furthermore, cells lacking *BEM1* were larger overall (~40%, Figs. 4.2, 4.3) than wild-type cells and, importantly, their vacuolar compartment was also disproportionately enlarged (about 2-fold, Figs. 4.2, 4.3). Finally, Cdc28p readily phosphorylated Bem1p (*P*-score =4.4) in the phosphorylation assays by Ubersax et al (Ubersax et al., 2003). Consequently, we decided to evaluate Bem1p as a putative Cln3p/Cdc28p effector in vacuolar biogenesis.

To test whether Cln3p might mediate its effects in vacuolar biogenesis through Bem1p, we measured the overall cell size and vacuolar size of *CLN3* and *BEM1* mutant combinations, and also microscopically examined their vacuolar morphology. Loss of Cln3p or Bem1p leads to cellular and vacuolar enlargement and vacuolar fragmentation (Fig. 4.3). Conversely, cells expressing a stabilized form of Cln3p from the dominant gain-of-function *CLN3-2*^{D} allele are smaller overall (Cross, 1988), and their vacuolar compartment is also smaller (see Fig. 4.3A and CHAPTER II). However, the *CLN3-2*^{D} allele was unable to reduce cell and vacuole size in the absence of Bem1p (Fig. 4.3A). Furthermore, combined loss of Bem1p and Cln3p did not lead to an additive cellular or

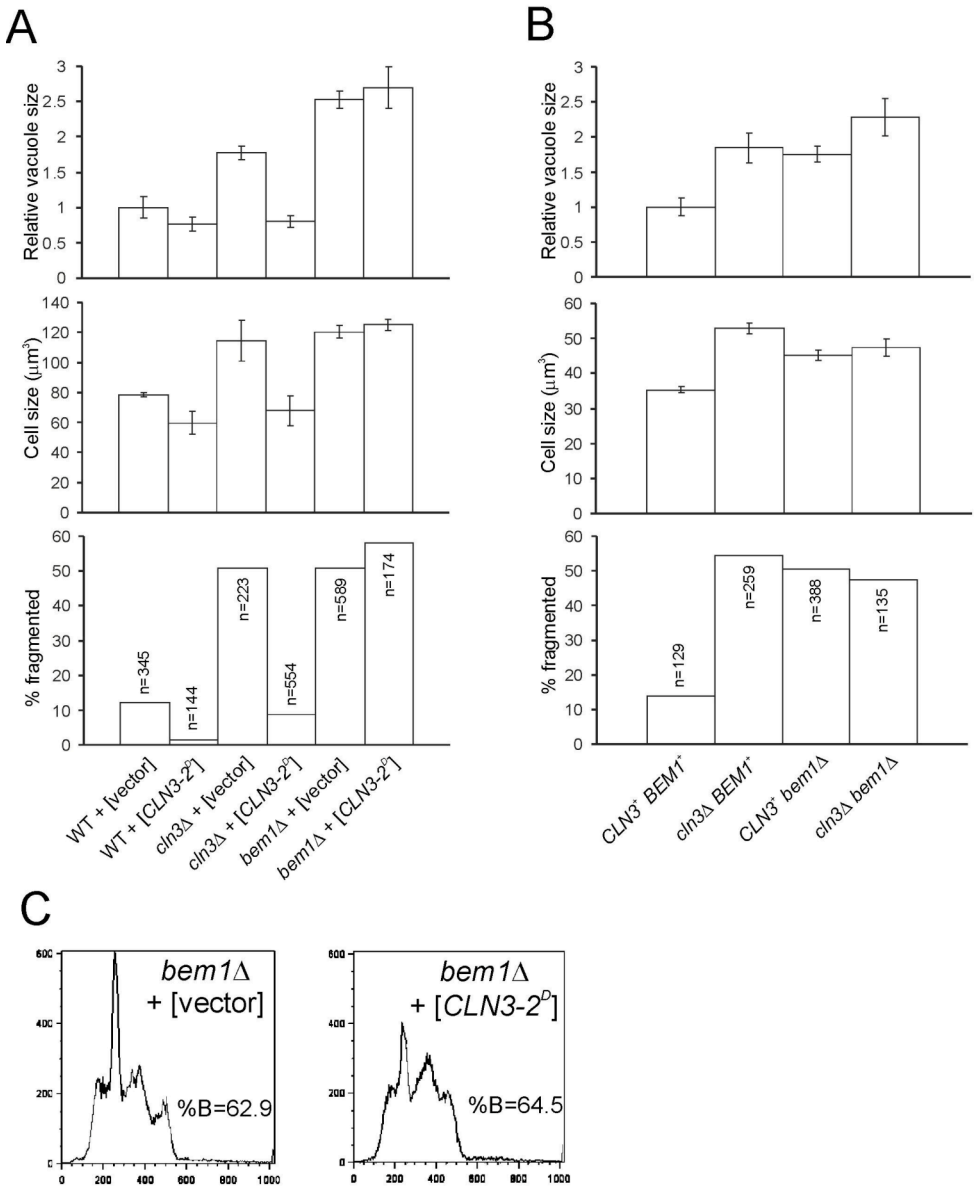

Figure 4.3. Cln3p requires Bem1p to affect cell and vacuole size and vacuolar morphology. *A*, The relative vacuole size of the indicated strains (all in the diploid BY4743 background) was measured as in Fig. 2, and cell size was measured with a channelyzer. The average and standard deviation from four independent measurements in each case is shown. The indicated strains were also stained with FM4-64 to observe their vacuolar morphology by fluorescence microscopy. The percent of cells with vacuolar fragmentation and the number of cells scored in each case (n) is shown. *B*, The indicated parameters were measured as in *A*, using the strains shown (in the haploid BY4741 background). *C*, The DNA content of the indicated strains (in the diploid BY4743 background) was measured by flow cytometry. The number of cells is shown on the y-axis, and the x-axis indicates fluorescence. The percentage of budded cells (%B) is also shown.

vacuolar enlargement or vacuolar fragmentation (Fig. 4.3B). These results are consistent with the idea that Bem1p is required for Cln3p's effects on cell and vacuole size, and that Bem1p and Cln3p do not affect vacuolar biogenesis through separate independent pathways.

Since Bem1p was required for Cln3p's effects on cell and vacuole size (Fig. 4.3A), we then evaluated cell cycle progression in *bem1*Δ *CLN3-2*^{D} cells. In synthetic complete media at 30°C the population doubling times of *bem1*Δ and *bem1*Δ *CLN3-2*^{D} cells were similar to each other (~200 min), but much slower than wild-type cells (~90 min). The percentage of budded cells (budding index) was similar in *bem1*Δ and *bem1*Δ *CLN3-2*^{D} cell populations (Fig. 4.3C). However, based on DNA content analysis by flow cytometry, it appears that *bem1*Δ cells carrying the *CLN3-2*^{D} allele have a shorter G1 phase (Fig. 4.3C). Thus, the *CLN3-2*^{D} allele still accelerated initiation of DNA replication in *bem1*Δ cells, even though the cell and vacuolar size of these cells did not decrease. The irregular DNA content profiles of *bem1*Δ cells (Fig. 4.3C) might be due to aneuploidy, which has been previously reported to result from the bud emergence defect of *bem1*Δ cells (Bender and Pringle, 1991).

Bem1p is phosphorylated in a Cdk-dependent manner

It was mentioned in an earlier report that Bem1p might be a phosphoprotein, because phosphatase treatment leads to faster migration of Bem1p during SDS-PAGE (Leeuw et al., 1995). Indeed, immunoprecipitated TAP-tagged Bem1p migrated faster upon phosphatase treatment (Fig. 4.4A). Bem1p has four potential Cdk phosphorylation sites: two [ST]-P-X-[KR] sites at Thr-51 and Ser-72, and two [ST]-P sites at Thr-26 and Ser-

Figure 4.4. Bem1p is phosphorylated in a Cdk-dependent manner. *A*, Schematic of the TAP-tagged Bem1p. Bem1p-TAP was isolated from cells carrying a chromosomal TAP-tagged BEM1 copy (*BEM1-TAP*, strain 7499374, see Table 2.1) by immunoprecipitation using IgG, and treated with calf intestinal phosphatase (CIP) as indicated. The samples were then processed for SDS-PAGE and immunobloting with the PAP reagent. *B*, Bem1p-TAP was isolated by tandem immunoprecipitations using IgG and Calmodulin beads. The IgG-immunoprecipitated material was treated with TEV protease as indicated, before immunoprecipitations with calmodulin beads. Immunobloting was done using the indicated antibodies. *C*, The immunoprecipitated samples from Bem1p-TAP cell extracts were treated as in *B*, and in addition with λ-phosphatase (λ-PPase) and phosphatase inhibitor (PPase-[I]) as indicated. The antibodies used for immunobloting are shown on the right, and the relative ratios of the signal intensities are shown at the bottom. *D*, The samples were processed as in *C*, but instead of phosphatase treatment, they were incubated with cytosolic extracts prepared from cells of the indicated genotype (200 µl in each case, containing 0.75 mg of total protein). Before addition to the immunoprecipitated Bem1p, the extracts were pre-cleared on calmodulin beads. *E*, Extracts from *CDC28*$^{+}$ and *cdc28-as1* cells carrying cMyc-tagged Bem1p on a low copy plasmid (plasmid pDLB2226; see Table 2.2) were prepared using a urea extraction buffer and analyzed by SDS PAGE and immunoblotting with an anti-Myc antibody. The cells were treated with DMSO alone or 1 NM-PP1 (at 5 µM) for the indicated times. *F*, Vacuole fusion activity using cytosol from *cdc28-as1* cells. DMSO alone or 1 NM-PP1 (at 5 µM for 15 min) was added as indicated. Fusion was evaluated colorimetrically and the average and standard deviation of the relative fusion activities from at least three independent experiments is shown. *G*, Extracts from cells of the indicated genotype (in the haploid BY4741 background) carrying cMyc-tagged Bem1p on a low copy plasmid (plasmid pDLB2226; see Table 2.2) were analyzed as in *E*. The same blot was sequentially processed first with an anti-Myc antibody and then with an anti-Pgk1p antibody. *H*, Extracts from synchronous cultures of wild-type haploid BY4741 cells carrying cMyc-tagged Bem1p on a low copy plasmid were obtained after release from a nocodazole block (used at 15 µg/ml for 4 hrs) at the indicated time points, and analyzed as in *G*. The corresponding percentage of budded cells in each case is shown at the bottom. Logarithmically growing cells (log) and cells that do not carry a cMyc-tagged copy of Bem1p (untagged) were also included in the analysis.

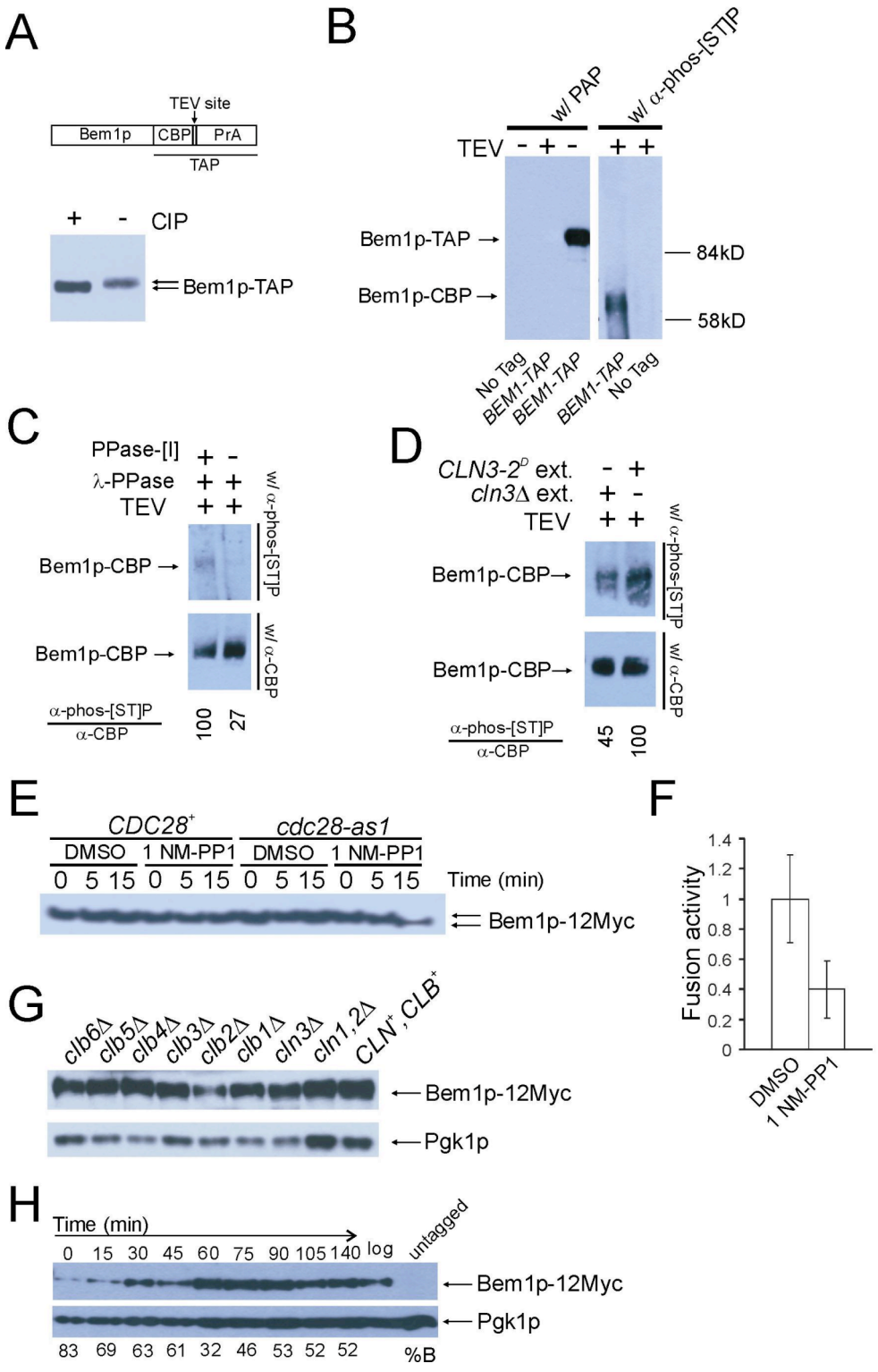
A
TEV site
Bem1p
CBP
PrA
TAP
+ - CIP
Bem1p-TAP
B
w/ PAP
w/ α-phos-[ST]P
TEV - + - + +
Bem1p-TAP
Bem1p-CBP
84kD
58kD
No Tag
BEM1-TAP
BEM1-TAP
BEM1-TAP
No Tag
C
PPase-[I] + -
λ-PPase + +
TEV + +
w/ α-phos-[ST]P
Bem1p-CBP
Bem1p-CBP
w/ α-CBP
α-phos-[ST]P / α-CBP
100
27
D
CLN3-2D ext. - +
cln3Δ ext. + -
TEV + +
w/ α-phos-[ST]P
Bem1p-CBP
Bem1p-CBP
w/ α-CBP
α-phos-[ST]P / α-CBP
45
100
E
CDC28+
cdc28-as1
DMSO 1 NM-PP1 DMSO 1 NM-PP1
0 5 15 0 5 15 0 5 15 0 5 15
Time (min)
Bem1p-12Myc
F
Fusion activity
1.4
1.2
1
0.8
0.6
0.4
0.2
0
DMSO
1 NM-PP1
G
clb6Δ clb5Δ clb4Δ clb3Δ clb2Δ clb1Δ cln3Δ cln1,2Δ CLN+,CLB+
Bem1p-12Myc
Pgk1p
H
Time (min)
0 15 30 45 60 75 90 105 140 log
untagged
Bem1p-12Myc
Pgk1p
83 69 63 61 32 46 53 52 52
%B

60, respectively. As a first step towards establishing possible Cdk-mediated phosphorylation events, we asked whether an antibody directed against phosphorylated [ST]-P recognized Bem1p immunoprecipitated from cell extracts. From these cell extracts, we sequentially immunoprecipitated Bem1p-TAP using IgG and Calmodulin beads (Fig. 4.4B). The immunoprecipitated protein was readily recognized by the PAP reagent, via the protein A domain (Fig. 4.4B). To use the anti phospho [ST]-P antibody, after immunoprecipitations with IgG beads, we cleaved the immunoprecipitated product with TEV protease to remove the protein A part of the TAP epitope. Immunoblotting with the anti phospho [ST]-P antibody recognized the cleaved Bem1p-CBP (which now lacks the protein A part of the TAP tag) (Fig. 4.4B). Recognition by the anti phospho [ST]-P antibody was phosphorylation-dependent, because the signal was significantly reduced after treatment with phosphatase (Fig. 4.4C). When normalized for Bem1p levels using an antibody that recognizes the remaining part of the TAP tag after TEV cleavage, treatment with phosphatase removed >70% of the signal (Fig. 4.4C, bottom). Furthermore, the Bem1p-associated phospho [ST]-P signal was about two times more intense when the immunoprecipitated product was incubated with extracts from cells carrying the *CLN3-2*^{D} allele compared to *cln3*Δ extracts (Fig. 4.4D).

To further evaluate whether Cdc28p activity contributes to Bem1p phosphorylation, we used *cdc28-as1* cells, which express an engineered version of Cdc28p that is inhibited by the ATP analog 1NM-PP1 (Bishop et al., 2000). These cells were then transformed with a low-copy centromeric plasmid carrying cMyc-tagged Bem1p (Irazoqui et al., 2003). Upon treatment with the inhibitory drug, the mobility of

Myc-tagged Bem1p increased on SDS-PAGE, consistent with dephosphorylation (Fig. 4.4E). No such effects were seen upon treatment with DMSO or in the isogenic strain that does not carry the engineered *cdc28-as1* allele (Fig. 4.4E). We had previously reported that shifting temperature-sensitive *cdc28-1* cells to their non-permissive temperature led to vacuolar fragmentation (CHAPTER II). To further confirm that Cdc28p-associated kinase activity is required for vacuole homotypic fusion, we performed the *in vitro* fusion reaction using cytosol from *cdc28-as1* cells, and we found that upon treatment with the inhibitory drug, fusion activity was reduced to ~40% of the activity when DMSO alone was added (Fig. 4.4F). Together, all of the above results support the hypothesis that Bem1p is phosphorylated in a Cdc28p-dependent manner *in vivo*.

We then examined the electrophoretic mobility of cMyc-tagged Bem1p in cells lacking mitotic or G1 cyclins (Fig. 4.4G). There was a slight mobility increase in cells lacking Cln3p (Fig. 4.4G; compare the *cln3*Δ and *clb1*Δ lanes that are equally loaded and electrophoresed next to each other; and see also Fig. 3.6, for related evidence). Finally, the electrophoretic mobility of Bem1p does not vary significantly during the cell cycle in synchronous cultures (Fig. 4.4H), but this perhaps is not surprising given that Cln3p/Cdc28p activity also does not oscillate during the cell cycle (Tyers et al., 1993; Tyers et al., 1992).

Ser72 is critical for Bem1p's role in vacuolar homeostasis

We then examined whether the Bem1p potential Cdk phosphorylation sites are conserved in other *Saccharomyces* species (Cliften et al., 2003; Kellis et al., 2003) and in *Candida* species for which genome information is available (Fig. 4.5A). Not surprisingly, all the sites are conserved in the *sensu stricto Saccharomyces* species (*S. mikatae, S. kudriavzevii*, *S. paradoxus* and *S. bayanus*). *S. castellii* is a more distantly related *sensu lato Saccharomyces* species, and alignment of Bem1p to its ortholog in this species is likely to be more useful (Cliften et al., 2003). In *S. castellii* only positions 26 and 72 are conserved, while in the two *Candida* species positions 51 and 72 are conserved (Fig. 4.5A). The extreme N-terminus of the *C. albicans* Bem1p does not show significant conservation with the *S. cerevisiae* Bem1p, and the highlighted position may not correspond to Ser51. Overall, the only conserved site in all of these cases is Ser72 (Fig. 4.5A), which is a preferred [ST]-P-X-[KR] Cdk consensus site. Ser72 also represents the first amino acid residue of the SH3-1 domain, which spans from position 72 to 132, based on PROSITE software predictions (Gattiker et al., 2002).

To test whether position 72 might be targeted for Cdk-mediated phosphorylation, we replaced Ser72 to Ala (to abolish phosphorylation) or Asp (to mimic phosphorylation) and evaluated the vacuolar morphology of *bem1*Δ or *cln3*Δ cells expressing these Bem1p mutants from low-copy plasmids as C- terminal cMyc fusions (Fig. 4.5B). The S72A and S72D mutants were expressed at levels similar to the wild-

Figure 4.5. Ser at position 72 in Bem1p is critical for vacuolar morphology. *A*, Bem1p amino acid sequences (positions 24-75) in *Saccharomyces* and *Candida* species. The numbering on top refers to *S. cerevisiae* Bem1p. The amino acids putatively targeted for Cdk-dependent phosphorylation are shown in bold, and the conserved Ser at position 72 is bracketed in red. *B,* Homozygous diploid WT, *bem1*Δ or *cln3*Δ cells (BY4743 background) were transformed with the low-copy empty vector, wild-type or mutant cMyc-tagged Bem1p as indicated. The transformants were then stained with FM4-64 to observe their vacuolar morphology by fluorescence microscopy. The percent of cells with vacuolar fragmentation and the number of cells scored in each case (n) is shown. Where indicated, the *P* value associated with a x^2 significance test is shown. *C,* Representative photographs of the indicated strains from *B*. The arrow indicates an example of vacuolar fragmentation. *D*, Homozygous diploid *bem1*Δ cells (BY4743 background) carrying the *CLN3-2*^{D} allele on a low copy plasmid were also transformed with the low copy wild-type or mutant cMyc-tagged Bem1p as indicated. Vacuolar morphology was evaluated as in *B*, above. *E*, Fusion reactions were performed as described in Materials and Methods, using cytosol from cells lacking both *CLN3* and *BEM1* (strain SMY01; Table 2.1) and recombinant proteins from bacteria as indicated. The average of the relative activities from two independent experiments is shown in each case. The data from the two experiments had a Pearson correlation value of 0.82, and a paired two-sample t-test value of 0.009.

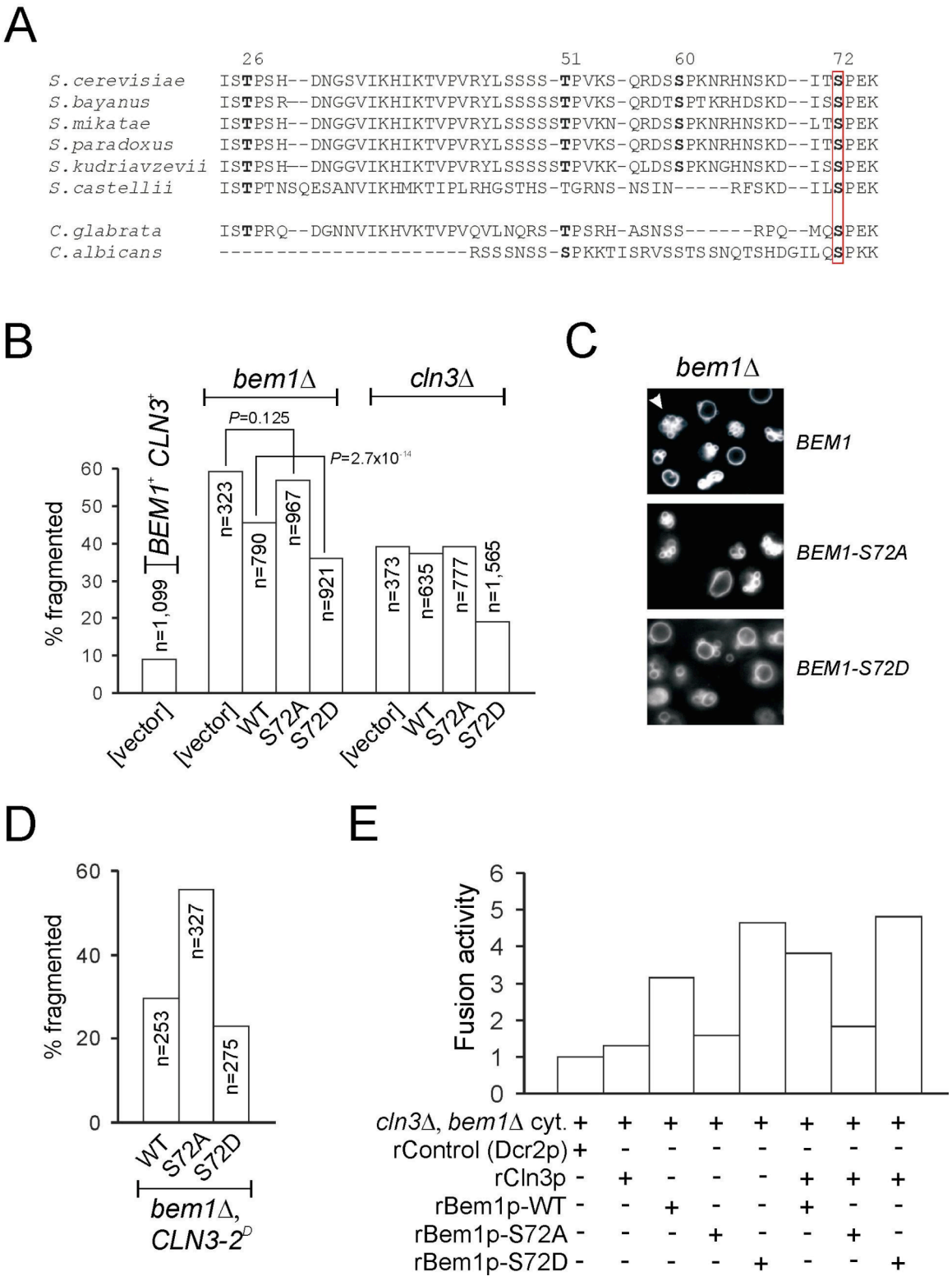
A
26
51
60
72
S.cerevisiae ISTPSH--DNGSVIKHIKTVPVRYLSSSS-TPVKS-QRDSSPKNRHNSKD--ITSPEK
S.bayanus ISTPSR--DNGGVIKHIKTVPVRYLSSSSSTPVKS-QRDTSPTKRHDSKD--ISSPEK
S.mikatae ISTPSH--DNGGVIKHIKTVPVRYLSSSSSTPVKN-QRDSSPKNRHNSKD--LTSPEK
S.paradoxus ISTPSH--DNGGVIKHIKTVPVRYLSSSS-TPVKS-QRDSSPKNRHNSKD--ITSPEK
S.kudriavzevii ISTPSH--DNGGVIKHIKTVPVRYLSSSSSTPVKK-QLDSSPKNGHNSKD--ISSPEK
S.castellii ISTPTNSQESANVIKHMKTIPLRHGSTHS-TGRNS-NSIN-----RFSKD--ILSPEK
C.glabrata ISTPRQ--DGNNVIKHVKTVPVQVLNQRS-TPSRH-ASNSS------RPQ--MQSPEK
C.albicans ----------RSSSNSS-SPKKTISRVSSTSSNQTSHDGILQSPKK
B
bem1Δ
cln3Δ
P=0.125
P=2.7x10-14
% fragmented
BEM1+ CLN3+
n=1,099
n=323
n=790
n=967
n=921
n=373
n=635
n=777
n=1,565
[vector]
[vector]
WT
S72A
S72D
[vector]
WT
S72A
S72D
C
bem1Δ
BEM1
BEM1-S72A
BEM1-S72D
D
% fragmented
n=253
n=327
n=275
WT
S72A
S72D
bem1Δ,
CLN3-2D
E
Fusion activity
cln3Δ, bem1Δ cyt. + + + + + + + +
rControl (Dcr2p) + - - - - - - -
rCln3p - + - - - + + +
rBem1p-WT - - + - - + - -
rBem1p-S72A - - - + - - + -
rBem1p-S72D - - - - + - - +

type cMyc-tagged Bem1p, and their sub-cellular localization was indistinguishable from wild-type (data not shown). We noticed that introduction of the otherwise wild-type cMyc-tagged Bem1p on a low-copy centromeric plasmid only partially suppressed the vacuolar fragmentation of *bem1*Δ cells (Fig. 4.5B). The plasmid is clearly functional because it does suppress the bud emergence defect of *bem1*Δ cells {see below and (Irazoqui et al., 2003)}. The lack of strong suppression of the vacuolar fragmentation might be due to the relative under-expression of cMyc-tagged Bem1p from this plasmid compared to endogenous levels (Irazoqui et al., 2003). Consistent with this interpretation, cMyc-tagged Bem1p expressed from a high-copy (2μ) plasmid at levels no more than 2-fold higher compared to endogenous Bem1p (Irazoqui et al., 2003), showed strong suppression of the vacuolar fragmentation of *bem1*Δ cells (see below).

Nonetheless, it is important to note that the fact that wild-type cMyc-tagged Bem1p from a low-copy plasmid only partially suppressed vacuolar fragmentation conveniently allows one to evaluate the effects of the S72D substitution even in *bem1*Δ (but $CLN3^{+}$) cells. It was clear that S72D Bem1p suppressed vacuolar fragmentation better than wild-type Bem1p and, conversely, the S72A Bem1p mutant did not suppress at all the vacuolar fragmentation of *bem1Δ* cells (Fig. 4.5B,C). Because the S72A mutant is functional in bud emergence (see below), the lack of suppression in vacuolar fragmentation is unlikely to be due to the production of a non-functional unfolded protein. Finally, introduction of the S72D, but not the S72A, Bem1p mutant in *cln3*Δ cells also significantly suppressed their vacuolar fragmentation (Fig. 4.5B,C).

To further test the role of Ser72, we over-expressed Cln3p in cells carrying wild-type or Ser72 Bem1p mutants (Fig. 4.5D). We found that cells carrying both the *CLN3-2*^{D} and *BEM1-S72A* alleles had fragmented vacuolar morphology (Fig. 4.5D). Thus, the S72A substitution blocks the ability of Cln3p to promote vacuole fusion *in vivo*. We then performed *in vitro* fusion reactions using cytosol from cells lacking both Cln3p and Bem1p, supplemented with various combinations of recombinant Cln3p, Bem1p, Bem1p-S72A, and Bem1p-S72D (Fig. 4.5E). The highest activity was observed upon addition of Bem1p-S72D with or without Cln3p, and the lowest upon addition of Bem1p-S72A. Also, addition of Cln3p alone or with Bem1p-S72A did not increase fusion activity (Fig. 4.5E). Therefore, these *in vitro* results completely support our *in vivo* evidence that Cln3p requires Bem1p to promote fusion. Furthermore, the S72A substitution in Bem1p blocks fusion, while the S72D mutation promotes it. Interestingly, addition of wild-type Bem1p also increased fusion activity in the absence of Cln3p, albeit not to the same level as Bem1p-S72D. Thus, it is possible that in the absence of Cln3p, when large amounts of exogenous Bem1p are added, Bem1p can still be modified in these extracts perhaps by other cyclin/Cdk complexes. Overall, our results from the *in vitro* fusion assays are in very good agreement with our *in vivo* evidence, and suggest that Cln3p and Bem1p play direct roles in vacuole fusion, with Bem1p acting downstream of Cln3p.

Overall, these results strongly support the notion that the conserved Ser at position 72 in the first SH3 domain of Bem1p might be targeted for Cdk-mediated phosphorylation, and that the phosphorylated form promotes vacuolar homotypic fusion.

It is possible that the other sites may also be phosphorylated. However, because the S72D mutant significantly suppressed the vacuolar fragmentation of *cln3*Δ and *bem1*Δ cells *in vivo* and *in vitro*, while the S72A mutant did not, it is reasonable to conclude that even if additional sites are phosphorylated, phosphorylation of Ser72 has the most significant biological consequences for vacuolar biogenesis.

Since the electrophoretic mobility shift of Bem1p using SDS-PAGE was not very pronounced in the absence of Cln3p (Figs. 4.4G and 4.6B), we used two-dimensional gel electrophoresis to better resolve putative Bem1p isoforms (Fig. 4.6A). Indeed, an acidic isoform present in wild-type Bem1p (Fig. 4.6A, top panel) was absent in cells lacking Cln3p (Fig. 4.6A, middle panel), or in cells carrying Bem1p-S72A (Fig. 4.6A, bottom panel). We also noticed that Bem1p-S72A migrated slightly faster than wild-type Bem1p in standard one-dimensional SDS-PAGE (Fig. 4.6B). Together, these results strongly suggest that Bem1p is phosphorylated at Ser72 in a Cln3p-dependent manner *in vivo*.

Finally, we examined whether Bem1p expressed in bacteria could be phosphorylated *in vitro*. For this experiment we over-expressed *CLN3* from a high-copy plasmid carrying epitope-tagged *CLN3* under the control of a galactose-inducible promoter. It has been previously shown that over-expression of Cln3p allows for the recovery of detectable Cln3p-associated kinase activity against histone H1, and that most of that activity is Cdc28p-dependent (Tyers et al., 1993; Tyers et al., 1992). Indeed, the immunoprecipitated Cln3p had associated kinase activity against recombinant Bem1p, albeit to significantly lower levels compared to histone H1 (Fig. 4.6C). We also performed similar reactions using commercially available preparations of human

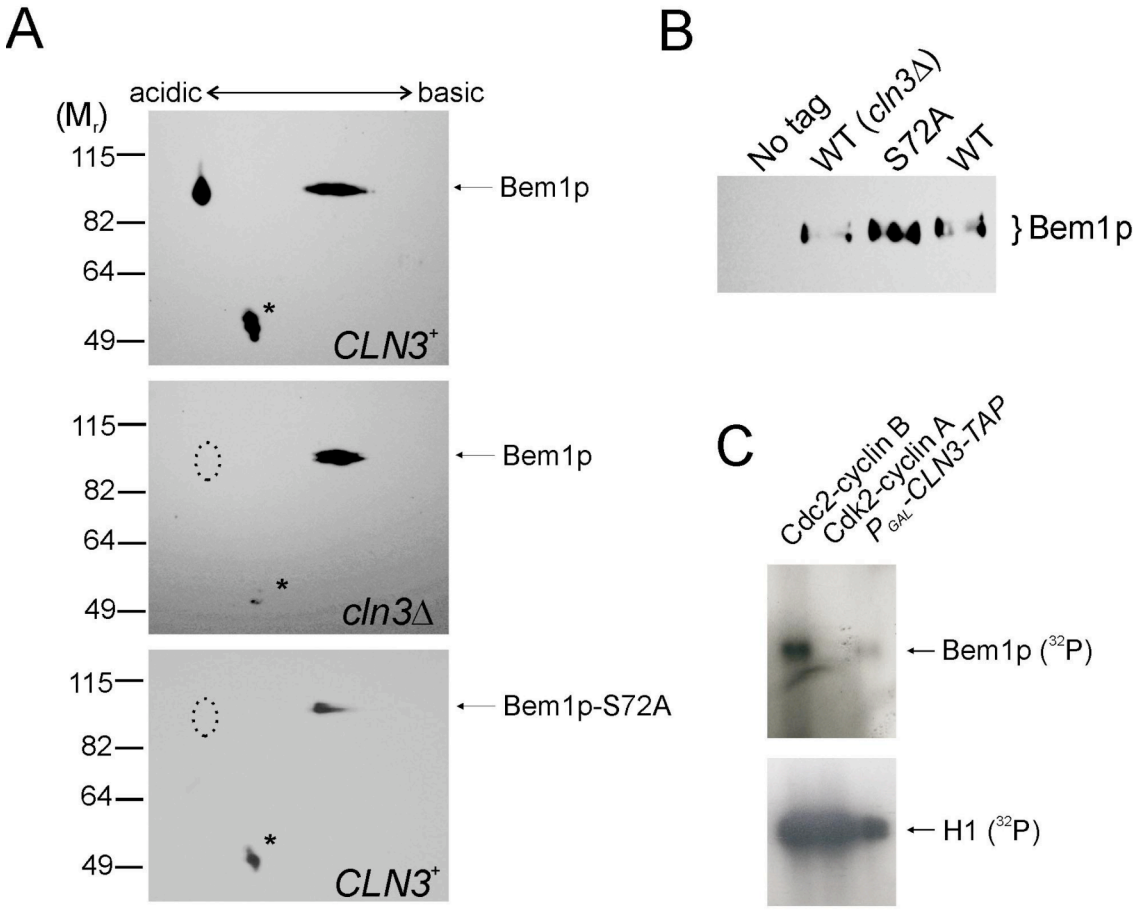

Figure 4.6. Gel electrophoresis analysis of Bem1p isoforms. *A*, Resolution of Bem1p isoforms by 2D gel electrophoresis. Extracts from cells of the indicated *CLN3* genotype were transformed with the low copy wild-type or mutant cMyc-tagged Bem1p as indicated, subjected to 2D gel electrophoresis, and immunoblotting with an anti-Myc antibody as described in the Materials and Methods. A degradation product is indicated by an asterisk (*). A broken line circles the location of the acidic full-length isoform absent from the two lower panels. *B*, The samples from *A* were also analyzed by standard one-dimensional SDS-PAGE and immunoblotting. *C*, Phosphorylation of Bem1p *in vitro*. (Top) autoradiogram of kinase reactions using recombinant Bem1p as a substrate and commercial preparations of human Cdk/cyclin complexes and Cln3p-associated kinase activity from yeast cells, as indicated. Exposure time was 10 days. (Bottom) autoradiogram of kinase reactions using histone H1 as a substrate and the same kinase preparations as in the top panel. Exposure time was 4 hrs.

Cdc2/cyclinB and Cdk2/cyclinA complexes. Surprisingly, Cdc2/cyclinB apparently phosphorylated Bem1p (Fig. 4.6C). Whether this reflects "background" non-specific levels of activity of this preparation is unclear at this point. Note that although the Cdc2 signal appears stronger than the signal from Cln3p (Fig. 4.6C), the commercial Cdc2 preparation we used was much more active against histone H1 than the Cln3p-associated activity we obtained from yeast cells.

Opposing role of Ser72 in bud emergence

Since Bem1p was originally identified for its role in bud emergence (Bender and Pringle, 1991), we next examined whether our Bem1p Ser72 mutants have phenotypes associated with bud emergence. To quantify the bud emergence defect we measured the frequency of unbudded cells containing spindles. The S72A mutant was fully functional in bud emergence (Fig. 4.7), in contrast to its total lack of complementing activity in vacuole fusion (Fig. 4.5). Interestingly, the S72D substitution did not fully complement the bud emergence defect of *bem1*Δ cells (Fig. 4.7). Thus, while phosphorylation of Ser72 promotes vacuole fusion, it is not required for and it might even negatively affect bud emergence.

Over-expression of Cdc42p or Cdc24p suppresses the vacuolar fragmentation of cln3Δ cells

We next examined whether Cln3p's requirement for vacuolar homotypic fusion might reflect perturbations of Cdc42p activity, since Bem1p is a well-established regulator of

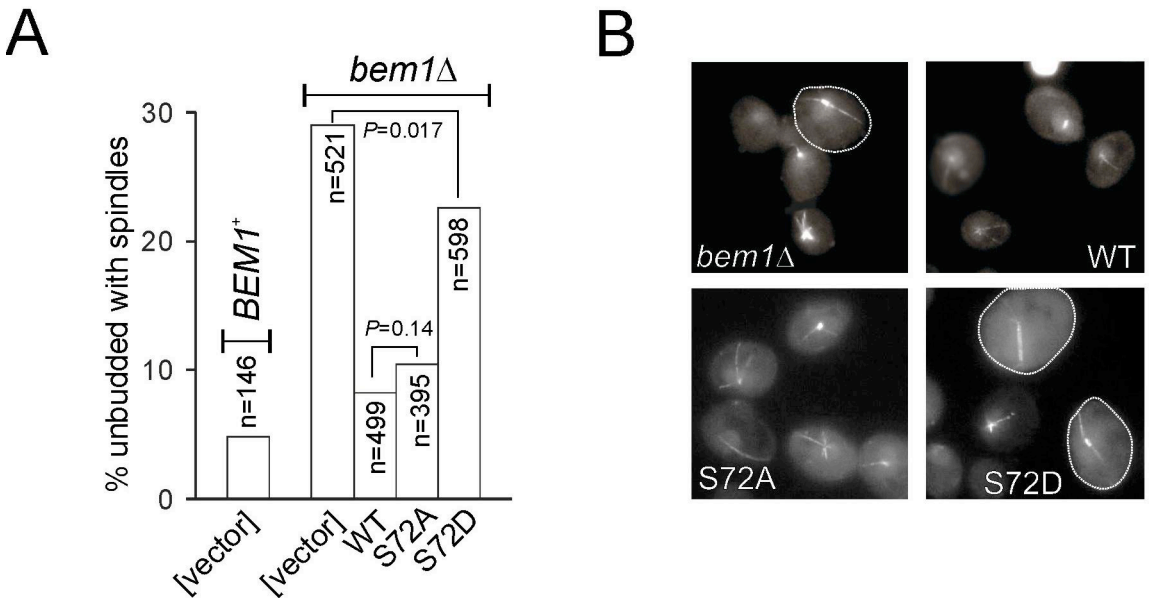

Figure 4.7. Rescue of bud emergence defect in *bem1*Δ cells by different *BEM1* alleles. Homozygous diploid WT or *bem1*Δ cells (BY4743 background) were transformed with the low copy empty vector, wild-type or mutant cMyc-tagged Bem1p as indicated. The cells were grown at 37 °C, fixed and processed for immunofluorescence to visualize tubulin. *A*, The percent of unbudded cells with spindles and the number of cells scored in each case (n) is shown. Where indicated, the *P* value associated with a χ^2 significance test is shown. *B*, Representative photographs of the indicated strains from *A*. Examples of unbudded cells with spindles are outlined.

Cdc42p, and Cdc42p is also required for the docking step of vacuolar homotypic fusion (Eitzen et al., 2001; Muller et al., 2001). To perhaps bypass the requirement for Cln3p, we activated the Cdc42p GTPase cycle by over-expressing wild-type *CDC42*, or its exchange factor *CDC24*, in c*ln3*Δ cells and evaluated their vacuolar morphology. Remarkably, over-expression of *CDC42* or *CDC24* completely suppressed the fragmented vacuolar morphology of *cln3*Δ cells (Fig. 4.8A,B). On the other hand, over-expression of *CDC42* did not significantly suppress the vacuolar fragmentation of *bem1*Δ cells (Fig. 4.8B). *CDC24* over-expression weakly suppressed the vacuolar fragmentation in *bem1*Δ cells (Fig. 4.8B). Overall, over-expression of Cdc42p, in the presence of Bem1p, is sufficient to bypass the requirement for Cln3p in vacuole fusion. Furthermore, in the *in vitro* fusion assay addition of Cdc42p did not rescue the fusion defect of *bem1*Δ cytosolic extracts (Fig. 4.8C), suggesting again that Bem1p is required for Cdc42p to promote fusion. Interestingly, when the extracts were supplemented with Bem1p-S72A together with Cdc42p there was an increase in fusion activity (~60%; Fig. 4.8C), but not to the same extent as when the extracts were supplemented with Bem1p-S72D (see Fig. 4.5E).

We next examined several other Bem1p amino acid substitutions at positions that are important for Bem1p's biological roles (Irazoqui et al., 2003), for their ability to suppress vacuolar fragmentation of *bem1*Δ cells (Fig. 4.8D). For example, a P208L substitution affects interactions with various effectors and scaffolds; P355A interferes with a postulated conformational change of Bem1p; R369A inhibits interactions with phosphoinositides; and K482A affects interaction with Cdc24p (Irazoqui et al., 2003).

Figure 4.8. *CDC42* or *CDC24* over-expression suppresses the vacuolar fragmentation of *cln3*Δ cells. *A*, Diploid *cln3*Δ cells (BY4743 background) were transformed with high copy plasmids as indicated. The transformants were then stained with FM4-64 to observe their vacuolar morphology and photographed through phase optics (top panels) and by fluorescence (bottom panels). *B*, The same analysis as in *A* was also done for *bem1*Δ and WT cells, and the percent of cells with vacuolar fragmentation and the number of cells scored in each case (n) is shown. Where indicated, the *P* value associated with a χ^2 significance test is shown. *C*, Fusion reactions were performed as described in Materials and Methods, using cytosol from *bem1*Δ cells and recombinant proteins from bacteria as indicated. Fusion was evaluated colorimetrically and the average and standard deviation of the relative fusion activities from at least three independent experiments is shown. *D*, Homozygous diploid *bem1*Δ cells (BY4743 background) were transformed with the empty high copy vector, or carrying wild-type or mutant cMyc-tagged Bem1p as indicated. The transformants were then stained with FM4-64 to observe their vacuolar morphology by fluorescence microscopy. The percent of cells with vacuolar fragmentation and the number of cells scored in each case (n) is shown. Where indicated, the *P* value associated with a χ^2 significance test is shown. *E*, Cells lacking Bem1p are not defective in vacuolar segregation. Exponentially growing cells of the indicated genotype were transferred in medium containing FM4-64 for 1 h, washed, re-suspended in fresh medium and allowed to grow for another 4h before they were examined microscopically. The number of cells examined is shown in parentheses. The scored cells had a bud diameter less or equal to 0.4 of the mother cell's diameter. The percentage of cells with the indicated vacuolar morphology is shown.

A

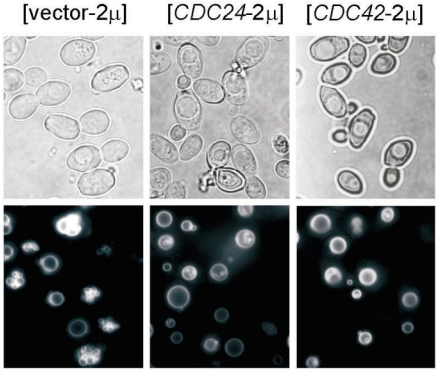

B

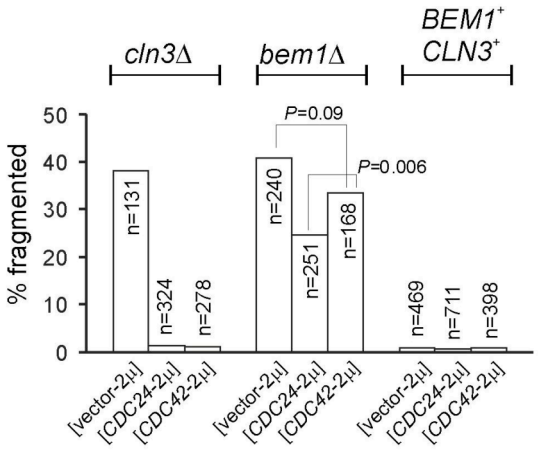

C

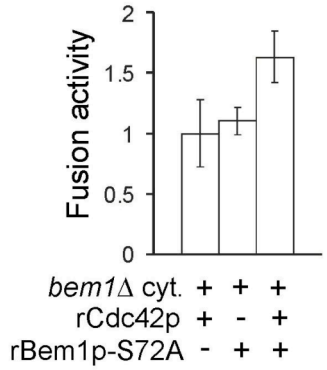

D

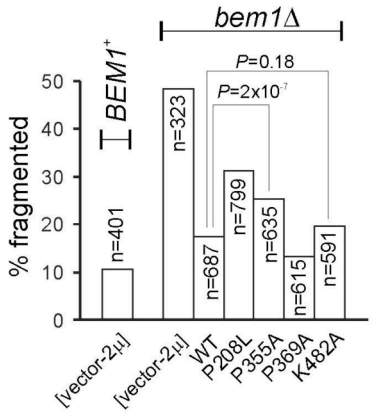

E

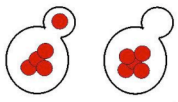

WT (n=234)	72%	28%
***cln3*Δ** (n=203)	53%	47%
***bem1*Δ** (n=125)	77%	23%

The R369A substitution did not have any effect (Fig. 4.8D), suggesting perhaps that lipid interactions are not important for Bem1p's function in vacuolar homotypic fusion. To varying degrees, the other Bem1p mutants also significantly suppressed vacuolar fragmentation of *bem1*Δ cells (Fig. 4.8D). Notably, the weakest suppression, albeit still significant, was observed with the P208L substitution (Fig. 4.8D), which affects protein-protein interactions through the SH3-2 domain (Irazoqui et al., 2003).

Finally, since the actin cytoskeleton plays a major role in vesicle transport in the bud and vacuole inheritance (Pruyne et al., 2004; Weisman, 2003), we decided to evaluate vacuolar segregation in *bem1*Δ cells. When we followed the "old" vacuolar compartment synthesized in previous cell divisions, we found that *bem1*Δ and wild-type cells equally distribute their vacuoles between the mother and the bud (Fig. 4.8E), unlike *cln3*Δ cells which have a weak but measurable defect (Fig. 3.8E and CHAPTER II). Furthermore, over-expression of *CDC42* did not alter the vacuolar segregation of *cln3*Δ cells (data not shown). Overall, these results suggest that it is unlikely that the mechanism we describe here linking Cln3p and Bem1p significantly affects vacuole segregation.

Discussion

In this study we present experiments that link the G1 cyclin Cln3p with vacuole fusion, through Bem1p and the Cdc42p GTPase. We discuss our findings in the context of the known roles of these proteins and how they might affect vacuolar homeostasis.

We were initially led to Bem1p because *bem1*Δ cells are large and their vacuolar compartment is also enlarged and fragmented, similar to the situation in *cln3*Δ cells (Fig. 4.2 and CHAPTER II). The experiments we report here suggest that Bem1p is phosphorylated in a Cdk-dependent manner. The biological significance of Ser72 phosphorylation is underscored by the fact that a substitution to Asp that probably mimics phosphorylation suppresses vacuolar fragmentation, while an Ala substitution does not (Fig. 4.5). Our data strongly point to the link between Cln3p and modification of Ser72 (Fig. 4.6). *In vitro*, however, it appears that multiple Cdk complexes can phosphorylate Bem1p. Addition of Bem1p from bacteria can still promote vacuole fusion *in vitro*, in the absence of Cln3p (Fig. 4.5E), suggesting that other cyclin/Cdk complexes might also be able to phosphorylate this exogenous pool of Bem1p. Furthermore, Clb2p/Cdc28p was previously shown to phosphorylate Bem1p (Ubersax et al., 2003) *in vitro*. This result was further extended in a follow-up study, where Loog and Morgan found that Clb5p/Cdc28p and Clb2p/Cdc28p phosphorylated Bem1p with equal efficiency (Loog and Morgan, 2005). Nonetheless, in living cells Cln3p certainly plays a unique role in vacuolar biogenesis because loss of any other cyclin does not lead to vacuolar fragmentation (CHAPTER II; Seeley et al., 2002).

Cln3p abundance and activity does not significantly oscillate in the cell cycle (Tyers et al., 1993; Tyers et al., 1992), and the same seems to be true for the electrophoretic mobility of Bem1p in synchronously cycling cells (Fig. 4.4H). While it is thought that overall vacuolar biogenesis is the result of reciprocal control between vacuole fusion and fission (Peters et al., 2004), there is no evidence that either of these

processes oscillate in the cell cycle. Vacuolar inheritance is thought to be coordinated with the cell cycle and we have previously reported that loss of Cln3p leads to mild defects in vacuolar segregation (CHAPTER II and see also Fig. 4.8E), but there are no such defects in *bem1*Δ cells (Fig. 4.8E). Thus, although the mechanism we describe here linking Cln3p with Bem1p certainly impacts on the "steady-state" overall vacuolar homeostasis, it may not necessarily impart an oscillatory feature to it.

On the other hand, Cln3p's vacuolar roles strongly affect the cell size phenotypes associated with *CLN3* mutations (see Fig. 4.3 and CHAPTER II). As we have discussed previously (CHAPTER II), this does not extend to all cell size mutants. Vacuolar enlargement is usually accompanied by cellular enlargement (Efe et al., 2005) but the converse is not necessarily true and not all large cell size mutants have large vacuoles. This is exemplified in double mutant *cln1,2*Δ cells, which are large overall although they have small vacuoles (CHAPTER II). A general correlation between vacuolar fragmentation and cell size also does not seem to exist (Fig. 4.2A). Nonetheless, our data also show that in *bem1*Δ cells *CLN3* over-expression accelerated initiation of DNA replication (Fig. 4.3C), without a concomitant reduction in cell size (Fig. 4.3A). All these observations suggest that Cln3p's role in vacuole fusion is separate from and probably does not impact on the other function of Cln3p in accelerating initiation of DNA replication.

How might cyclin-dependent phosphorylation of Bem1p impact on vacuole fusion? Cdc42p is involved in actin dynamics (Etienne-Manneville, 2004; Irazoqui and Lew, 2004) and vacuole fusion (Eitzen et al., 2001; Muller et al., 2001). Importantly, the

temporal requirement of Cln3p or Cdc42p for fusion appears to be similar. Loss of either Cln3p or Cdc42p leads to vacuolar fragmentation, but once the docking step of fusion is completed neither Cln3p (Fig. 4.1) nor Cdc42p (Eitzen et al., 2001; Muller et al., 2001) are required anymore for fusion. While it is clear that non-cytoskeletal actin is found on the surface of vacuoles and remodeling of this actin pool is required for vacuole fusion (Eitzen et al., 2002), it is not known how it contributes to fusion. This requirement is distinct from the actin cytoskeleton-dependent processes of vacuole segregation (Pruyne et al., 2004; Weisman, 2003). Since we find no evidence for a defect in vacuolar segregation in *bem1*Δ cells (Fig. 4.8D), there is no reason to think that the cyclin-dependent phosphorylation of Bem1p we describe here affects this process. Consequently, our data placing Bem1p downstream of Cln3p (Figs. 4.3,4.5), and the ability of Cdc42p to suppress vacuole fragmentation in *cln3*Δ cells (Fig. 4.8), probably reflect the non-cytoskeletal role of actin for vacuole fusion that has been proposed by the Wickner and Mayer labs (Eitzen et al., 2001; Eitzen et al., 2002; Muller et al., 2001).

Organelle bound actin could also act as a fusion barrier, which must transiently disassemble for vesicles to dock, while later promoting actin assembly is thought to somehow help the docked vesicles to finally fuse (Eitzen, 2003). Based on chemical inhibition experiments, it appears that the actin depolymerizing drug latrunculin B inhibits the last fusion step of vacuole homotypic fusion (Eitzen et al., 2001). Interestingly, the F-actin binding and stabilizing drug jasplakinolide inhibited the docking step of fusion only, and not the last latrunculin B-sensitive step (Eitzen et al., 2001). Given that Cln3p (Fig. 4.1) and Cdc42p (Eitzen et al., 2001; Muller et al., 2001)

are not required after the docking step of fusion; the fact that Ser72 of Bem1p has distinct and even opposing roles in vacuole fusion vs. bud emergence (Figs. 4.5 and 4.7); and the fact that other Bem1p mutants that affect bud emergence do not affect vacuole fusion (Fig. 4.8), it is possible that the effects we are observing reflect the "actin as a barrier" model of fusion (Eitzen, 2003).

Does cyclin-dependent phosphorylation of Bem1p affect other Bem1p-regulated processes? The S72A substitution is incapable of suppressing vacuolar fragmentation in *bem1*Δ cells, but it is still fully active in bud emergence (Figs. 4.5 and 4.7). On the other hand, the S72D substitution fully suppresses vacuole fragmentation but it only partially suppresses bud emergence (Figs. 4.5 and 4.7). These results suggest that Bem1p has distinct roles in bud emergence and vacuole fusion. While presumably locking Ser72 to the phosphorylated state (in the S72D mutant) suffices to suppress vacuolar fragmentation (Fig. 4.5), it might adversely affect bud emergence (Fig. 4.7).

The notion that Bem1p's roles in vacuole fusion and bud emergence may be distinct is also suggested by the fact that other Bem1p mutants (for example the K482A mutant) that were shown to be unable to suppress bud emergence defects (Irazoqui et al., 2003), retain full complementing ability in vacuole fusion (Fig. 4.8D). Even the P208L mutant, which cannot complement bud emergence (Irazoqui et al., 2003), partially suppressed vacuolar fragmentation (Fig. 4.8D). The P208L mutant affects interactions between the SH3-2 domain of Bem1p with various effectors, including the Cla4p kinase. Interestingly, loss of Cla4p leads to vacuolar fragmentation (Seeley et al., 2002), and it is possible that interactions mediated by the SH3-2 domain of Bem1p might be important

for vacuole fusion, explaining the incomplete suppression of vacuolar fragmentation we got from the P208L mutant (Fig. 4.8D).

In any case, since the actin remodeling necessary for vacuole fusion is not the same as the rearrangement of the actin cytoskeleton that takes place during bud emergence, probably identical mechanisms/effectors do not operate in both processes. It should also be noted that while Cln1p and Cln2p have established roles in bud emergence (Bose et al., 2001; Gulli et al., 2000; Moffat and Andrews, 2004), they do not affect vacuole fusion (CHAPTER II). Finally, although there are no known protein-protein interactions mediated by the SH3-1 domain of Bem1p, it is possible that Ser72 might impact on vacuole fusion through interactions with effectors that have specific roles in fusion. Given the scaffold role of Bem1p and the fact that addition of Cdc42p in the presence of the Bem1p-S72A mutant did not promote fusion as efficiently as the Bem1p-S72D mutant alone (compare Figs. 4.8C and 3.5E), it is possible that phosphorylation of Ser72 is important for some kind of protein-protein interactions that promote vacuole fusion. Future experiments need to address in full detail the mechanisms that account for the differences between Bem1p's roles in vacuole fusion and bud emergence.

CHAPTER V

SUMMARY AND PERSPECTIVES

We found a novel role of Cln3p in vacuolar fusion and biogenesis independent of its well-established function in the activation of G1 transcription. Cln3p/Cdc28p directly regulates vacuolar homotypic fusion and vacuolar copy number by a post-translational mechanism. Overall vacuole size disproportionately increases in *cln3Δ* cells, which accounts for most of their cell size increase.

Furthermore, we identified a scaffold protein, Bem1p, as the target of Cln3p/Cdc28p in vacuolar fusion. Bem1p is required for the vacuolar function of Cln3p both *in vivo* and *in vitro*. Our results indicate that Ser72 on Bem1p is phosphorylated by Cdc28p in a Cln3p-dependent manner and that Cln3p's vacuolar function is executed by the regulation of this phosphorylation. In contrary, bud emergence was promoted by an unphosphorylated Ser72 isoform but not by a phosphorylated Ser72 isoform. Over-expression of Cdc42p GTPase bypasses the requirement of Cln3p for vacuolar homotypic fusion only in the presence of Bem1p, suggesting that the Ser 72 phosphorylation by Cln3p/Cdc28p impacts on the regulation of Bem1p/Cdc42p-dependent actin polymerization and as a result vacuolar homotypic fusion.

Our results are remarkable in several respects. First, they contain the first demonstration in yeast that a cell cycle regulator directly regulates an organelle's membrane fusion. Second, they suggest that organelle biogenesis and membrane trafficking, rather than the conventional molecule-to molecule interactions, should be

taken into account to better understand cell size control. Third, they provide high resolution details of a molecular mechanism such that phosphorylation of a single amino acid on a protein is exclusively dependent on a specific cyclin *in vivo*. Fourth, they add an important, rare illustration to the currently brief list of examples of how Cdk-dependent phosphorylation of a single amino acid on a protein gives rise to a distinct and significant biological consequence, as seen in the differential effect of Bem1p's Ser72 phosphorylation on vacuolar homotypic fusion versus bud emergence.

Actin polymerization is of fundamental importance in that it provides the structural basis of cytoskeleton and cell morphogenesis and motility, as well as it plays a role in vacuolar homotypic fusion and neural signaling. A further mechanistic study on how a single phosphorylation on Bem1p results in such a significant impingement on Cdc42p activity and actin polymerization will provide an important insight into these actin-involving processes.

REFERENCES

Adams, A. E., and Pringle, J. R. (1984). Relationship of actin and tubulin distribution to bud growth in wild-type and morphogenetic-mutant *Saccharomyces cerevisiae*. J Cell Biol *98*, 934-945.

Altman, R., and Kellogg, D. (1997). Control of mitotic events by Nap1 and the Gin4 kinase. J Cell Biol *138*, 119-130.

Barelle, C. J., Bohula, E. A., Kron, S. J., Wessels, D., Soll, D. R., Schafer, A., Brown, A. J., and Gow, N. A. (2003). Asynchronous cell cycle and asymmetric vacuolar inheritance in true hyphae of *Candida albicans*. Eukaryot Cell *2*, 398-410.

Bender, A., and Pringle, J. R. (1991). Use of a screen for synthetic lethal and multicopy suppressee mutants to identify two new genes involved in morphogenesis in *Saccharomyces cerevisiae*. Mol Cell Biol *11*, 1295-1305.

Benton, B. K., Tinkelenberg, A. H., Jean, D., Plump, S. D., and Cross, F. R. (1993). Genetic analysis of Cln/Cdc28 regulation of cell morphogenesis in budding yeast. Embo J *12*, 5267-5275.

Bishop, A. C., Ubersax, J. A., Petsch, D. T., Matheos, D. P., Gray, N. S., Blethrow, J., Shimizu, E., Tsien, J. Z., Schultz, P. G., Rose, M. D*., et al.* (2000). A chemical switch for inhibitor-sensitive alleles of any protein kinase. Nature *407*, 395-401.

Bonifacino, J. S., and Glick, B. S. (2004). The mechanisms of vesicle budding and fusion. Cell *116*, 153-166.

Bose, I., Irazoqui, J. E., Moskow, J. J., Bardes, E. S., Zyla, T. R., and Lew, D. J. (2001). Assembly of scaffold-mediated complexes containing Cdc42p, the exchange factor Cdc24p, and the effector Cla4p required for cell cycle-regulated phosphorylation of Cdc24p. J Biol Chem *276*, 7176-7186.

Breeuwer, P., Drocourt, J.-L., Bunschoten, N., Zwietering, M. H., Rombouts, F. M., and Abee, T. (1995). Characterization of uptake and hydrolysis of fluorescein diacetate and carboxyfluorescein diacetate by intracellular esterases in *Saccharomyces cerevisiae*, which result in accumulation of fluorescent product. Appl. & Environ. Microbiol. *61*, 1614-1619.

Bryan, B. A., McGrew, E., Lu, Y., and Polymenis, M. (2004). Evidence for control of nitrogen metabolism by a START-dependent mechanism in *Saccharomyces cerevisiae*. Mol Genet Genomics *271*, 72-81.

Bryant, N. J., and Stevens, T. H. (1998). Vacuole biogenesis in *Saccharomyces cerevisiae*: protein transport pathways to the yeast vacuole. Microbiol Mol Biol Rev *62*, 230-247.

Burd, C. G., Babst, M., and Emr, S. D. (1998). Novel pathways, membrane coats and PI kinase regulation in yeast lysosomal trafficking. Semin Cell Dev Biol *9*, 527-533.

Casamayor, A., and Snyder, M. (2002). Bud-site selection and cell polarity in budding yeast. Curr Opin Microbiol *5*, 179-186.

Catlett, N. L., and Weisman, L. S. (2000). Divide and multiply: organelle partitioning in yeast. Curr Opin Cell Biol *12*, 509-516.

Chau, B. N., and Wang, J. Y. (2003). Coordinated regulation of life and death by RB. Nat Rev Cancer *3*, 130-138.

Chen, Y. A., and Scheller, R. H. (2001). SNARE-mediated membrane fusion. Nat Rev Mol Cell Biol *2*, 98-106.

Cliften, P., Sudarsanam, P., Desikan, A., Fulton, L., Fulton, B., Majors, J., Waterston, R., Cohen, B. A., and Johnston, M. (2003). Finding functional features in *Saccharomyces* genomes by phylogenetic footprinting. Science *301*, 71-76.

Conradt, B., Shaw, J., Vida, T., Emr, S., and Wickner, W. (1992). *In vitro* reactions of vacuole inheritance in *Saccharomyces cerevisiae*. J Cell Biol *119*, 1469-1479.

Costanzo, M., Nishikawa, J. L., Tang, X., Millman, J. S., Schub, O., Breitkreuz, K., Dewar, D., Rupes, I., Andrews, B., and Tyers, M. (2004). CDK activity antagonizes Whi5, an inhibitor of G1/S transcription in yeast. Cell *117*, 899-913.

Cross, F. R. (1988). *DAF1*, a mutant gene affecting size control, pheromone arrest, and cell cycle kinetics of *Saccharomyces cerevisiae*. Mol Cell Biol *8*, 4675-4684.

Cross, F. R. (1990). Cell cycle arrest caused by *CLN* gene deficiency in *Saccharomyces cerevisiae* resembles START-I arrest and is independent of the mating- pheromone signalling pathway. Mol Cell Biol *10*, 6482-6490.

Cvrckova, F., and Nasmyth, K. (1993). Yeast G1 cyclins CLN1 and CLN2 and a GAP-like protein have a role in bud formation. Embo J *12*, 5277-5286.

De Bondt, H. L., Rosenblatt, J., Jancarik, J., Jones, H. D., Morgan, D. O., and Kim, S. H. (1993). Crystal structure of cyclin-dependent kinase 2. Nature *363*, 595-602.

de Bruin, R. A., McDonald, W. H., Kalashnikova, T. I., Yates, J., 3rd, and Wittenberg, C. (2004). Cln3 activates G1-specific transcription via phosphorylation of the SBF bound repressor Whi5. Cell *117*, 887-898.

Dirick, L., Bohm, T., and Nasmyth, K. (1995). Roles and regulation of Cln-Cdc28 kinases at the start of the cell cycle of *Saccharomyces cerevisiae*. Embo J *14*, 4803-4813.

Doree, M., and Hunt, T. (2002). From Cdc2 to Cdk1: when did the cell cycle kinase join its cyclin partner? J Cell Sci *115*, 2461-2464.

Edgington, N. P., and Futcher, B. (2001). Relationship between the function and the location of G1 cyclins in *S. cerevisiae*. J Cell Sci *114*, 4599-4611.

Efe, J. A., Botelho, R. J., and Emr, S. D. (2005). The Fab1 phosphatidylinositol kinase pathway in the regulation of vacuole morphology. Curr Opin Cell Biol *17*, 402-408.

Eitzen, G. (2003). Actin remodeling to facilitate membrane fusion. Biochim Biophys Acta *1641*, 175-181.

Eitzen, G., Thorngren, N., and Wickner, W. (2001). Rho1p and Cdc42p act after Ypt7p to regulate vacuole docking. Embo J *20*, 5650-5656.

Eitzen, G., Wang, L., Thorngren, N., and Wickner, W. (2002). Remodeling of organelle-bound actin is required for yeast vacuole fusion. J Cell Biol *158*, 669-679.

Eitzen, G., Will, E., Gallwitz, D., Haas, A., and Wickner, W. (2000). Sequential action of two GTPases to promote vacuole docking and fusion. Embo J *19*, 6713-6720.

Elledge, S. J., and Spottswood, M. R. (1991). A new human p34 protein kinase, CDK2, identified by complementation of a cdc28 mutation in *Saccharomyces cerevisiae*, is a homolog of Xenopus Eg1. Embo J *10*, 2653-2659.

Etienne-Manneville, S. (2004). Cdc42--the centre of polarity. J Cell Sci *117*, 1291-1300.

Gari, E., Volpe, T., Wang, H., Gallego, C., Futcher, B., and Aldea, M. (2001). Whi3 binds the mRNA of the G(1) cyclin CLN3 to modulate cell fate in budding yeast. Genes Dev *15*, 2803-2808.

Gary, J. D., Wurmser, A. E., Bonangelino, C. J., Weisman, L. S., and Emr, S. D. (1998). Fab1p is essential for PtdIns(3)P 5-kinase activity and the maintenance of vacuolar size and membrane homeostasis. J Cell Biol *143*, 65-79.

Gattiker, A., Gasteiger, E., and Bairoch, A. (2002). ScanProsite: a reference implementation of a PROSITE scanning tool. Appl Bioinformatics *1*, 107-108.

Gulli, M. P., Jaquenoud, M., Shimada, Y., Niederhauser, G., Wiget, P., and Peter, M. (2000). Phosphorylation of the Cdc42 exchange factor Cdc24 by the PAK-like kinase Cla4 may regulate polarized growth in yeast. Mol Cell *6*, 1155-1167.

Guo, W., Sacher, M., Barrowman, J., Ferro-Novick, S., and Novick, P. (2000). Protein complexes in transport vesicle targeting. Trends Cell Biol *10*, 251-255.

Guzman, L. M., Belin, D., Carson, M. J., and Beckwith, J. (1995). Tight regulation, modulation, and high-level expression by vectors containing the arabinose PBAD promoter. J Bacteriol *177*, 4121-4130.

Haas, A., and Wickner, W. (1996). Homotypic vacuole fusion requires Sec17p (yeast alpha-SNAP) and Sec18p (yeast NSF). Embo J *15*, 3296-3305.

Hadwiger, J. A., Wittenberg, C., Richardson, H. E., de Barros Lopes, M., and Reed, S. I. (1989). A family of cyclin homologs that control the G1 phase in yeast. Proc Natl Acad Sci USA *86*, 6255-6259.

Han, B.-K., Aramayo, R., and Polymenis, M. (2003). The G1 cyclin Cln3p controls vacuolar biogenesis in *Saccharomyces cerevisiae*. Genetics *165*, 467-476.

Hartwell, L. H., and Unger, M. W. (1977). Unequal division in *Saccharomyces cerevisiae* and its implications for the control of cell division. J Cell Biol *75*, 422-435.

Hay, J. C., and Scheller, R. H. (1997). SNAREs and NSF in targeted membrane fusion. Curr Opin Cell Biol *9*, 505-512.

Heinisch, J. J., Lorberg, A., Schmitz, H. P., and Jacoby, J. J. (1999). The protein kinase C-mediated MAP kinase pathway involved in the maintenance of cellular integrity in *Saccharomyces cerevisiae*. Mol Microbiol *32*, 671-680.

Henchoz, S., Chi, Y., Catarin, B., Herskowitz, I., Deshaies, R. J., and Peter, M. (1997). Phosphorylation- and ubiquitin-dependent degradation of the cyclin-dependent kinase inhibitor Far1p in budding yeast. Genes Dev *11*, 3046-3060.

Hill, K. L., Catlett, N. L., and Weisman, L. S. (1996). Actin and myosin function in directed vacuole movement during cell division in *Saccharomyces cerevisiae*. J Cell Biol *135*, 1535-1549.

Irazoqui, J. E., Gladfelter, A. S., and Lew, D. J. (2003). Scaffold-mediated symmetry breaking by Cdc42p. Nat Cell Biol *5*, 1062-1070.

Irazoqui, J. E., and Lew, D. J. (2004). Polarity establishment in yeast. J Cell Sci *117*, 2169-2171.

Jones, E. W., Webb, G. C., and Hiller, M. A. (1997). Biogenesis and function of the yeast vacuole. In: The Molecular Biology of the Yeast *Saccharomyces*, J. R. Pringle, J. R. Broach, and E. W. Jones, eds. (Cold Spring Harbor, NY, Cold Spring Harbor Laboratory Press), pp. 363-470.

Jorgensen, P., Nishikawa, J. L., Breitkreutz, B. J., and Tyers, M. (2002). Systematic identification of pathways that couple cell growth and division in yeast. Science *297*, 395-400.

Jorgensen, P., and Tyers, M. (2004). How cells coordinate growth and division. Curr Biol *14*, R1014-1027.

Kaiser, C., Michaelis, S., and Mitchell, A. (1994). Methods in Yeast Genetics (Cold Spring Harbor, Cold Spring Harbor Laboratory Press).

Katzmann, D. J., Odorizzi, G., and Emr, S. D. (2002). Receptor downregulation and multivesicular-body sorting. Nat Rev Mol Cell Biol *3*, 893-905.

Kellis, M., Patterson, N., Endrizzi, M., Birren, B., and Lander, E. S. (2003). Sequencing and comparison of yeast species to identify genes and regulatory elements. Nature *423*, 241-254.

Klionsky, D. J., and Emr, S. D. (2000). Autophagy as a regulated pathway of cellular degradation. Science *290*, 1717-1721.

Laemmli, U. K. (1970). Cleavage of structural proteins during the assembly of the head of bacteriophage T4. Nature *227*, 680-685.

Langan, T. A., Gautier, J., Lohka, M., Hollingsworth, R., Moreno, S., Nurse, P., Maller, J., and Sclafani, R. A. (1989). Mammalian growth-associated H1 histone kinase: a homolog of cdc2+/CDC28 protein kinases controlling mitotic entry in yeast and frog cells. Mol Cell Biol *9*, 3860-3868.

Lee, M. G., and Nurse, P. (1987). Complementation used to clone a human homologue of the fission yeast cell cycle control gene cdc2. Nature *327*, 31-35.

Leeuw, T., Fourest-Lieuvin, A., Wu, C., Chenevert, J., Clark, K., Whiteway, M., Thomas, D. Y., and Leberer, E. (1995). Pheromone response in yeast: association of Bem1p with proteins of the MAP kinase cascade and actin. Science *270*, 1210-1213.

Leeuw, T., Wu, C., Schrag, J. D., Whiteway, M., Thomas, D. Y., and Leberer, E. (1998). Interaction of a G-protein beta-subunit with a conserved sequence in Ste20/PAK family protein kinases. Nature *391*, 191-195.

Levine, K., Huang, K., and Cross, F. R. (1996). *Saccharomyces cerevisiae* G1 cyclins differ in their intrinsic functional specificities. Mol Cell Biol *16*, 6794-6803.

Lew, D. J., Dulic, V., and Reed, S. I. (1991). Isolation of three novel human cyclins by rescue of G1 cyclin (Cln) function in yeast. Cell *66*, 1197-1206.

Liakopoulos, D., Kusch, J., Grava, S., Vogel, J., and Barral, Y. (2003). Asymmetric loading of Kar9 onto spindle poles and microtubules ensures proper spindle alignment. Cell *112*, 561-574.

Loog, M., and Morgan, D. O. (2005). Cyclin specificity in the phosphorylation of cyclin-dependent kinase substrates. Nature *434*, 104-108.

Lowe, M., Rabouille, C., Nakamura, N., Watson, R., Jackman, M., Jamsa, E., Rahman, D., Pappin, D. J., and Warren, G. (1998). Cdc2 kinase directly phosphorylates the cis-Golgi matrix protein GM130 and is required for Golgi fragmentation in mitosis. Cell *94*, 783-793.

Maffucci, T., and Falasca, M. (2001). Specificity in pleckstrin homology (PH) domain membrane targeting: a role for a phosphoinositide-protein co-operative mechanism. FEBS Lett *506*, 173-179.

Mayer, A., Wickner, W., and Haas, A. (1996). Sec18p (NSF)-driven release of Sec17p (alpha-SNAP) can precede docking and fusion of yeast vacuoles. Cell *85*, 83-94.

Mayo, LD and Donner, DB (2002). The PTEN, Mdm2, p53 tumor suppressor-oncoprotein network. Trends Biochem. Sci. *27*, 462-467.

McNew, J. A., Parlati, F., Fukuda, R., Johnston, R. J., Paz, K., Paumet, F., Sollner, T. H., and Rothman, J. E. (2000). Compartmental specificity of cellular membrane fusion encoded in SNARE proteins. Nature *407*, 153-159.

Mellman, I., and Warren, G. (2000). The road taken: past and future foundations of membrane traffic. Cell *100*, 99-112.

Mendenhall, M. D., and Hodge, A. E. (1998). Regulation of Cdc28 cyclin-dependent protein kinase activity during the cell cycle of the yeast *Saccharomyces cerevisiae*. Microbiol Mol Biol Rev *62*, 1191-1243.

Miller, M. E., and Cross, F. R. (2000). Distinct subcellular localization patterns contribute to functional specificity of the Cln2 and Cln3 cyclins of *Saccharomyces cerevisiae*. Mol Cell Biol *20*, 542-555.

Moffat, J., and Andrews, B. (2004). Late-G1 cyclin-CDK activity is essential for control of cell morphogenesis in budding yeast. Nat Cell Biol *6*, 59-66.

Muller, O., Johnson, D. I., and Mayer, A. (2001). Cdc42p functions at the docking stage of yeast vacuole membrane fusion. Embo J *20*, 5657-5665.

Nash, P., Tang, X., Orlicky, S., Chen, Q., Gertler, F. B., Mendenhall, M. D., Sicheri, F., Pawson, T., and Tyers, M. (2001). Multisite phosphorylation of a CDK inhibitor sets a threshold for the onset of DNA replication. Nature *414*, 514-521.

Nash, R., Tokiwa, G., Anand, S., Erickson, K., and Futcher, A. B. (1988). The WHI1+ gene of *Saccharomyces cerevisiae* tethers cell division to cell size and is a cyclin homolog. Embo J *7*, 4335-4346.

Nasmyth, K. (1996). At the heart of the budding yeast cell cycle. Trends Genet *12*, 405-412.

Nelson, W. J. (2000). W(h)ither the Golgi during mitosis? J Cell Biol *149*, 243-248.

Novick, P., Ferro, S., and Schekman, R. (1981). Order of events in the yeast secretory pathway. Cell *25*, 461-469.

Novick, P., Field, C., and Schekman, R. (1980). Identification of 23 complementation groups required for post-translational events in the yeast secretory pathway. Cell *21*, 205-215.

Nurse, P. (2002). Cyclin dependent kinases and cell cycle control (Nobel lecture). Chembiochem *3*, 596-603.

Nurse, P., and Thuriaux, P. (1980). Regulatory genes controlling mitosis in the fission yeast *Schizosaccharomyces pombe*. Genetics *96*, 627-637.

O'Farrell, P. H. (1975). High resolution two-dimensional electrophoresis of proteins. J Biol Chem *250*, 4007-4021.

Ogas, J., Andrews, B. J., and Herskowitz, I. (1991). Transcriptional activation of CLN1, CLN2, and a putative new G1 cyclin (HCS26) by SWI4, a positive regulator of G1-specific transcription. Cell *66*, 1015-1026.

Palade, G. (1975). Intracellular aspects of the process of protein synthesis. Science *189*, 347-358.

Pardee, A. B. (1974). A restriction point for control of normal animal cell proliferation. Proc Nat Acad Sci USA *71*, 1286-1290.

Parker, L. L., Atherton-Fessler, S., and Piwnica-Worms, H. (1992). p107wee1 is a dual-specificity kinase that phosphorylates p34cdc2 on tyrosine 15. Proc Natl Acad Sci USA *89*, 2917-2921.

Pathak, R., Bogomolnaya, L. M., Guo, J., and Polymenis, M. (2004). Gid8p (Dcr1p) and Dcr2p function in a common pathway to promote START completion in *Saccharomyces cerevisiae*. Euk Cell *3*, 1627-1638.

Pelham, H. R. (1999). SNAREs and the secretory pathway-lessons from yeast. Exp Cell Res *247*, 1-8.

Peter, M., Gartner, A., Horecka, J., Ammerer, G., and Herskowitz, I. (1993). FAR1 links the signal transduction pathway to the cell cycle machinery in yeast. Cell *73*, 747-760.

Peters, C., Baars, T. L., Buhler, S., and Mayer, A. (2004). Mutual control of membrane fission and fusion proteins. Cell *119*, 667-678.

Pfeffer, S. R. (1996). Transport vesicle docking: SNAREs and associates. Annu Rev Cell Dev Biol *12*, 441-461.

Pfeffer, S. R. (1999). Transport-vesicle targeting: tethers before SNAREs. Nat Cell Biol *1*, E17-22.

Polymenis, M., and Schmidt, E. V. (1997). Coupling of cell division to cell growth by translational control of the G1 cyclin CLN3 in yeast. Genes Dev *11*, 2522-2531.

Preston, R. A., Manolson, M. F., Becherer, K., Weidenhammer, E., Kirkpatrick, D., Wright, R., and Jones, E. W. (1991). Isolation and characterization of PEP3, a gene required for vacuolar biogenesis in *Saccharomyces cerevisiae*. Mol Cell Biol *11*, 5801-5812.

Preston, R. A., Murphy, R. F., and Jones, E. W. (1989). Assay of vacuolar pH in yeast and identification of acidification- defective mutants. Proc Natl Acad Sci USA *86*, 7027-7031.

Pringle, J. R., and Hartwell, L. H. (1981). The *Saccharomyces cerevisiae* cell cycle. In: The molecular biology of the yeast *Saccharomyces*, J. D. Strathern, E. W. Jones, and J.

R. Broach, eds. (Cold Spring Harbor, NY, Cold Spring Harbor Laboratory Press), pp. 97-142.

Pruyne, D., Legesse-Miller, A., Gao, L., Dong, Y., and Bretscher, A. (2004). Mechanisms of polarized growth and organelle segregation in yeast. Annu Rev Cell Dev Biol *20*, 559-591.

Raught, B., Gingras, A. C., and Sonenberg, N. (2001). The target of rapamycin (TOR) proteins. Proc Natl Acad Sci USA *98*, 7037-7044.

Richardson, H. E., Wittenberg, C., Cross, F., and Reed, S. I. (1989). An essential G1 function for cyclin-like proteins in yeast. Cell *59*, 1127-1133.

Richman, T. J., Toenjes, K. A., Morales, S. E., Cole, K. C., Wasserman, B. T., Taylor, C. M., Koster, J. A., Whelihan, M. F., and Johnson, D. I. (2004). Analysis of cell-cycle specific localization of the Rdi1p RhoGDI and the structural determinants required for Cdc42p membrane localization and clustering at sites of polarized growth. Curr Genet *45*, 339-349.

Rigaut, G., Shevchenko, A., Rutz, B., Wilm, M., Mann, M., and Seraphin, B. (1999). A generic protein purification method for protein complex characterization and proteome exploration. Nat Biotechnol *17*, 1030-1032.

Roberts, C. J., Raymond, C. K., Yamashiro, C. T., and Stevens, T. H. (1991). Methods for studying the yeast vacuole. Methods Enzymol *194*, 644-661.

Rothman, J. E. (1994). Mechanisms of intracellular protein transport. Nature *372*, 55-63.

Rothman, J. E. (2002). Lasker Basic Medical Research Award. The machinery and principles of vesicle transport in the cell. Nat Med *8*, 1059-1062.

Schaefer, J. B., and Breeden, L. L. (2004). RB from a bud's eye view. Cell *117*, 849-850.

Schneider, B. L., Yang, Q. H., and Futcher, A. B. (1996). Linkage of replication to start by the Cdk inhibitor Sic1. Science *272*, 560-562.

Seeley, E. S., Kato, M., Margolis, N., Wickner, W., and Eitzen, G. (2002). Genomic analysis of homotypic vacuole fusion. Mol Biol Cell *13*, 782-794.

Shintani, T., and Klionsky, D. J. (2004). Autophagy in health and disease: a double-edged sword. Science *306*, 990-995.

Shorter, J., and Warren, G. (2002). Golgi architecture and inheritance. Annu Rev Cell Dev Biol *18*, 379-420.

Sollner, T., Bennett, M. K., Whiteheart, S. W., Scheller, R. H., and Rothman, J. E. (1993). A protein assembly-disassembly pathway *in vitro* that may correspond to sequential steps of synaptic vesicle docking, activation, and fusion. Cell *75*, 409-418.

Spellman, P. T., Sherlock, G., Zhang, M. Q., Iyer, V. R., Anders, K., Eisen, M. B., Brown, P. O., Botstein, D., and Futcher, B. (1998). Comprehensive identification of cell cycle-regulated genes of the yeast *Saccharomyces cerevisiae* by microarray hybridization. Mol Biol Cell *9*, 3273-3297.

Stuart, D., and Wittenberg, C. (1995). CLN3, not positive feedback, determines the timing of CLN2 transcription in cycling cells. Genes Dev *9*, 2780-2794.

Sudbery, P. E., Goodey, A. R., and Carter, B. L. (1980). Genes which control cell proliferation in the yeast *Saccharomyces cerevisiae*. Nature *288*, 401-404.

Sutton, R. B., Fasshauer, D., Jahn, R., and Brunger, A. T. (1998). Crystal structure of a SNARE complex involved in synaptic exocytosis at 3.4 A resolution. Nature *395*, 347-353.

Tang, F., Kauffman, E. J., Novak, J. L., Nau, J. J., Catlett, N. L., and Weisman, L. S. (2003). Regulated degradation of a class V myosin receptor directs movement of the yeast vacuole. Nature *422*, 87-92.

Thuriaux, P., Nurse, P., and Carter, B. (1978). Mutants altered in the control co-ordinating cell division with cell growth in the fission yeast *Schizosaccharomyces pombe*. Mol Gen Genet *161*, 215-220.

Tyers, M. (1996). The cyclin-dependent kinase inhibitor p40SIC1 imposes the requirement for Cln G1 cyclin function at Start. Proc Natl Acad Sci USA *93*, 7772-7776.

Tyers, M., Tokiwa, G., and Futcher, B. (1993). Comparison of the *Saccharomyces cerevisiae* G1 cyclins: Cln3 may be an upstream activator of Cln1, Cln2 and other cyclins. Embo J *12*, 1955-1968.

Tyers, M., Tokiwa, G., Nash, R., and Futcher, B. (1992). The Cln3-Cdc28 kinase complex of *S. cerevisiae* is regulated by proteolysis and phosphorylation. Embo J *11*, 1773-1784.

Ubersax, J. A., Woodbury, E. L., Quang, P. N., Paraz, M., Blethrow, J. D., Shah, K., Shokat, K. M., and Morgan, D. O. (2003). Targets of the cyclin-dependent kinase Cdk1. Nature *425*, 859-864.

Verma, R., Annan, R. S., Huddleston, M. J., Carr, S. A., Reynard, G., and Deshaies, R. J. (1997). Phosphorylation of Sic1p by G1 Cdk required for its degradation and entry into S phase. Science *278*, 455-460.

Vida, T. A., and Emr, S. D. (1995). A new vital stain for visualizing vacuolar membrane dynamics and endocytosis in yeast. J Cell Biol *128*, 779-792.

Wang, H., Gari, E., Verges, E., Gallego, C., and Aldea, M. (2004). Recruitment of Cdc28 by Whi3 restricts nuclear accumulation of the G1 cyclin-Cdk complex to late G1. Embo J *23*, 180-190.

Wang, Y. X., Kauffman, E. J., Duex, J. E., and Weisman, L. S. (2001). Fusion of docked membranes requires the armadillo repeat protein Vac8p. J Biol Chem *276*, 35133-35140.

Wang, Y. X., Zhao, H., Harding, T. M., Gomes de Mesquita, D. S., Woldringh, C. L., Klionsky, D. J., Munn, A. L., and Weisman, L. S. (1996). Multiple classes of yeast mutants are defective in vacuole partitioning yet target vacuole proteins correctly. Mol Biol Cell *7*, 1375-1389.

Warren, G., and Wickner, W. (1996). Organelle inheritance. Cell *84*, 395-400.

Weber, T., Zemelman, B. V., McNew, J. A., Westermann, B., Gmachl, M., Parlati, F., Sollner, T. H., and Rothman, J. E. (1998). SNAREpins: minimal machinery for membrane fusion. Cell *92*, 759-772.

Weisman, L. S. (2003). Yeast vacuole inheritance and dynamics. Annu Rev Genet *37*, 435-460.

Wickner, W. (2002). Yeast vacuoles and membrane fusion pathways. Embo J *21*, 1241-1247.

Wickner, W., and Haas, A. (2000). Yeast homotypic vacuole fusion: a window on organelle trafficking mechanisms. Annu Rev Biochem *69*, 247-275.

Wiemken, A., and Durr, M. (1974). Characterization of amino acid pools in the vacuolar compartment of *Saccharomyces cerevisiae*. Arch Microbiol *101*, 45-57.

Wijnen, H., and Futcher, B. (1999). Genetic analysis of the shared role of CLN3 and BCK2 at the G(1)-S transition in *Saccharomyces cerevisiae*. Genetics *153*, 1131-1143.

Wittenberg, C., and Reed, S. I. (1996). Plugging it in: signaling circuits and the yeast cell cycle. Curr Opin Cell Biol *8*, 223-230.

Wittenberg, C., Sugimoto, K., and Reed, S. I. (1990). G1-specific cyclins of *S. cerevisiae*: cell cycle periodicity, regulation by mating pheromone, and association with the p34CDC28 protein kinase. Cell *62*, 225-237.

Yang, H. C., Palazzo, A., Swayne, T. C., and Pon, L. A. (1999). A retention mechanism for distribution of mitochondria during cell division in budding yeast. Curr Biol *9*, 1111-1114.

Zachariae, W., Schwab, M., Nasmyth, K., and Seufert, W. (1998). Control of cyclin ubiquitination by CDK-regulated binding of Hct1 to the anaphase promoting complex. Science *282*, 1721-1724.

Zettel, M. F., Garza, L. R., Cass, A. M., Myhre, R. A., Haizlip, L. A., Osadebe, S. N., Sudimack, D. W., Pathak, R., Stone, T. L., and Polymenis, M. (2003). The budding index of *Saccharomyces cerevisiae* deletion strains identifies genes important for cell cycle progression. FEMS Microbiol Lett *223*, 253-258.

Zhang, J., Schneider, C., Ottmers, L., Rodriguez, R., Day, A., Markwardt, J., and Schneider, B. L. (2002). Genomic scale mutant hunt identifies cell size homeostasis genes in *S. cerevisiae*. Curr Biol *12*, 1992-2001.

VITA

NAME:	Bong Kwan Han
EDUCATION:	B.S., Food Science and Engineering (1990) Seoul National University, South Korea
	M.S., Biotechnology (1992) Korea Advanced Institute of Science and Technology, South Korea
	Ph.D., Biochemistry (2005) Texas A&M University College Station, TX
PROFESSIONAL EXPERIENCE:	Researcher, Institute of Doo San (Oriental Brewery Co.), South Korea (1994-1995)
	Researcher, Mogam Biotechnology Research Institute, South Korea (1995-1998)
	Researcher, Korea University Medical School, South Korea (1998-1999)
PERMANENT ADDRESS:	Department of Biochemistry and Biophysics College Station, TX 77843-2128